POLITECNICO DI MILANO

Polo Regionale di Lecco

Faculty of Industrial Engineering

Master of Science in
Mechanical Engineering

Application of Optical Emission Spectroscopy Method for Characterization of Laser Micro Drilling

Supervisor: Prof. Barbara Previtali

Co - Supervisors: Eng. Daniele Colombo (Ph.D)

Eng. Ali Gokhan Demir

Master of Science Thesis by:

Endalkachew Mekonnen Aragaw (Matr. N. 737578)

Academic Year 2009-2010

Acknowledgement

This thesis marks the end of the remarkable journey I took in the last two years carrying out my master's study. Its successful completion, however, would not have been possible without the support of several people.

First and foremost, I would like to thank Politecnico Di Milano and UNIVER LECCO for offering me the scholarship to cover my tuition fees and living expense for the entire study period.

My deepest gratitude goes to my supervisors at Politecnico Di Milano, Prof, Barbara Previtali, Eng. Daniele Colombo and Eng. Ali Gokhan Demir for their sincere guidance, constant attention and support in the course of this thesis. Without their encouragement for the good works and comfort in the time of frustrations, it would have been difficult for me to bring this work to completion. I thank them for treating and understanding me with personal touches.

I'm grateful for those in SITEC lab helping me with technical things and support in many activities with special credit going to Giovanni Riva. I also like to express my gratitude to my friends Roza, Henok, Endris and Anteneh for motivating me through numerous personal and academic discussions we had which were an indispensable to my work and energy.

Last but not least, I would like to thank my family for the love they always nourish me as for their unshakable confidence on me, which is the driving force of my life.

Contents

Abstract

In this thesis work the use of fiber laser source for micro drilling and implementation of Optical emission spectroscopy to characterize laser induced plasma during the process is studied. Commercially pure (cp) grade II titanium is micro drilled using IPG Photonics YLP-50 fiber laser source at SITEC laboratory of Politecnico di Milano. Titanium is chosen as a work piece for the reason it is one of the commonly applicable engineering material in the field of micro drilling for enormous fields like aerospace, automotive and medical.

The characterization of laser induced plasma is performed on 1.5 mm thick cp titanium. Approach is with experimental technique in all part of the thesis work. First of all, the fiber laser source is studied which include the temporal behavior and process parameters like pulse width and shape. Secondly, once the laser source and its characteristics are defined, micro drilling process is performed for measurement of drilling time. The main aim of this phase was to understand the process duration and use it to fix gate width for spectrometer. Thirdly, laser micro drilling with spectroscopic measurement setup for optical emission (optical emission spectroscopy) is carried out to characterize induced plasma. Analysis and examination of experimental result using the analytical tool presented was targeting the determination of physical parameters of plasma during micro drilling. Atomic excitation temperature and electron density are the two physical parameters under consideration with the intention of characterizing the temporal behavior, relative amount and distribution of plasma formation. Finally the thesis work presents potential further implementation of the technique used in laser induced plasma for process characterization and monitoring in laser micro drilling.

Keywords: laser induced plasma, micro drilling, fiber laser, optical emission spectroscopy

Introduction

Modern products are getting more and more compact in design and demanding. In recent years, laser micro drilling has emerged as the prominent choice for the production of a large quantity of holes. Aerospace industry employ this technique to produce millions of small effusion cooling holes in turbine engine components such as combustion chambers and nozzle guide vanes. Electronic components such as print circuit board and printer ink nozzle, as well as mechanical parts such as fuel nozzle and filter are manufactured commonly. Biomedical engineering uses laser micro drilled commercially pure titanium (cp - Ti) these days as the most popular biomaterials for dental implantation because of its good specific strength, excellent corrosion resistance and bio-inertness. Other applications include automotive spare parts manufacturing, micro valves, drilling of flow filters and strainers, sub micron drilling in flexography ceramic rolls and drilling of aesthetic materials [H.C. Man, Q.Wang, X.Guo 2009, A. De Giacomo 2002].

In an industrial application, the type of manufacturing process has to be competitive, efficient, and cost effective so as to get preference over other methodological approaches. Laser material processing has proved its feasibility well in micro scale operating efficiently, flexibly and in better controllable fashion. Laser micro drilling has the advantage of no mechanical forces on work piece, flexibility for various materials, and applicability on small products dimension with high aspect ratio.

Pulsed fiber laser source are suitable for micro processing of engineering materials. The recently emerging technology of fiber laser could enable to deliver highly efficient power with excellent beam quality for inside of fiber with doping of rare Earth elements like Nd, Yb, Er, and others, with excellent electrical to optical power conversion efficiency (wall plug efficiency). As a challenge in fiber laser micro processing, from industrial practice point of view optimizing manufacturing cost, efficiency, product quality free from spatter, dimensional accuracy of hole diameter and taper would be mentioned.

In chapter 1 the aims of the work are discussed clearly and concisely. Basic point about micro machining, problem definition and plasma formation are raised.

The whole chapter 2 deals with states of the art. Section 2.2 is dedicated to discussion on technical aspects and state of the art of fiber laser sources and internal components such as gain media, pulse generation and modulation. Section 2.3 covers a literature review to characterization of Laser Induced Plasma (LIP). State of the art for Optical Emission Spectroscopy (OES), theory, and mathematical equations are discussed.

Once the state of the art portion of this work reviews the theoretical background and literature, focus is given to specific aim of this work on experimental set up and design in chapter 3. The first part of the experimental work of this thesis is dedicated to investigate the response behaviour of pulsed laser source in the initial transitory phase. The experimental oriented study is conducted at SITEC laboratory at Politecnico di Milano which is equipped with a pulsed IPG Photonics fiber laser source, whose gain medium is Ytterbium doped glass and is pumped with a diode system. Method of controlling the transient behaviour for generated pulses (in nano seconds region) is by acusto optic Q- switched device. Specifically, the amount of time required for laser pulse to reach peak power, number of pulses before nominal power reached and pulse width are measured considering two of the main laser parameters, pumping current (which determine laser power) and pulse repetition rate as factors altering the response. These factors influence manufacturing processes such as micro drilling (with drilling time commonly in ms) that operate the process in laser ablation of materials. Accordingly, it is inevitable that laser power amount and its duration can play significant effect on material laser beam interaction, and ultimately obtained product quality. The measuring technique used in this experimentation is off axis laser beam detection with fast responding photodiodes. The experimental approach is rigorous with two configurations used with spot diameter focused ON and OFF the surface of reflecting copper mirror used. Section 3.1 deals with the deep description of technical aspect of experimental set up, configurations, and components used for measurement of the above mentioned laser parameters. Detailed discussion is presented on set up of triggering mechanism for laser, specification and performance of photodiode with its alimentation circuit, and oscilloscope used to acquire measurement signal. Next, detailed presentation for OES experimental setup in laser drilling is covered. An overview of experimental setup description is presented first followed by a discussion on individual components specification, performance and working principle.

In chapter 4 experimental design is discussed in detail for all the experimentations performed followed by chapter 5 with results, explanation and discussion. Important parameters that describe the type of the laser source such as rise time to peak power, number of pulses, and the half width at half maximum pulse width (which is in nano seconds regime) is discussed.

Finally, study of process characterization during percussion micro drilling on commercially pure titanium specimen was performed with a target to evaluate physical parameters that can define the process. Spectroscopic analysis is used as a method for examination with optical emission lines of titanium atom and ion identified for analysing temporal evolution during the process. LIP physical parameters atomic excitation temperature and electron density values are computed and discussed for a selected technological laser parameter full power (100% pumping current) and 50 KHz operating condition. Finally, the paper presents summary of results, conclusions, and recommendation with the view point for potential further study and implementation of the results obtained by this thesis work.

Chapter 1: Aims of the Work

1.1 Problem definition

Laser micro drilled holes for various applications can be successfully produced by laser trepanning, though it is a relatively slow process compared with laser percussion drilling and there is limitation of micro drilled size. With percussion drilling however the control of hole parameters such as taper, entrance hole variation and roundness is much more difficult and these parameters are of the utmost importance for such applications. There are a large number of factors which can potentially affect this process. Determining number of pulses sufficient, insufficient or surplus irradiance, excessive plasma formation resulting spatter and dross are some of the factors to mention.

Laser micro machining basics is thermal process with absorption of the laser beam from the material to process followed by thermal filed and material ablation [Annemie Bogaerts et. al 2005, A. Ancona et.al 2008)]. The process is dependent on characteristics of the laser source especially on laser irradiance, pulse width and emission wavelength. Effectiveness of micro machining process with a goal of material removal like cutting and drilling depends mainly with pulse duration property of the laser source and heat diffusion capacity of base material in process. The longer the pulse width and the poorer the heat diffusion capacity of the base material, worse will become the resulting micro machined product [A. Ancona et .al 2009, A. Semerok et al 2000]. Especially micro drilling of holes quality is highly dependent on beam duration and is usually performed with shorter pulsed laser sources rather than continuous wave (CW) laser beam emission.

To characterize the process so that it enables to understand what is going on during that short period of time is the aim of this work. Characterization of the process with physical variables and interpretation of the value for drilled hole dimensional accuracy and state is a method applicable in various monitoring techniques. There have been different research approaches including parameter identification and modelling to monitor the process, but the present challenge is due to the lack of flexibility, since results are highly dependent on statistical modelling techniques of experimental results on specific material and laser interaction [L.Li, D.K.Y.Low and M.Ghoreshi 2007, R. Biswas et. Al 2009]. In this thesis work characterisation of

drilling process physical parameters is performed using experimental results performed on commercially pure grade 2 titanium using pulsed fiber laser source.

1.2 Micro drilling of titanium

The wide area of engineering and medical application of titanium makes it one of the research interest of materials in recent years. On the other hand, its physical properties like high melting point (in the order of 1933 K), reactivity with surrounding, poor thermal conductivity (21.9 $Wm^{-1}K^{-1}$) and low machinability due to high specific strength makes it a challenge from industrial point of view. Especially machining process in micro scale (generally from 1μ to 1mm) makes the task more difficult and is demanding because of the thermal process and short process duration. Micro drilling of titanium with short and ultra short pulse laser beam is a competitive and adoptable technique to encounter some of these challenges, and is widely implemented recently [A. Ancona et al 2009, S. Döring et. al 2010].

In micro drilling of titanium, its low thermal diffusivity (6.99 $\mu m^2 s^{-1}$) makes it more demanding for short pulsed fiber laser source in order to enable energy pumping time become shorter than the amount of time need for heat diffusion generated. Accordingly, it is interesting to determine and worth important to understand the behaviour of the laser source in use for the intended percussion micro drilling of titanium.

1.3 Formation of plasma

During the interaction of high power laser beam with surface of metallic targets, the laser causes heating of the solid state target, followed by melting and evaporation of some of the target material. The evaporated material expands, and because of the high temperature, plasma is formed (if plasma threshold is reached) in the material plume which is ionized by Bremsstrahlung (braking radiation emitted by particles change) and photo ionization processes. This plasma contains electrons, ions, neutral species, as well as excited species and is referred as laser induced plasma (LIP) which expands perpendicularly to the surface of target material.

For LIP expansion, the main mechanism of transition of bound electrons from the lower level to the upper level and vice versa is driven by inelastic collisions of electrons with heavy particles. The concentration of charged particles is controlled by

the electron impact ionization and the recombination of electrons with ions. Radiative processes as re-absorption, spontaneous and stimulated emission are also important in determining the concentration of emitting levels. During the plume expansion, the temperature drops down, and evaporated atoms will undertake condensation to small size particles [M. Capitelli et. al 2003].

The material ejection mechanism involved in percussion drilling has three distinct stages [P W French et. al 1999]. The first involves material being ejected as a plasma and a liquid conical sheet. This melt cone will continue to be ejected after the plasma has disappeared. The second stage involves material being ejected in a column like structure in a random direction from the hole. In the third stage of hole development droplets of melt can be seen leaving the hole. The extent of these droplets formation, which is directly proportional to the amount LIP and rate of ejection determines the efficiency of the drilling from quality point of view [B.S. Yilbas 2001]. For laser percussion drilling processes on metals, drilling efficiency related to re solidified materials is strongly dependent on the phenomenon of laser plasma formation and associated expansion. Plasma formation at the workpiece surface due to laser/material interaction severely decreases laser drilling effectiveness because it absorbs a significant portion of the incoming beam energy and thus shielding the workpiece surface [Annemie Bogaerts et. al 2005]. Quantity of re solidified and spattered materials depend on the amount of LIP formation and spread on material surface.

Laser parameters, mainly, laser irradiance, pulse duration and wavelength plays significant roll on the formation of LIP, evaporation process and formed plume (plasma) characteristics. The effect of laser process parameters on the formation of plasma and evaporation process during laser material interaction, and its effect on efficiency of micro drilling is discussed with depth in laser induced plasma section of state of the art.

1.4 Characterization of plasma for process behaviour study

The formation of droplets and defect associated to the final stage condensation of LIP in laser material interaction during micro drilling is a function of various factors. Beam quality, emission wavelength, material to process, process parameters like laser power (pulse energy), pulse width, repetition rate, shielding gas, in use are some to mention. Characterizing the physical state of the process and interpretation of the

result using spectroscopic technique is a methodological approach to understand what is being experienced in laser machining of metals. In this thesis work, micro drilling of a 1.5 mm commercially pure grade II titanium is performed with nano second regime pulsed fiber laser source, and spectroscopic method of approach is performed for characterization.

The experimental spectroscopic measurement aims exploring the temporal behavior of physical parameters of plasma; temperature and electron density. Previous works on the area has indicated the technique and are taken as consideration during decision in selecting process parameters [M. Capitelli 2003, C. Aragon 2008, A. De Giacomo 2002, Chengde Li 2006]. Temporal behaviour of the physical parameters of the laser induced plasma are investigated using time resolution into parts for the whole drilling process. Focus is given on designing an accurate methodological tool to implement in optical emission spectroscopy that enables processing of experimental data. It is suggested that the experimental setup and tool used for determination of induced plasma physical parameters could be used for monitoring technique and comparison between micro drill holes when performed in variable laser process parameters combination.

The first part of the work is dedicated to measurement with an experimental approach to investigate the behaviour of the pulse laser power when triggered externally. Here an experimental approach is used to investigate the behaviour of fiber laser source (IPG Photonics YLP 50, 50 watt average power pulsed laser in nano second regime). Specifically, the amount of time required for laser pulse to reach peak power, pulse width and shape are evaluated considering pumping current (laser power) and pulse repetition rate as factors altering the response, keeping focal length, beam diameter, and emission wavelength constant. It is known these parameters influence micro drill hole quality (with drilling time commonly expected in ms for 1.5 mm thick titanium) that is produced with laser ablation of materials [H.C. Man 2009, Chengde Li 2006].

The second target of the thesis is once again experimentally approached determination of drilling time for commercial pure titanium with 1.5mm thickness. The result obtained will be a key design decision for the third aim of the work during spectrometry. With 1.5mm thickness, it was possible to obtain through hole and drilling time that enables spectroscopic record that matches well good relative intensity and integration time.

Chapter 2: State of the Art

2.1 Introduction

State of the art for fiber laser source, laser micro drilling and characterization of laser induced plasma with optical emission spectroscopy is covered in this chapter. Focus of discussion in the first section is on Ytterbium ion doped type fiber pulsed laser with acusto –optic modulation for generation of nano second regime pulse width. Then, laser micro machining in general and micro drilling in specific is discussed. Finally methodological approach and theory of optical emission spectroscopy is dealt at the end sub section of the chapter.

2.2 Fiber Laser Source

In this section of the work the state of the art of the recently emerged laser sources (fiber laser) is discussed with focus on Ytterbium ion doped type.

Fiber lasers are solid state lasers (gain media is solid state with glass or ceramic used as common) with an active medium of passive host crystal and the active ion. It is these components that give the laser its name. The laser consists of pumping source which could be optically pumped ordinarily by flash lamps or using laser diodes, a coil of appropriate double clad doped fiber (with rare earth elements), and two reflectors.

Compared to traditional broadband arc or flash-lamps pump sources, a laser diode pump source possesses greatly increased spectral brightness, with an emission bandwidth of typically a few nanometers. Power efficiency is improved very well in case of diode pumped fiber laser sources, and they are commonly referred as All Solid State Lasers. Diode pumped fiber lasers are preferred nowadays due to their advantage in delivering high beam quality, long life time and compact setup.

The double-clad fiber consists of an inner single-mode core doped with the appropriate rare-earth ions such as Neodymium Nd^{3+}, Ytterbium Yb^{3+}, Erbium Er^{3+}, Thulium Tm^{3+}, Holmium Ho^{3+}, Praseodymium Pr^{3+}, Cerium Ce^{3+}. The cladding is made of un-doped glass that has a lower index of refraction. The pump light is injected into the cladding and then propagates along the structure, passing through the active core and producing a population inversion.

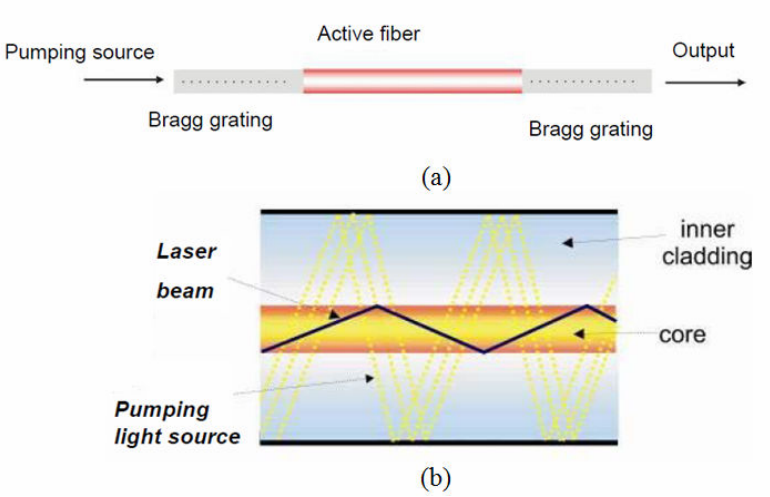

Figure 2.1: Fiber active laser source (a) fundamental components (b) double cladding

2.2.1 Pumping with diode power source

Diode pumping is optically efficient in comparison to the ordinary lamp pumping. It is possible to generate a range of laser power using the technique which makes it preferable and competitive. There is a possibility to find diode pumps for low power lasers (up to 200mw), little watt power with broad area diodes, high power laser with diode bars (greater than 100w) and highest power laser with diode stacks.

The following are some of the main advantages of diode pumping [Rudiger Paschotta 2008]:

- ⊕ A high electrical-to-optical efficiency of the pump source (of the order of 50%) leads to a high overall power efficiency
- ⊕ The narrow optical bandwidth of diode lasers makes it possible to pump directly certain transitions of laser-active ions without losing power in other spectral regions. It thus also contributes to a high efficiency.
- ⊕ Although the beam quality of high-power diode lasers is not perfect, it often allows for end pumping of lasers with very good overlap of laser mode and pump region, leading to high beam quality and power efficiency.
- ⊕ The lifetime of laser diodes is long compared with that of discharge lamps: typically many thousands of hours, often even well above 10 000 hours.
- ⊕ The compactness of the pump source, the power supply and the cooling arrangement makes the whole laser system much smaller and easier to use.
- ⊕ Diode pumping makes it possible to use a very wide range of solid-state gain media for different wavelength regions, including e.g. up conversion lasers.

For many solid-state gain media, the lower brightness of discharge lamps would not be sufficient.

- The low intensity noise of laser diodes leads to low noise of the diode-pumped laser.

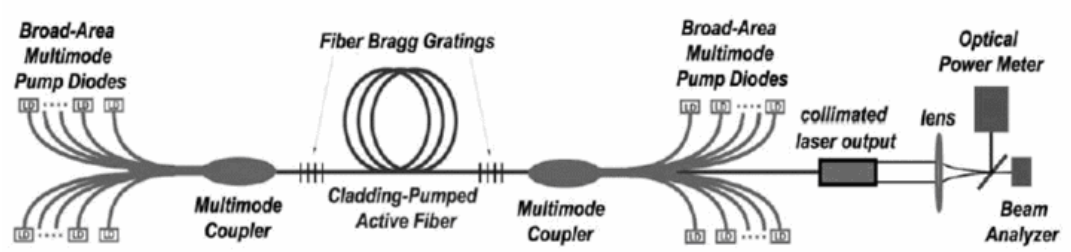

Figure 2.2: fiber laser source generation and delivery
(source: Valentin Gapontsev and William Krupke, Laser Focus World, August 2002)

2.2.2 Gain

In Photonics, the term gain is usually used to quantify the amplification of optical amplifiers. In fiber laser technology large gains are implemented and are expressed in decibel (dB) 10 times the logarithm (to base 10) of the amplification factor.

The width of the optical frequency range in which significant gain is available from an amplifier is referred as the gain bandwidth or spectral band width. It can limit the pulse duration of Q switched fiber laser. It is worth to remember though the pulse duration achievable actually depends on the "curvature" of the gain spectrum within the range of the pulse spectrum, and also on the magnitude of gain [C. Cuadrado-Laborde et. al 2007].

2.2.3 Gain Saturation

For high pumping power delivery, the gain of optical amplifier in fiber laser reduces. This is termed as gain saturation and is associated to the amount of power needed to add to an already amplified power.

Inside the laser gain medium, the gain does not instantly adjust to the level according to the optical input power, because the gain medium stores some amount of energy, and the stored energy determines the gain. For example, a sudden increase in the input power of a laser gain medium will reduce the gain only within a certain time,

because the population of excited laser ions is only reduced with a certain finite rate. This has important consequences for the laser dynamics [William F. Krupke 2001]. Very high amount of power do not also guarantee maximum gain because the population of excited laser ions is only reduced with a certain finite rate (at lower level).

2.2.4 Ytterbium Yb 3+ doping

Inside the laser gain medium which compensate for resonator losses, transparent crystals with laser active dopants is used to amplify light by absorption at laser wavelength with stimulated emission when energy is pumped to the crystal [Rudiger Paschotta 2008]. The type of dopant determines the absorbed light wavelength (emission wavelength of the laser and the amount of energy absorbed). The type of doping rare earth element determines the emission wave length of the laser beam. Oscillator strength which is related to upper state lifetime during laser transition is also a function of doping ion.

In many industrial laser applications Neodymium Nd^{3+} and Ytterbium Yb^{3+} are the preferable doping ions due to their laser emission wavelength close to engineering materials and energy storage capacity [William F. Krupke et. al 2000]. As it has been mentioned in the very first of this chapter, and the fact SITEC lab at Politechnico di Milano is equipped with Yb^{3+} diode pumped solid state laser (DPSSL) with pulsed mode, the focus area of discussion will be on it from here onwards.

Ytterbium-doped laser crystals have a number of interesting properties, which differ from other gain media. They have a very simple electronic level structure, with only one excited state manifold within reach from the ground-state manifold with near-infrared or visible photons. Pumping and amplification involve transitions between different sublevels of the ground-state and excited-state manifolds [J. Limpert et. al 2005] .

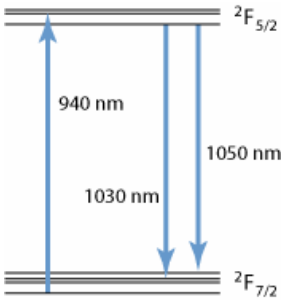

Figure 2.3: Energy levels of Yb^{3+} ions in Yb: YAG, and the usual pump and laser transitions.

In addition to its simple electronic level structure, Yb^{3+}ions in Yb: YAG enjoy larger gain width of laser transitions that allows wide wavelength tuning ranges for generating ultra short pulses in the range of 850nm to 1070nm. The upper-state lifetimes are relatively long (typically of the order of 1–2 ms), which is beneficial for Q switching.

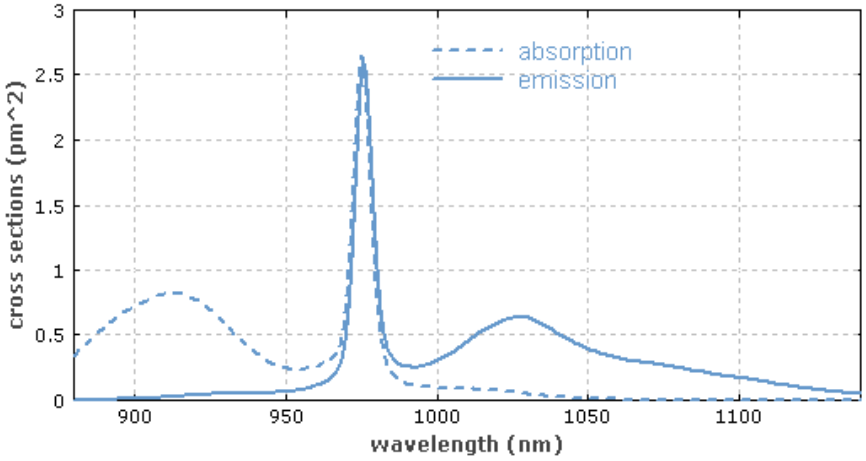

Figure 2.4: Absorption and emission cross sections of ytterbium-doped germano-silicate glass, as used in the cores of ytterbium-doped fibers.
(Source: spectroscopic measurements by R. Paschotta)

The dynamics of energy level populations in laser gain media with doped Ytterbium fiber (Yb^{3+}) are dependent on rate of temporal evolution of level populations under the influence of optically induced and non-radiative transitions [Rudiger Paschotta 2008].

Absorption processes include excited state absorption, spontaneous and stimulated emission, and multi phonon transitions energy transfers. Rate condition describes the spatial distribution of optical powers in fiber amplifiers and dynamic behavior of Q-switching. Thus it helps in understanding the operation of laser source, and allows evaluating the response behavior.

2.2.5 Generation of pulsed laser with Q-switching

Short and concentrated laser energy facilitates micro drilling of holes. One of the practical methods used in fiber laser technology is Q-Switching. It is possible with this technique to produce short and high peak power pulses by modulating the intra cavity losses (Q factor) of the laser resonator. It involves interrupting the optical resonator in some fashion so that the population inversion process can progress with little or no feedback present to cause lasing. At the beginning, the resonator losses are kept at a high level. As lasing cannot occur at that time, the energy fed into the gain

medium by the pumping mechanism accumulates there. The amount of stored energy is often limited only by spontaneous emission, the onset of lasing, and by the pump energy available. The stored energy can be a multiple of the saturation energy. When the population inversion has reached some high level, the resonator interruption is removed and the laser gives out a short pulse with very high peak power. The scalability to enormous average powers without the need for active cooling, high efficiency and high spatial beam quality is also achievable in the short pulse regime [J. Limpert et al 2005]. Therefore, Q-switching of fiber lasers has attracted considerable attention.

The name Q-switched laser is also associated to the Q value of the laser.

$$Q = \frac{2\pi * Energy\ stored}{Energy\ lost\ \ percycle}$$
$$= 2\pi f \tau_c$$

Where τ_c is life time of a photon in the cavity and f is the central frequency of the oscillator.

The Q value can be related to the central frequency of the oscillator and losses in the cavity (particularly to mirror reflectance). Q–switching can be passive (losses modulated with automatically saturating absorber) or active modulation type. Passive Q switching is simple with no electronic modulation and cost effective but suffers a drawback of lower pulse energy and inability to operate with external trigger mechanism.

For active modulation losses inside gain media are controlled with active control element. Rotating mirrors and mechanical choppers techniques active Q-switching for pulses operates on the order of 0.001 sec. The fiber pulsed laser source at SITEC lab of Politechnico di Milano is operated with Acousto-optic modulators, and operates in the order of 10^{-6} sec. It is also possible these days to have Q-switching in the order of 10^{-9} using Pockels and Kerr cells.

2.2.6 Acousto-optic modulators (AOM)

The acoustic wave modulates periodically the effective index profile of the FBG and changes its reflection features. A transducer generates a sound wave, at which a light

beam is partially diffracted. This allows controlling the Q-factor of the cavity [C. Cuadrado-Laborde et.al 2007, M. Delgado-Pinar et.al 2006].

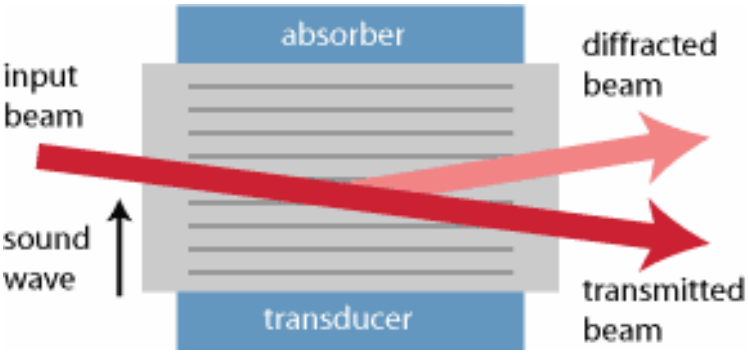

Figure 2.5: schematic set up of AOM (source: Encyclopedia of laser physics and technology)

Main component of AOM is the piezoelectric transducer which is attached to the crystal is used to excite a sound wave with a very high frequency. Light pumped from diode source experience Bragg diffraction at the traveling periodic refractive index grating generated by the sound wave enabling pulsed laser formation.

Below figure 2.6 shows a typical temporal evolution of gain and losses in an actively Q-switched laser. The Q switch is activated at t=0. The power starts to rise exponentially at this point, but becomes high only after some time approximately in micro second range.

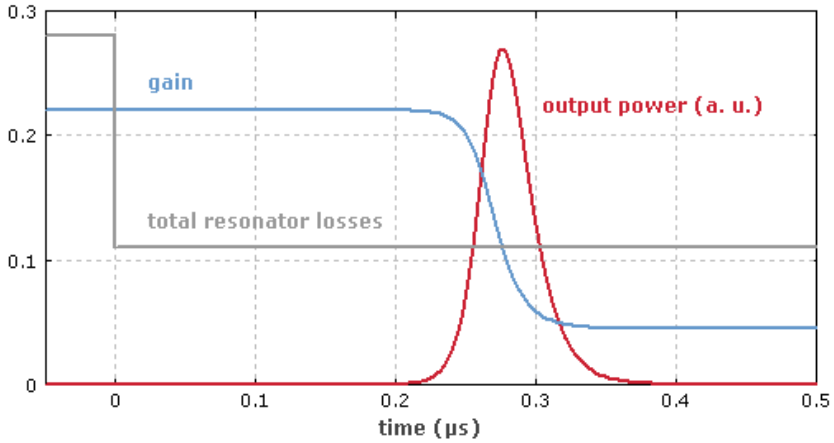

Figure 2.6: Temporal evolution in Active Q switch laser (source: Encyclopedia of laser physics and technology)

For active Q switching, pulse energy decreases at very higher pulse repetition rates. This is because of a weaker modulation of the net gain. At lower pumping power, the amount of power reaching to the resonator is low and below the saturation energy inside leading to a slower rise and decay of the optical power. When the pulse

repetition rate of an actively Q-switched laser falls just below the inverse upper-state lifetime (τ_c), the maximum gain and pulse energy is achieved.

According to M. Delgado-Pinar et.al 2006, the peak power of laser pulses increases with pump power, and there is a corresponding reduction of pulse width. Also increase in repetition rate tends fall down peak power and increase pulse width due to recovery time of the system. For short pulse durations, a short laser resonator and high laser gain are required. Short pulse durations (in nanoseconds) combined with milli Joule pulse energies is achieved by IPG Photonics YLP 50 fiber laser in SITEC with compact solid-state diode laser power pumping, particularly with end-pumped versions due to their higher gain. The energy of the generated pulse is typically higher than the saturation energy of the gain medium.

2.3 Laser micro machining

2.3.1 Introduction

Micro machining is one of the key processes for these days and future technology. Conventional mechanical machining face increasing physical limitation when product dimension is decreased to micron scale. Below some critical dimension, friction surpasses the mechanical strength of the tool and machining is possible only by choosing especially designed tools made of high modulus materials. Additionally processing time may be increased and tool lifetime may be sacrificially reduced [Sylvain Lazare, Vladimir Tokarev 2004]. Laser micro machining offers an attracting alternative to mechanical machining and is already widely used in numerous applications.

Micro machining basics is thermal process with absorption of the laser beam from the material to process followed by thermal filed and material ablation. The process is dependent on characteristics of the laser source, especially on beam quality, beam width and emission wavelength. Pulsed laser sources are frequently used for micro drilling because of their high energy concentration in a short duration of time [G.P. Pinho et al 1999]. It enables to perform the drilling process fast and achieve less heat affected hole. Wavelength of emission determines the size of beam spot diameter together with focal length. Small beam diameter is favoured by choosing a short laser wavelength and small focal length [K. F. Kleine and K. G. Watkins 2004]. Effectiveness of micro machining process with a goal of material removal like cutting

and drilling depends mainly with pulse duration property of the laser source and heat diffusion capacity of base material in process. The longer the pulse width and the poorer the heat diffusion capacity of the base material, worst will become the resulting micro machined product. Especially micro drilling of holes quality is highly dependent on beam duration and is usually performed with shorter pulsed laser sources rather than continuous laser beam emission [B.S. Yilbas 2001].

2.3.2 Laser micro drilling

Micro drilling with laser source is the future for technological and industrial applications in the field. It is foreseeable the old conventional drilling technique can not be as competitive and demand fulfilling with continuous need and expectation in micro drilled products. Laser micro drilling is considered as the only solution for dimensions with less than 50μm yet with relative depth (high aspect ratio). It also offers the ability to produce small dimension hole with no mechanical contact unlike conventional drilling at high speed, tolerance, and excellent quality with high aspect ratio is achievable. Laser micro drilling also offers drilling of wide variety of materials, drilling at different hole orientation, and accurate positioning or alignment.. Some of the draw backs of laser micro drilling includes the high cost of the equipment, its limitation in drilling through hole in case of thick materials, taper encountered again in case of increased thickness, presence of heat affected and molten zone, and formation of spatter and re melted materials on top of surface [P W French et al 1999].

Depending on the laser drilling application there are two common methods used for laser hole drilling; Percussion and Trepanning. It is sometimes common to see other categories like on the fly laser micro drilling (which is similar to Percussion drilling except the whole process is performed with one shoot) and Helical micro drilling which is close to Trepanning except the path of laser beam is helical path from center of hole to peripheral (breaking up of the process into a multitude of ablation steps in order to enhance the accuracy). In contrast to trepanning, the helical drilling reaches the breakthrough only after many turns of spiral describing the path of the ablation front. Each method depends on depth requirement, hole diameter, number of holes, edge quality and production quantity.

Trepanning Laser Drilling

With trepanning, the laser beam pierces the work piece material and is then moved in a circular motion, cutting out the hole. Trepanning, when performed on a galvo system, yields holes with the best circularity and smallest taper. Trepanned laser drilling is a method used to remove a cylindrical core, or circular disc from a substrate. Unlike percussion laser drilling, the position of the beam or substrate is moved in conjunction with a predetermined laser beam overlap to achieve the desired edge quality and production throughput. Less overlap trepanning laser drilling increases throughput but produces a more sharp edge quality. More overlap creates finer hole resolution and edge quality.

Certain types of trepanning laser drilling can completely exterminate first pulse suppression which is a common concern in laser micromachining. Laser drilling in a trepanned, spiral pattern beginning in the approximate center of the laser drilled hole prevents hole inconsistency related to the start/stop of the laser beam.

Trepanned laser drilling results with better edge quality in comparison to percussion drilling. On the other hand percussion drilling is preferable and posses the advantage in micro drilling application due to its simplicity. Laser spot dimension govern the quality and dimension of the hole at most and there is no motion control for the trajectory of the laser beam. But this costs on the quality of the drilled hole which is characterized with diameter at top and bottom, tapperness or barrel shape, and spatter formation both at top and bottom again.

Percussion Laser Drilling

In theses types of laser micro drilling a rapid-fire burst-of-pulses micromachining are used. Varying the laser pulse duration, spot size, optics and beam characteristics percussion laser drilling produces high-quality hole with minimal residue and consistent edge quality from entry to exit point. Percussion laser drilling evaporates the machined substrates layer by layer without noticeable strata or striations. Percussion laser drilling technology is especially suitable for metal, ceramic, polycarbonate, Pyrex, quartz and composite substrates [P. Bassani 2004].

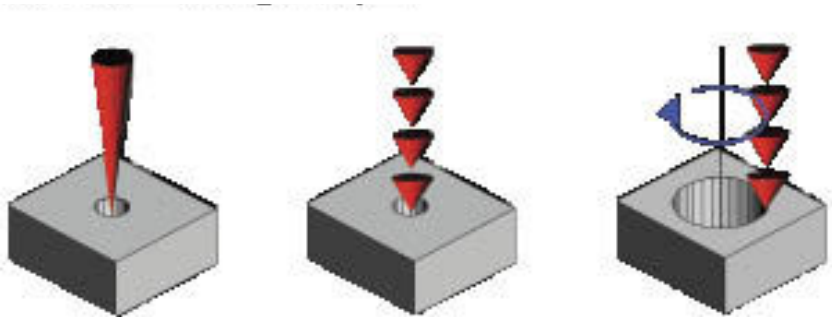

Figure 2.7: from left to right single shot (on the fly), percussion, and trepanned laser drilling.

This work is focused on laser percussion micro drilling and how characterization of the process is possible from quality point of view. As it has been mentioned in classification of laser micro drilling, though percussion drilling is simpler and do not need for trajectory control of the laser beam there has been a question of quality delivered at different operating conditions.

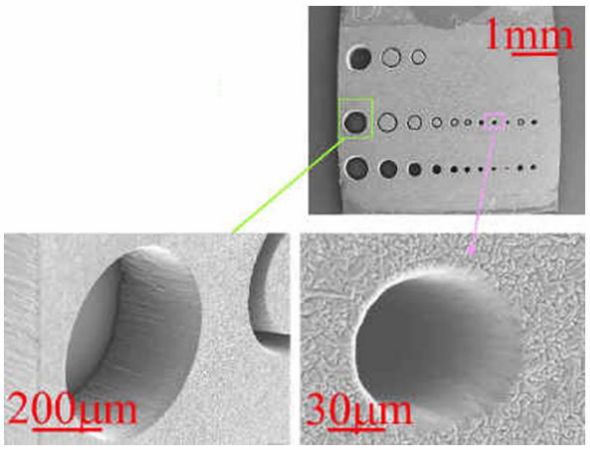

Figure 2.8: percussion laser drilling (picture courtesy Laserod home page http://www.laserod.com/)

Hole taper, formation of barrel shape, recasts and spatter on top of drilled material surface are some of the defects encountered in percussion laser micro drilling. In the following section, definition, state of the art, and research works on improving hole quality and drilling efficiency in percussion drilling is discussed. In line with the aim of the work, focus is given more on the effect of plasma formation, and effect of laser process parameters.

2.3.3 Laser micro drilling of titanium

Laser micro drilling of titanium is a prior choice for the production of a large quantity of holes for various applications of the material. Aerospace industry employ this technique to produce millions of small effusion cooling holes in turbine engine components such as combustion chambers and nozzle guide vanes of titanium. Biomedical engineering uses laser micro drilled commercially pure titanium (cp-Ti) as the most popular biomaterials for dental implantation because of its good specific strength, excellent corrosion resistance and bio-inertness. Other applications of micro drilling of titanium include automotive spare parts manufacturing, micro valves, drillingg of flow filters and strainers.

The wide area of engineering and medical application of titanium makes it one of the research interest of materials in recent years. Different researchers study micro drilling of titanium with laser. C.A. Biffi 2009 on his work 'characterization of process and reduction of spatter in micro drilling of titanium with pulsed fiber laser source' studied the effect of main process parameters on through hole quality features.

Though, property of titanium is attractive from application point of view, it is not easy as process micro drilling it. Its physical properties of high melting point (around 1933 K), reactivity with surrounding, poor thermal conductivity (21.9 $Wm^{-1}K^{-1}$) and low machinability due to high specific strength makes it a challenge from industrial point of view [R. Biswas 2009]. Especially machining process in micro scale (generally from 1μ to 1mm) makes the task more difficult and demanding. Micro drilling of titanium with short and ultra short pulse laser beam is a competitive and adoptable technique to encounter some of these challenges, and is widely implemented recently.

In micro drilling titanium, its low thermal diffusivity (6.99 $\mu m^2 s^{-1}$) makes it more demanding for short pulsed fiber laser source in order to enable energy pumping time shorter that time need for heat diffusion [A. De Giacomo 2002]. Accordingly, it is important determining and understanding behaviour of laser source in use, and physical characteristics of drilling process for intended percussion micro drilling of titanium.

2.4 Laser micro drilling quality and efficiency

2.4.1 Introduction

In industrial applications of laser drilling, the quality of drilled holes is the important factor. The laser drilled hole quality can be judged by internal shape, taper and related geometrical features, as well as the extent of the heat affected zone. The quality of micro drilled hole is a measure of how predetermined diameter and aspect ratio is obtained free from excessive spatter on top on workpiece surface. Assessing hole quality in micro drilling is analyzing features of geometric sections. Hole diameter and depth, formation of taper and barrel, and amount of re melted spatter are parameters used to characterise quality of micro drilled hole [B.S. Yilbas 2001].

Identifying drilling parameters which produce holes with less taper parallel sided walls, re-melt and solidified particles need to be identified. The laser and material parameters include laser output energy, pulse length, work distance of focusing lens, drilling shield gas pressure and workpiece thickness. The optimum performance in laser drilling depends on the proper selection of these factors.

2.4.2 Features of micro drill hole quality measure

It has been mentioned in the introduction part the quality of micro drilled hole is a measure of how predetermined diameter and aspect ratio is obtained free from excessive spatter on top on workpiece surface. These parameters are used commonly for the inspection and control of final drill product and to characterise the effectiveness of the whole drilling process. Below figure illustrates the schematics of representation for these geometric representation.

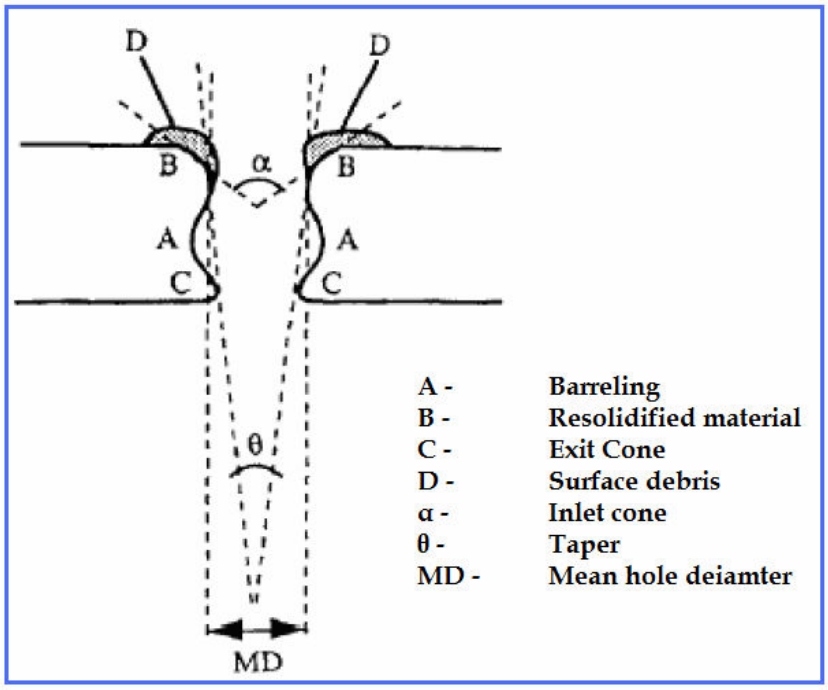

Figure 2.9 Laser micro drilled hole geometry to quantify quality (Source: B.S. Yilbas 2001)

Barrel is a measure of straightness of the inside part of the hole unlike taper which indicates the angle between entrance and exit of the hole. It is important to notice taper angle do not include the entrance and exit cone angles. Re solidification material represents the amount of melt and spattered solid state particles. The higher the content of these re solidified materials in comparison with the size of the hole, the worst is the quality of micro drilling using laser. Taper formation and re melts on top of surface, which are due to erosion during expulsion of melted and vaporized materials from the hole are more critical micro drill hole defects. Where as barrelling which is formed mainly due to ejection of material from local site of the hole cavity can be minimized with reducing gas pressure.

Hole-taper is one of the main challenges in percussion laser micro drilling. The entry hole diameter is normally larger than the exit hole diameter and thus the holes drilled are generally positively tapered [L.Li, D.K.Y.Low and M.Ghoreshi July 2007]. In certain engineering applications, parallel holes (zero taper) and negatively tapered (entrance hole diameter is smaller than the exit hole diameter) are needed. Zero taper can be achieved with Trepanned laser drilling, but production rate will be very less. This could be unacceptable from industry point of view. Thus examining the possibility of improving percussion laser drilled hole quality is a better way.

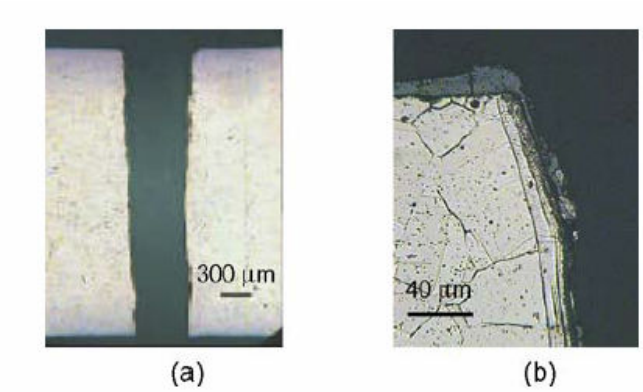

Figure 2.10: Typical hole taper characteristic during laser percussion drilling. (a) Cross section of a hole. (b) A close up view of the entrance wall cross section showing extensive erosion (L.Li, D.K.Y.Low and M.Ghoreshi 2007)

Decrease in laser power intensity as depth of hole increase downwards is the main reason behind taper formation and diameter change. Laser material interaction irradiance of the laser beam continuously drop down in its magnitude with ablation process and thickness of the workpiece. In fact, irradiance of laser beam is a function of thermal diffusivity of ablated material, time and irradiance of the laser beam before interaction ($I = I_o . e^{-\alpha t}$). Hence the material behaviour and source laser beam irradiance are significant parameters in preventing hole taper and barrel formation.

In addition to laser irradiance, in an experimental study to model micro drill hole quality, researched have shown hole taper has been found to be sensitive to focal plane position variations followed by pulse width, peak power and number of pulses [X. Zhu et.al 1999, D.K.Y . Low et.al 2000, L.Li, D.K.Y.Low and M.Ghoreshi 2007, S. Doring, A. Ancona et.al 2010]

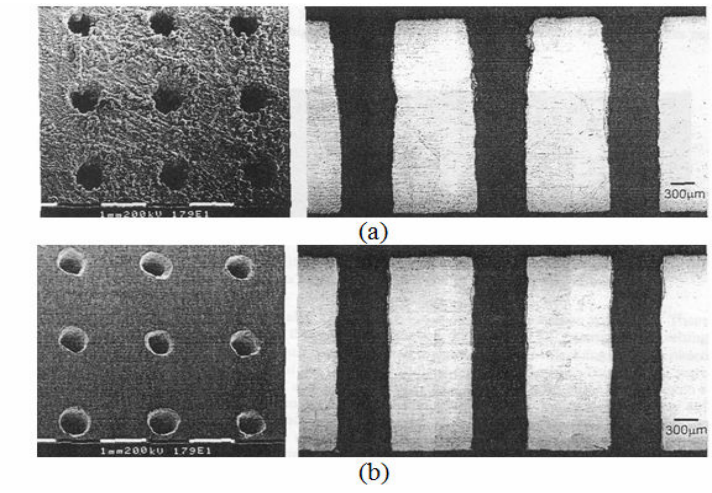

Figure 2.110: Typical micrographs of (a) normal percussion drilled holes showing strong spatter and taper, and (b) spatter free and taper free laser percussion drilled holes produced by combined use of anti-spatter coating and Sequential Pulse Delivery Pattern Control (D. K. Y. Low, et al., 2000)

For laser percussion drilling processes on metals, drilling efficiency related to re solidified materials is strongly dependent on the phenomenon of laser plasma formation and associated expansion. Plasma formation at the workpiece surface due to laser - material interaction severely decreases laser drilling effectiveness because it absorbs a significant portion of the incoming beam energy and thus shielding the workpiece surface [Annemie Bogaerts et. al 2005, R. Biswas et. al 2009]. This transient phenomenon propagates the plasma volume and effectively shields the workpiece surface from the laser beam.

At the entrance, material is frequently eroded with multiple hot flowing melts. The situation is the main factor responsible for the formation of spatter on top of material surface. It is understood from this fact laser power plays an important roll in monitoring quality of micro drill, but it should be put in mind the irradiated power need to be enough for the formation of through hole for the entire thickness of the workpiece. Amongst the factors that rule the quality of percussion micro drill with pulsed laser source, the following ones are the main:

- Irradiance
- Laser beam process parameters: frequency and pulse width
- Wavelength of laser beam
- Beam quality (M^2), beam waist diameter and divergence
- Type of shielding gas
- Pressure of shielding gas
- Type of material to drill
- Time required to drill

2.5 Laser Induced Plasma (LIP) in micro drilling

Interaction between high power laser beam and surface of metallic targets results in heating then melting and finally evaporation of some of the target material. The evaporated material expands, and because of the high temperature, plasma is formed in the material. Formation of plasma during laser material interaction is referred as laser induced plasma (LIP). In laser micro drilling, this plasma is ejected from the hole as a conical sheet in the early stage of its formation. At the same time plume expansion continue resulting temperature drop, and evaporated atoms start condensation to small size particles [Taras V Kononenko 2009]. It results to ejection of melted particles out of the hole and spread on top of the material surface. The extent of these droplets (spatter) on top surface of the material is proportional to the formation of LIP and determined the quality of the hole and drilling efficiency.

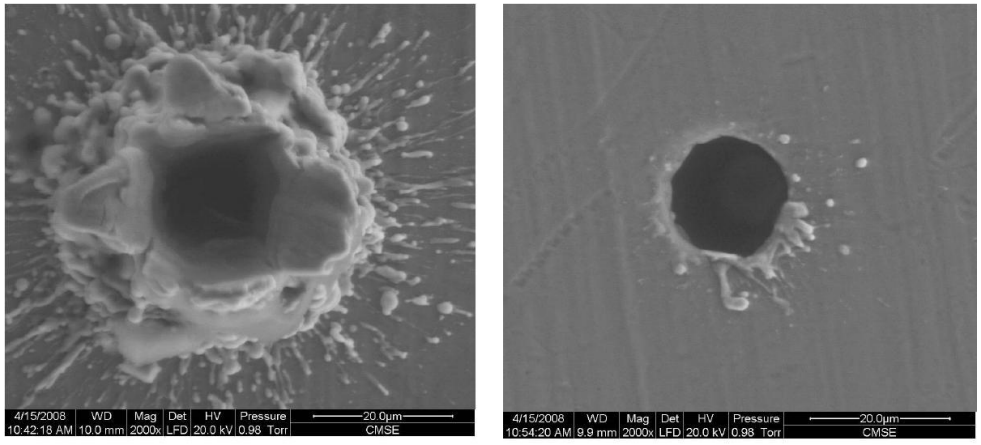

Figure 2.12: effect of LIP and re-melts on micro drill hole quality (source: www.edmmatters.com last visited October 4, 2010)

A. De Giacomo 2000 in his study 'Optical emission spectroscopy and modelling of plasma produced by laser ablation of titanium oxides', states the interaction of laser light with the solid targets is a complicated process. It consists of different stages: the laser ablation of the target; plasma generation; laser interaction with the plasma; plasma expansion and collision with a substrate. The stages of the plasma generation, laser interaction with plasma and plasma expansion play a very important role in the thin film growth process. In fact, during temporal evolution of the laser induced plasma (LIP), excitation and ionization of the evaporated material occurs, therefore, it is important to define its thermodynamic parameters, such as electron number density N_e , temperatures atoms T_a and ions T_i .

The quality of laser ablation processing depends highly on the pulse energy, pulse duration, emission wavelength and material properties. Pulse width and laser fluence are widely recognized as critical parameters that determine the ablation regime, depending on the thermo-physical properties of the irradiated material [Taras V Kononenko 2009]. These parameters play significant roll on formation of LIP, evaporation process and formed plume (plasma) characteristics. Different researches are and will be performed to analyze laser irradiance and pulse width related melting effect during engineering materials processing and optimal parameter is suggested for better quality and efficient laser machining. Effect of laser process parameters on the formation of plasma and evaporation process during laser material interaction, and its effect on efficiency of micro drilling is discussed as below.

Effect of laser irradiance/Energy

In micro drilling with pulsed laser source, the amount of energy supplied need to be high enough for interaction with material, melt it, and even evaporate from the surface to ablate. The main reason for the preference of pulsed laser sources than continuous wave is due to their characteristics of delivering very highly concentrated energy in each pulse. Single pulse energy is the product of laser irradiance (laser power per spot area of laser beam) and pulse duration. Laser beam sources with low irradiance deliver less energy, resulting to inability to form through hole for a predetermined material thickness or even inability to drill. Increase in pulse energy improves drilling efficiency as proved with lots of experimental researched on the area [A. Ancona 2009, Annemie Bogaerts 2005, Chengde Li et. Al 2006]. On the other hand, higher pulse energy will not necessarily work better or faster. The ablated plasma cloud gets denser and can no longer dissociate from the surface. Even worse, it may thermally alter the material and destroy the hole quality.

[S. Conesa et.al 2004] studied the influence of laser irradiance on the temporal evolution of the plasma with a dynamic microphone, for a Nd:YAG laser at 1064 nm, in the irradiance range of 10^9–10^{10} W/cm^2, and it is observed that a higher laser irradiance yields larger plasma volumes. [W. Sdorra, K. Niemax 1992] studied the effect of laser energy, in the range of 2–20 mJ/pulse, for a Nd:YAG laser of 1064 nm and five different background gases, and it was reported that the measured plasma temperature and the emission intensity in the laser induced plasma generally increase with laser energy. Finally, hole diameter and hole depth are proportional to pulse

energy, but excess energy introduces deformation and large entrance cone angle with recristallized material.

Effect of pulse width

The most frequently used definition of pulse duration is based on the full width at half-maximum (FWHM) of the power versus time graph. In laser micro machining there are three main regimes of pulse duration each possessing its own behaviour and delivering its own application area. General classification proposed in many literatures is:

- Long pulse width
- Short pulse width
- Ultra short pulse width

The following three paragraphs discuss the definition of these pulse width types of laser beam and their effect on micro drilling processes.

Long pulse duration, usually in the order of mill second have less contribution in laser micro drilling recently. In long pulse width machining, the time required for thermal diffusion by the material and pulse duration are nearly similar resulting heat diffusion to the surrounding and increase heat affected zone during the process. More over, long pulse width laser contain lesser pulse energy concentration as compared to other pulsed laser sources. These types of pulses are more preferable for laser welding process rather that drilling.

Short pulse durations which range from micro second to nano second on the other hand can be generated using Q-switching technique and are commonly used for micro machining processes. In short pulsed laser, ablation of metals is always accompanied by the formation of a superheated melt layer [A. Ancona et. al 2009]. In the case of pulse durations comparable to the heat conduction time, the removal mechanism is governed by the evaporation and a throw out of cluster like liquid droplets via fragmentation. The ablated structures display large heat-affected zones and recast layers that affect not only the accuracy but also the reliability of the process.

A Femto second pulse width is laser pulse width which is emitted with a duration well below 1 ps, i.e., in the domain of Femto seconds (1 fs = 10^{-15} s). The generation of such short pulses is achieved with the technique of passive mode

locking. Micro machining process with ultra short pulsed laser in Femto seconds delivers highly concentrated pulse energy with in the short duration of time and material ablation is performed in vaporization phenomenon directly from solid state with the vapour taking away the heat formation. This delivers sufficient time for thermal diffusion of heat especially needed for metals like commercially pure titanium with low thermal diffusivity [R. Biswas 2009]. Ultimately this results with better quality in comparison with short pulses of micro and nano second sources.

It could be understood from this short and ultra short pulses are those used for micro drilling metallic targets. Comparing these two regimes, in micro machining with short pulses, formation of more molten material with thermal effected zone is apparently happening resulting with spatter, cracks associated with formation of plasma [J. Meijer]. This is associated the transformation of solid state materials to melt pool and inability to eject out as vaporized state one due to lack of pulse energy concentration or the other distribute over longer period of time unlike ultra short pulses.

In contrary, the use of ultra short pulses in industrial areas suffers a big draw back of lesser material removal rate and production rate. Accordingly, the trade off between product quality and production rate is a challenge and tricky concept to tackle in the field. Nano second regime pulse attract the focus in industrial application compromising the better hand of quality than short pulses in micro scale and reasonable quality though lower than Femto second pulses, and good rate of production.

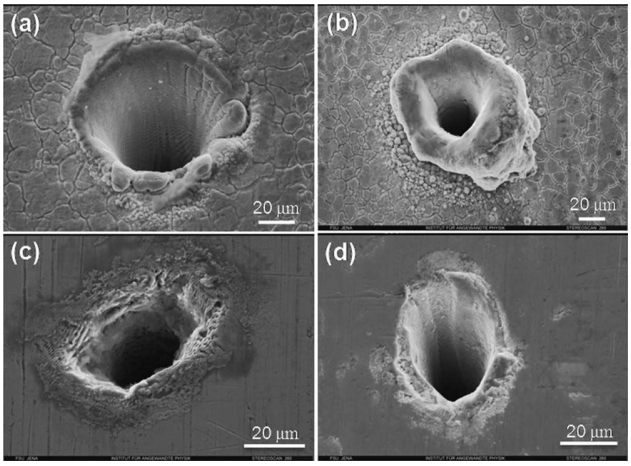

Figure 2.13: SEM images of the hole entrances in stainless steel (thermal conductivity: 0.16 W cm^{-1} K^{-1}) at 50 µJ, (a) 800 fs and 200 kHz, (b) 19 ps and 300 kHz, and in copper (thermal conductivity: 3.86 W cm^{-1} K^{-1}) at 50 µJ, (c) 800 fs and 975 kHz, (d) 19 ps and 975 kHz. (Source: A. Ancona 2009)

[C. Y. Chien and M.C. Gupta 2004] studied based on the experimental results; effect of pulse duration for laser material processing on silicon and stainless steel using laser pulse energy of 2 mJ and 1 KHz frequency at 800 nm emission wavelength. The result reveal optimal pulse width to avoid significant melting damage was 5 ps for silicon and 2.5 ps for stainless steel.

[X. Liu, D. Du, and G. Mourou, 1997] discussed some aspects of laser–material interaction with ultrashort pulses and emphasized the differences between short and long pulses. Because ultrashort laser pulses have precise breakdown thresholds and negligible thermal diffusion, they are ideally suited to precision micromachining applications with ablation mechanism mainly direct vaporization of materials.

[Sami T. Hendoe and Sami A. Shakir 2010], with their study on structuring materials with nanosecond laser pulses demonstrated that pulses of high peak powers have shallow penetration depths, while longer pulses with lower peak powers have a higher material removal rate with deeper scribes. It is also mentions key reason for the phenomenon is non linear change in material absorption coefficient with temperature increase.

[A. Ancona et al 2007] states controllable ablation, characterized by minimized collateral damage to the material and negligible heat affected zones, takes place during ultra-short pulsed laser machining. As a consequence, the accuracy of the produced structures is improved. On the other hand, laser ablation with longer pulses is accompanied by a large volume of molten material that solidifies resulting in burrs and rounded edges. In this way it is not possible to reliably control the accuracy of the produced microstructures.

Effect of laser emission wavelength

There is a wide range of emission wavelength for laser sources ranging from UV to infrared zone. The two main effects of laser emission wavelength are controlling the dimension of spot diameter related of laser source and impact on absorption coefficient related to material processing [R. Biswas 2009]. In the first case, smaller emission wavelength (higher resolution) gives minimal laser spot diameter which is required to focalize laser energy keeping other factors (beam quality, focal length and collimated beam diameter) constant. In many industrial application laser sources with emission wavelength in near infrared zone (Nd-YAG at 1064 nm and fiber laser sources close to visible 850 nm and near infrared 1064 nm) are used for metallic target processing. on the other hand, excimer lasers with emission wavelength in UV range are commonly used for micro machining organic materials. This is mainly due to the high laser absorption behaviour of the materials at the specified emission wavelengths.

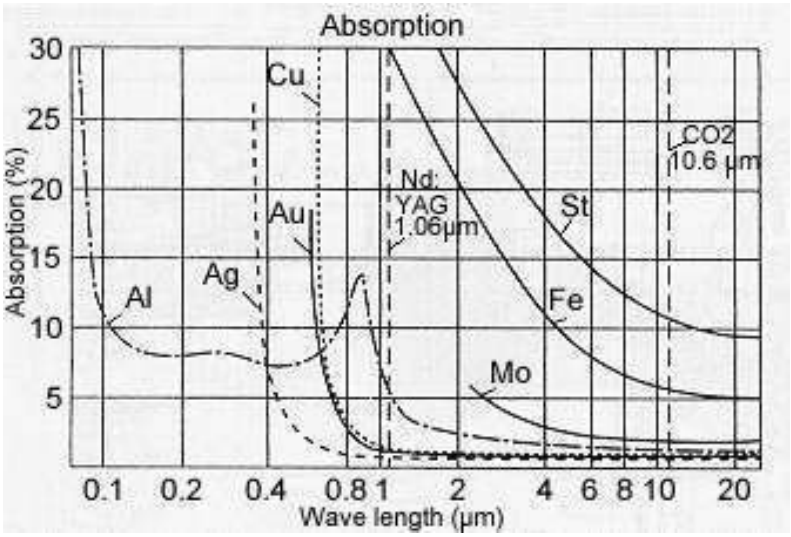

Figure 2.14: Absorption coefficient for different metals at laser wave lengths (Source: http://www.tubenet.org site for tube and pipe industry, last visited October 4, 2010)

2.6 Base material titanium

2.6.1 Introduction

Titanium is one of the widely applicable engineering metals in recent years. Aerospace is the prime consumer of titanium and its alloys, but other markets such as architecture, chemical processing, medicine, power generation, marine and offshore, sports and leisure, and transportation are gaining increased acceptance [M. Peters et al 2003]. Titanium is not a rare substance as it ranks as the ninth most plentiful element and the fourth most abundant structural metal in the Earth's crust exceeded only by aluminium, iron, and magnesium. Unfortunately, it is seldom found in high concentrations and never found in a pure state. Thus, the difficulty in processing the metal makes it expensive. Even today it is produced only in a batch process, and no continuous process exists as for other structural metals.

Titanium alloys primarily stand out due to two properties: high specific strength and excellent corrosion resistance. This also explains their preferential use in the aerospace sector, the chemical industry, and medical engineering. The high affinity of titanium for oxygen in air at room temperature enables the formation of a very thin dense oxide layer (TiO_2) on the metal surface. This is the reason for the excellent corrosion resistant behavior of titanium alloys. Only at temperatures below 300^0C do carbon fiber reinforced plastics have a higher specific strength than titanium alloys. At higher temperatures the specific strength of titanium alloys is particularly attractive.

2.6.2 Titanium alloys and classification

Depending on their influence on β transus temperature, the alloying elements of titanium are classified as neutral, α stabilizers, or β stabilizers. The α stabilizing elements extend the α phase field to higher temperatures, while β stabilizing elements shift the β phase field to lower temperatures.

Amongst α stabilizer, aluminium is the most important alloying element of titanium. The interstitial elements oxygen, nitrogen, and carbon also belong to this category. In addition to extending α phase field to higher temperatures, α stabilizer develops a two-phase α + β field. α stabilizing elements are subdivided into β isomorphous and β eutectic elements. Of these, the β isomorphous elements, e.g. Mo, V, and Ta, are by

far more important due to their much higher solubility in titanium. On the other hand, even very low volume fractions of β eutectic elements, e.g. Fe, Mn, Cr, Co, Ni, Cu, Si, and H, can lead to the formation of intermetallics compounds.

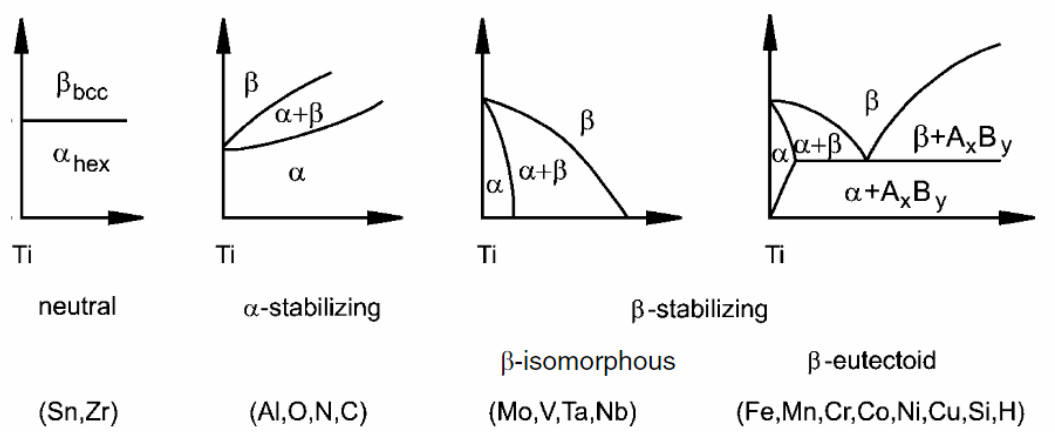

Fig. 2.15 Influence of alloying elements on phase diagrams of Ti alloys.

Source- M. Peters et al (2003)

2.6.3 Commercially pure (CP) titanium alloys

Usually titanium alloys are classified as α, α +β, and β alloys, with further subdivision into near α and metastable β alloys. This is schematically outlined in a three dimensional phase diagram, which is composed of two phase diagrams with an α and a β stabilizing element respectively. According to this scheme, the α alloys comprise commercially pure (cp) titanium and alloys exclusively alloyed with α stabilizing and neutral element. If minor fractions of β stabilizing elements are added, they are referred to as near α alloy. The α +β alloys is the most widely used alloy group. In the end, the single-phase β alloys mark the end of the alloying scale of the conventional titanium alloys.

This thesis work is focused on the use of α alloyed commercially pure titanium alloy. For here onwards discussion will be limited of this group when base materials are mentioned.

The various commercially pure (cp) titanium grades differ primarily in oxygen content. As an interstitial alloying element, oxygen drastically increases strength with a simultaneous reduction in ductility. To reach the required strength levels of cp

titanium grades, only oxygen is intentionally alloyed; while elements like carbon and iron are considered impurities brought into the alloy via the manufacturing process. The four cp titanium grades 1 to 4 covers a room temperature tensile strength level of 240 to 740 MPa. Of these, Grade 1 has the lowest strength level and excellent cold formability. Therefore, it is used commonly for parts which require excellent corrosion resistance but only low strength. Grade 2, with tensile strength levels between 390 and 540 MPa, is the most popular cp titanium grade and is the one in use during our experimentation. Higher strength grade 3 is exclusively used for pressure vessel applications. Grade 4 has the highest strength of up to 740 MPa and is preferentially used for mountings and fittings. Figure 2.16 to 2.21 show typical morphological structure of α alloyed commercially pure titanium specimen observed at various scanning resolutions.

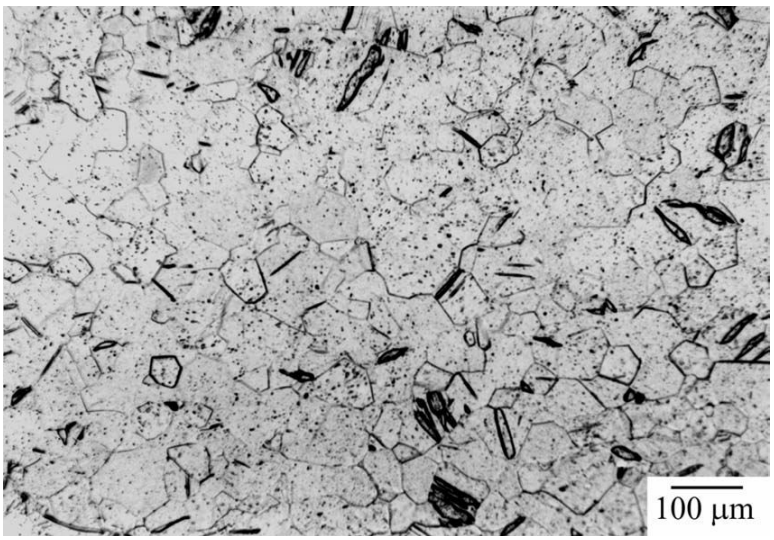

Figure 2.16: Commercial titanium, 675°C. Optical micrograph shows equiaxed α grains.

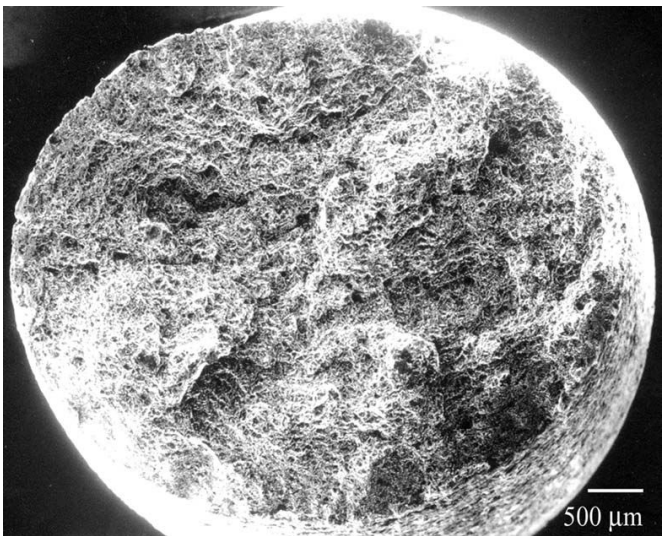

Figure 2.17: Commercial titanium, 675°C. Low-magnification scanning electron microscope (SEM) fractograph shows the fracture surface.

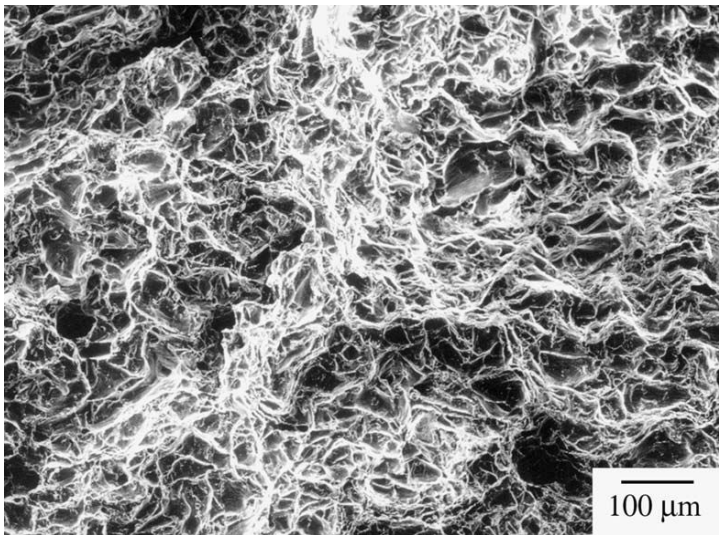

Figure 2.18: Commercial titanium, 675°C. High-magnification SEM fractograph of Figure 3.2 shows overload fracture with fine dimples.

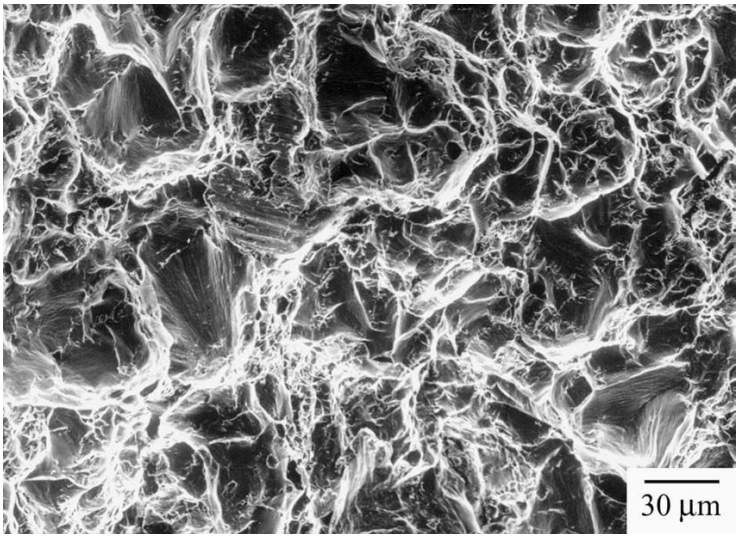

Figure 2.19: Commercial titanium, 675°C; SEM fractograph of a different area of figure 3. shows overload fracture with fine dimples and a few conical dimples.

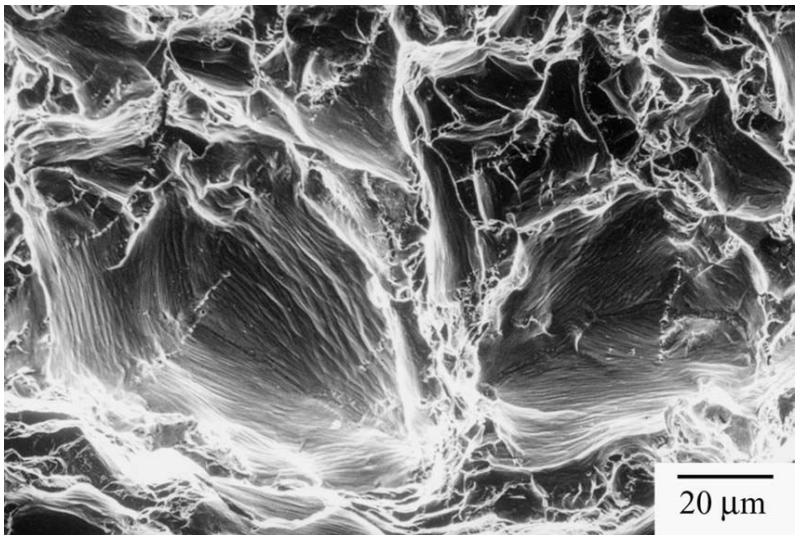

Figure 2.20: Commercial titanium, 675°C; High-magnification SEM fractograph of the conical dimples shows winding glide (stretch-like regions) surrounded by fine dimples.

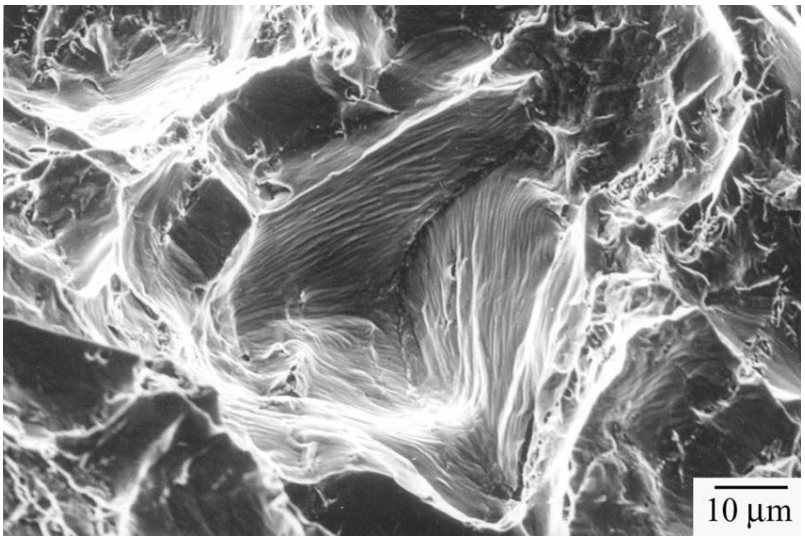

Figure 2.21: Commercial titanium, 675°C; High-magnification SEM fractograph of a different area shows the conical dimple.

Source for figure 2.16 to 2.21is the book 'Titanium alloys: An Atlas of structures and fracture features by Joshi, Vydehi Arun (2006)'

Table 2.1 summary important physical and thermal characteristics of CP titanium.

Young's Modulus	100 - 120	GPa
Yield Strength	480 - 655	MPa
Ultimate Strength	> 550	MPa
Hardness Vicker	260	HV
Beta transformation temperature	1223	K
Melting point	1933	K
Boiling point	3560	K
Density (at 293 K)	4.54	g/cm^3
Latent heat of vaporization	425	kJ/mol
Latent heat of fusion	419	kJ/kg
Specific heat	520	J/(kg K)
Thermal conductivity	21.9	W/(m K)
Thermal diffusivity	6.99	$\mu m^2/s$

2.7 Characterizing LIP by Optical Emission Spectroscopy (OES)

2.7.1 Introduction

Prediction of thermal processes induced by a short pulse width laser source is important in most of its application areas. The laser interaction with material becomes more complicated when high power density laser light is applied to material and melting or plasma formations occur [Sami T. Hendow and Sami A. Shakir 2010]. Characterizing this state of the process with physical parameters is a way of understanding what is going on exactly, and is a method for process monitoring and control. The spectroscopy of the radiation emitted by the LIP can be used to obtain the characteristic physical parameters, such as the temperature, the electron number density and the atom and ion number densities [Sang-Ho Nam and Young Jo Kim 2001, Nikolai V. Tkachenko 2005, J. Hermann, C. Boulmer-Leborgne, D. Hong 1998]. Since the spectral line and continuum emission of plasma depends in turn on these parameters, there is an interest of plasma characterization in order to understand a process and achieve improvements in engineering applications.

Process monitoring of laser machining is practicable with quite a few different proposed approaches for the analysis of processes, including the measurement of the charge voltage induced by the plasma, acoustic emissions measurement, imaging in different spectral bands; and single point optical methods, with photodiodes or optical spectroscopy through fiber transmission of light. Each method has its own advantage over the other and also limitation that it suffers. The optical fiber measurement chain methodology is suitable in many cases except its limitation that sensor need to be placed close and around the laser material interaction region and plasma pool [Nikolai V. Tkachenko 2005]. Even though, the spectroscopic analysis of plasmas is a widely used technique, with applications in many fields, like chemical characterization or industrial process monitoring. Process monitoring and study of micro drilling behavior is achievable using the technique called optical emission spectroscopy (OES). Plasma emission spectrum is characterized by the presence of several emission lines, whose examination offers relevant information about the process responsible of the plasma formation.

OES monitoring is capable mainly with the investigation and study of:

- Many spectra data such as line intensities and line widths for process characterization
- Measurement of two or three dimensional distributions of plasma parameters

The main aim of this work is to perform experimental micro drilling of titanium and demonstrate characterization method to determine induced plasma parameters used to describe the process. The result will help in measuring micro drill hole quality and identify a better laser and process parameter. It has been demonstrated that there can be a relationship between these parameters and the resulting quality [J. Mirapeix et al. 2005, Ferrara M. et al. 2000].

2.7.2 OES definition and approach

Optical spectroscopy studies absorption and emission of light by matter. The term optical spectroscopy can be attributed to any kind of optical photon interactions with matter. Two most general classes of such interactions are absorption and emission. Consequently, one can distinguish between absorption spectroscopy and emission spectroscopy. In the former case we will speak about absorption spectra and in the later the emission spectra will be the subject of measurements. Technically, in both cases the light spectra have to be measured, however, the arrangement of the measurements, application range and interpretation of the results have their specific characters and may differ significantly [Nikolai V. Tkachenko 2005].

Optical spectroscopy methods have numerous applications in physics, chemistry, material, biological and medical sciences. Two of the most exciting achievements of the optical spectroscopy are single molecule detection and ultra fast time resolution. The later extends the time scale to Femto seconds making possible direct studies of physical and chemical states on the level of the chemical bond dynamics at the atomic scale. One of the main advantages of the optical spectroscopy methods is their non-destructive nature and possibility to monitor the studied object without physical contact to it. This makes them popular in applications such as technological process control.

For OES techniques and analysis to operate very well, plasma formation, or at least partially ionized metallic vapour need to be reached. The first condition can be attained when vapour temperature is higher than 5000°C, threshold temperature at which the vapour is generally considered in a hot plasma state [H.R. Griem 1997, S. Petzoldt, J. Reif, E. Matthias 1995]. In the other case, partial ionization condition should be fulfilled in order the plume temperature is above the surface melting threshold temperature and enable at least atomic emission of the metal.

Once plasma formation is reached, there will be a transition from lower to higher energy level (E_i to E_k) of atoms and ions depending on electronic configuration of material in process. Thus there will be photon emission flux during relaxation from the higher energy level to a lower one, at frequency proportional to the difference between the energy level [C. Aragon 2008]. Accordingly, for atoms of the same element at different energy level, various emission lines at variable intensity are

observed. Below is reported some observed spectra for commonly interesting engineering materials gathered from literature.

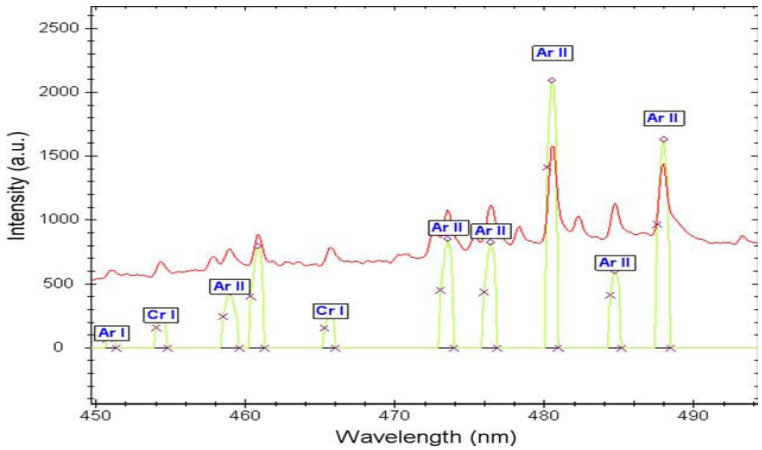

Figure 2.22: LIP Spectral emission lines of Argon during TIG welding (J. Mirapeix 2005)

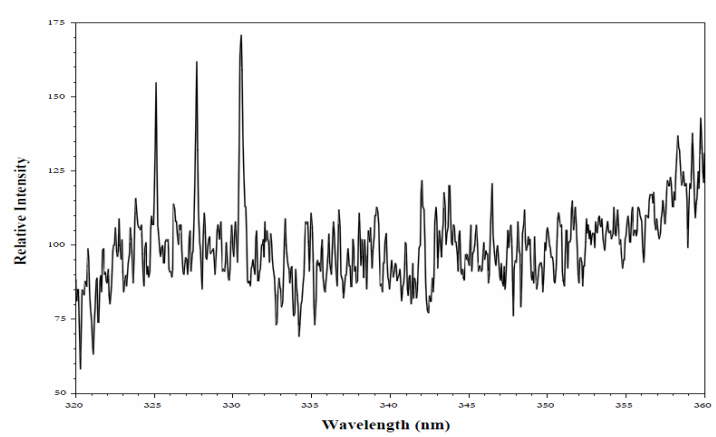

Figure 2.23: Spectral emission lines of Copper in hybrid rocket plume (M. Keith Hudson et al.)

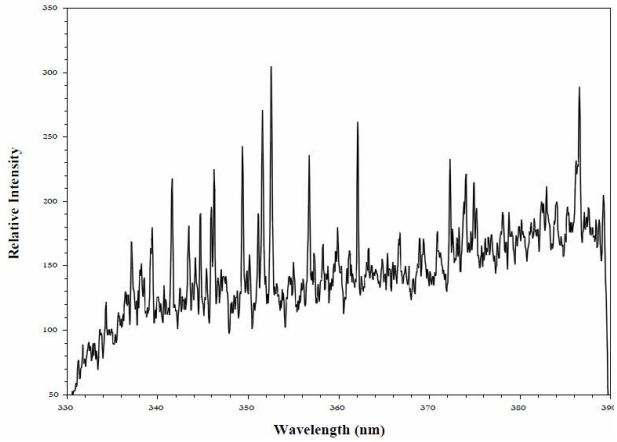

Figure 2.24: Spectral emission lines of Nickel (M. Keith Hudson et al.)

It is important to understand laser induced plasma generation depends on the experimental conditions, including laser parameters, laser emission wavelength, laser irradiance, spot size, sample morphology and surrounding atmosphere [C. Aragon

and J.A. Aguilera 2008]. In order for laser beam exposed material to transform from sub threshold heating to dense plasma generation:

- The incident fluence must be high enough to bring the surface to boil and provide metal vapour above the surface.
- The laser intensity must be high enough to promote dielectric breakdown in the metal vapour.

Which condition is harder depends on the thermal properties of the irradiated metal, in particular the thermal diffusivity which, together with the laser pulse duration, has an important influence on the boiling fluence [S. Petzoldt, J. Reif Matthias 1995]. For titanium with poor thermal conductivity the heated volume and therefore the necessary boiling fluence is small, so that 2^{nd} criteria is decisive for the plasma threshold.

Once the spectra emission lines of atoms of interest are acquired (commonly in near UV, visible and NIR spectral regions), a widely used classical technique is used to compute the physical parameters based on the measurement of relative intensities of lines from the same elements and ionization stage (Atomic or Ionic). For those parameters obtained from the plasma spectrum, a precise analysis of the emission peaks from the various species contributing to the plasma must be carried out, involving central peak wavelength, amplitude (Intensity count) and width. The method will enable to compute the physical parameters of induced plasma with the assumption of local thermodynamic equilibrium (LTE) and optically thin spectral line emission.

2.7.3 Local Thermodynamic Equilibrium (LTE)

The most frequently used methods for the determination of the temperature of LIPs by OES, are based on the application of two equilibrium relations; the Boltzmann equation, which describes the population densities N_j^z of excited energy levels as a function of temperature T, and the Saha equation which relates the densities of subsequent ionization species for a temperature T.

$$\frac{N_j^z}{N^z} = \frac{g_j . e^{-\frac{E_j^z}{kT}}}{U^z(T)} \qquad eq.\ 2.1$$

$where:\ N_j^z$ *polulation density*

N^z *total number density*

E_j^z *Energy at level z*

g_j^z *degeneracy of level z*

$U^z(T)$ *partition function*

k *Boltzmann const.*

$$\frac{N_e N^z}{N^{z-1}} = \frac{2U^z(T)}{U^{z-1}(T)}\left(\frac{2\pi m_e K_b T}{h^2}\right)^{\frac{3}{2}} e^{\frac{E_\infty^{z-1} - \Delta E_\infty^{z-1}}{K_b T}} \qquad eq.2.2$$

$where:\ N_e$ *electron number density*

E_∞^{z-1} *ionization Energy of* $z-1$ *species*

ΔE_∞^{z-1} *correction for interaction in plasma*

K_b *Boltzmann constant* $= 1.38*10^{-23}\,[J][K^{-1}] = 8.61734*10^{-5}\ [eV][K^{-1}]$

h *Plank's const.* $= 6.625*10^{-34}\,[J][Sec] = 4.135667*10^{-15}\,[eV][Sec]$

m_e *mass of electron* $= 9.10938215*10^{-31}\,[Kg] = 0.51099891\left[M\,{eV}/{c^2}\right]$

In LTE the loss of radiative energy is small compared to the energy exchange between material particles so that Maxwell, Boltzmann and Saha relations described above are still valid locally.

2.7.4 Optically thin line emission

The most widely used methods for determining the plasma parameters are based on the optically thin emission of spectral lines. The determinations of the electron density, as well as the measurement of temperature using the Boltzmann and Saha–Boltzmann equations require that the spectral lines used are optically thin. For accurate measurements of the electron density, spectral lines as isolated as possible and emitted in optically thin conditions have to be selected [C. Aragón and J.A. Aguilera 2008].

2.7.5 The Boltzmann relation to determine temperature

From a set of measured energy level transition emission lines of a species, temperature of plasma can be computed with a good accuracy using the wave length integrated emissivity equation of Boltzmann (Eq. 2.1).

$$I_{ki} = \frac{1}{4\pi} \cdot \frac{h.c}{\lambda} \cdot \frac{N^z}{U(T)} \cdot g_k \cdot A_{ki} \cdot e^{-\frac{E_k}{k.T}}$$

Where the subscripts 'i' stands for lower level, 'k' upper level, N^z is total number density, λ spectral emission wavelength, g_k upper level degeneracy, A_{ki} transition probability and U(T) is partition function.

Taking the natural logarithm of both side of the equation after rearranging:

$$\ln\left(\frac{I_{ki}.\lambda}{g_k.A_{ki}}\right) = \ln\left(\frac{h\ c\ N^z}{4\pi.U(T)}\right) + \frac{-1}{k\ .\ T}E_k \qquad eq.2.3$$

Equation 2.3 is of the linear form y = mx + c with the term on the left considered as ordinate axis and E_k (upper energy level) considered as abscissa.

For the reason number of spectra lines are used to determine the ordinate and abscissa, the term in the middle (constant term) is not needed from our target point of view, which is excitation temperature determination. Accordingly, there is no need for studying the partition function of the process in this case. The slope of the linear fit which is the negative inverse of the product between Boltzmann constant and excitation temperature is going to be obtained directly from the linear fitting of the data. It is later used to determine excitation temperature computing slope = $-\frac{1}{k.T_{exc}} = -\frac{0.625}{T_{exc}}$ if E_i is taken as [cm-1] or $-\frac{5040}{T_{exc}}$ if E_i is in [eV]. For increasing accuracy of fitting, the range of upper level energy needs to be as large as possible.

2.7.6 Electron density from Stark broadening

The second plasma physical parameter under study here from OES is electron density number (physical quantity indicating number of electrons per volume [$1/cm^3$]). Stark broadening, stark shift and the Saha-Boltzmann (Saha–Eggert Ionization theory) relation are the common methodologies for the determination of electron number density. But in this work we'll focus on stark broadening method because it is the reliable approach in analyzing Titanium spectral line emissions [J. Hermann et al. 1998, A. De Giacomo et al. 2007].

Stark effect

The stark effect is due to collision of the emitting atoms with electrons and ions, resulting in a broadening of the line and a shift of the peak wavelength. The method is based on the fact the stark broadening is dominant compared to other causes of broadening. The most important experimental considerations for choosing spectral lines for plasma density measurements are their strengths and separations from neighbouring lines; and also the wavelength range, i.e., the relative ease of obtaining sufficient resolution and signal. On the theoretical side, it is important that broadening mechanisms other than Stark effects can be ruled out, or at least accounted for.

With Stark dominated broadening, the electron density (N_e (cm^{-3})) is related to the Full width at half maximum (FWHM) $\Delta\lambda$ of the stark broadening line is given by:

$$N_e = \left[\frac{\Delta\lambda}{2w}\right] * 10^{16} \qquad eq.2.4$$

Where w is the electron impact parameter (nm) which can be obtained corresponding to different plasma temperature and $\Delta\lambda$ is commonly the Lorentzian fit of the spectral line at selected emission wavelength.

Saha-Boltzmann

Under the assumption of LTE state, the electron number density can be determined using the Saha-Boltzmann relation using relative emission intensities from the neutral atom and singly ionized species [Sang-Ho Nam and Young Jo Kim 2001]. The relation is stated in the following equation 2.5.

$$\left(\frac{I_i}{I_a}\right) = \frac{1}{N_e}.2\left(\frac{2\pi m_e k_b}{h^2}\right)^{\frac{3}{2}} \frac{g_i A_i \lambda_a}{g_a A_a \lambda_i} T^{\frac{3}{2}} \exp\left(\frac{-E^i + \Delta E_i}{K_b T}\right).\exp\left(\frac{E^a - E_i}{K_b T}\right)$$

Rearranging the Saha-Boltzmann equation to the topic of out interest, and utilizing the numerical values of the constants that are already used in equation 2.2 of section 2.2.3, electron number density is evaluated using:

$$N_e = \left(\frac{I_a}{I_i}\right).2\left(\frac{2\pi m_e k_b}{h^2}\right)^{\frac{3}{2}} \frac{g_i A_i \lambda_a}{g_a A_a \lambda_i} T^{\frac{3}{2}} \exp\left(\frac{-E^i + \Delta E_i}{K_b T}\right).\exp\left(\frac{E^a - E_i}{K_b T}\right) \quad eq.2.5$$

Where the labels ‘a’ and ‘i’ stands for atomic and Ionic respectively, and the constants m_e, h and K_b as described in equation 2.1.

Chapter 3: Experimental Setup

3.1 Experimental setup for laser beam characterization

The first portion of this work is dedicated for experimental investigation of laser beam characterisation. Focus is given in measuring transient behaviour of laser emission determining amount of time required for laser to reach nominal power, number of pulses required to reach nominal power and pulse duration at various selected laser processing parameters.

Methods used as measuring technique in this experimentation are off laser beam axis in two configurations using fast photodiode, in order to detect the reflected beam from surface of copper mirror. Measurement for off laser axis is done twice with a setup of laser waist diameter spot focused on surface (OFF axis ON focus), and above the mirror surface (OFF axis OFF focus), the well polished copper surface that could act as a perfect reflector for the incident laser beam. Thorlabs FGA 10 photodiode is positioned 80 mm far from laser incident point in horizontal trajectory.

Figure 3.1 and 3.2 below shows the experimental configuration and equipments used for the setup of OFF axis ON axis arrangement.

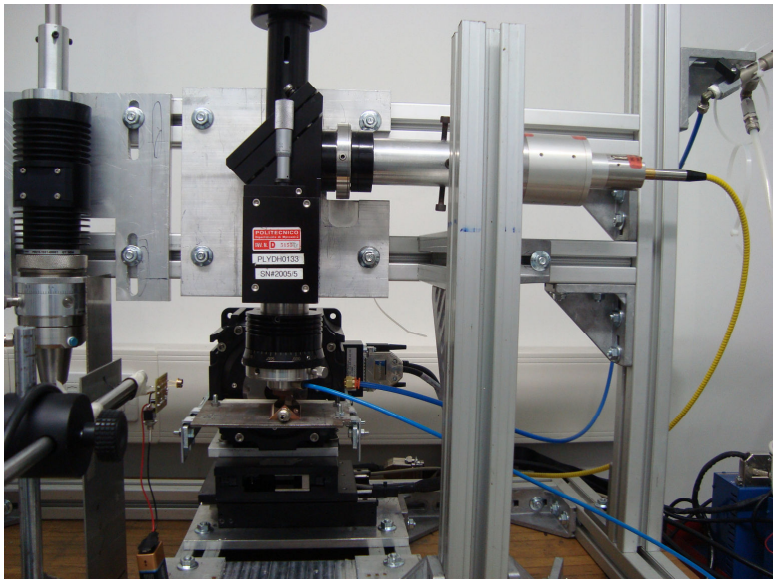

Figure 3.1: Experimental setup- picture for pulse characterization at SITEC lab

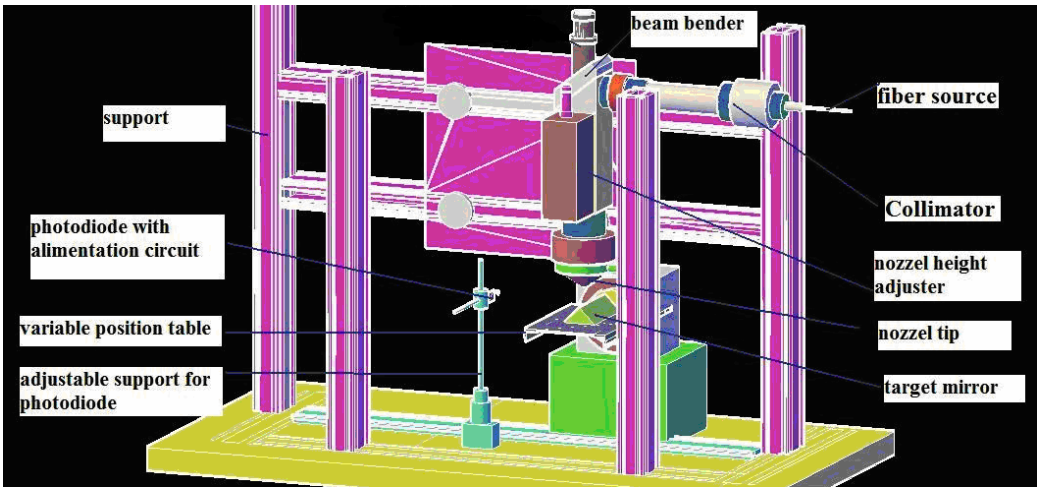

Figure 3.2: OFF axis ON focus measurement configuration and components

The OFF axis OFF focus configuration uses a similar set up with laser beam focused above the mirror surface. Further 2 mm above from focus condition is calibrated leading to a beam off focus from mirror surface.

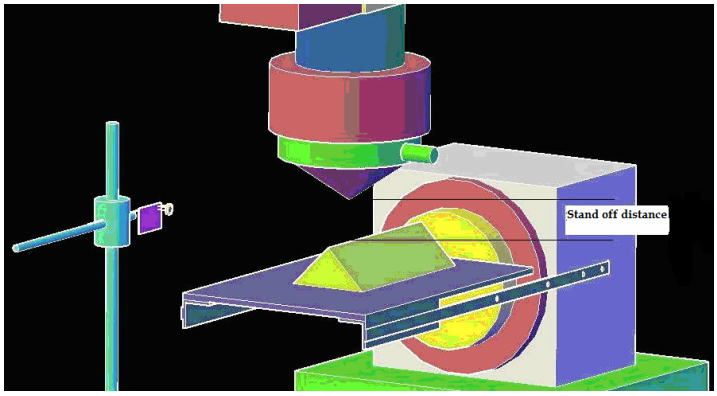

Figure 3.3 OFF axis OFF focus measurement configuration - a close view

3.1.1 Fiber laser source

The SITEC laboratory in Politecnico di Milano is equipped with a pulsed IPG Photonics fiber laser source (YLP 50) for micro drilling, which is Ytterbium doped glass type gaining medium with diodes pumping system. Laser pulses are generated (in nano seconds region) by acusto optic Q-switched device. It is also possible to modulate pulse frequencies in the regime of Kilo Hertz..

Figure 3.4: YLP -50 pulsed fiber laser source

Laser Mech' micro machining laser head is used attached to laser source YLP-50. It is used to focalize the laser beam and is capable of delivering a true perpendicular laser beam. It also include features of independent adjustment of laser beam, laser safety protection, X-Y tip centering, and external focal point to gas jet.

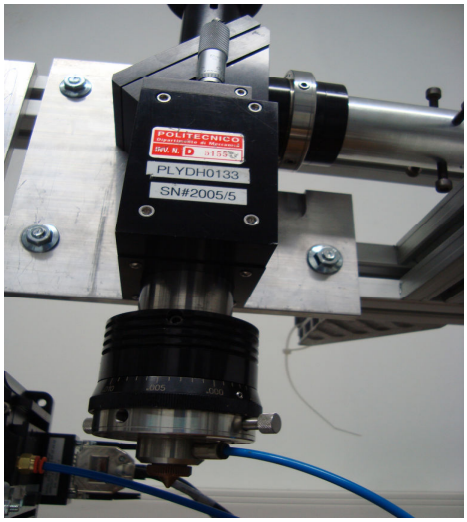

Figure 3.5: Laser Mech's micro machining laser head

Average output power	50W
Pulse repetition rate	20-80 kHz
Emission wavelength	1064 nm
Minimum pulse duration	100ns
Pulse energy at 50 kHz	1.09 mJ
Beam quality factor M^2	1.7
Output beam diameter	5.9 mm
Output power adjustment range	10 – 100%

Table 3.1 main characteristics of the laser system

3.1.2 Signal generator

Emission of laser pulse is with a trigger mechanism using Tektronix AFG310-Arbitirary Function signal Generator used for triggering laser modulation with in a determined amount of time. Square wave with 50/50 on and off with 5 volt amplitude is in use.

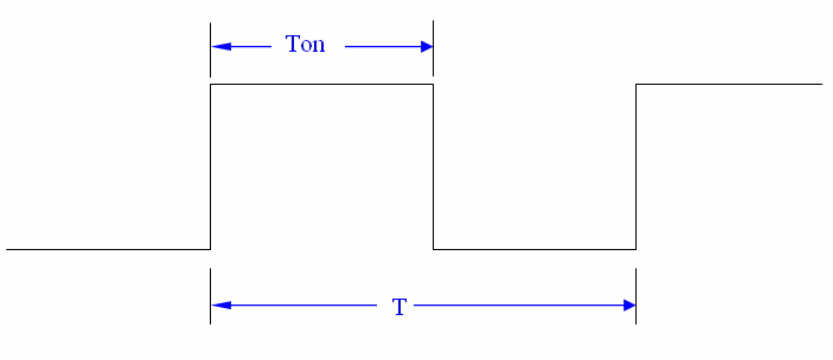

Figure 3.6: square wave trigger signal

$$frequency = \frac{1}{T} = \frac{1}{2 * T_{on}} = \frac{1}{2 * 2.5 * 10^{-3}} = 200 Hz$$

Table below summarizes other setting parameters from the signal generator to acquire pulse type signal form photodiode.

Signal type	Pulse
Amplitude	2.5 Volt
Offset	1.25
Mode	Trigger
Modulation	OFF
Phase	0

Table 3.2: Fixed parameters set for signal generator

3.1.3 Photo diode

A fast responding photodiode (Thorlabs FGA 10 InGaAs with 7ns rise time and 700 – 1800 nm responsivity) capable of measuring both pulsed and CW fiber light sources is used to detect signal from reflected laser beam. Photodiodes operate by absorption of photons or charged particles and generate an electrical current, which classify it to a trans-impedance photodiode category.

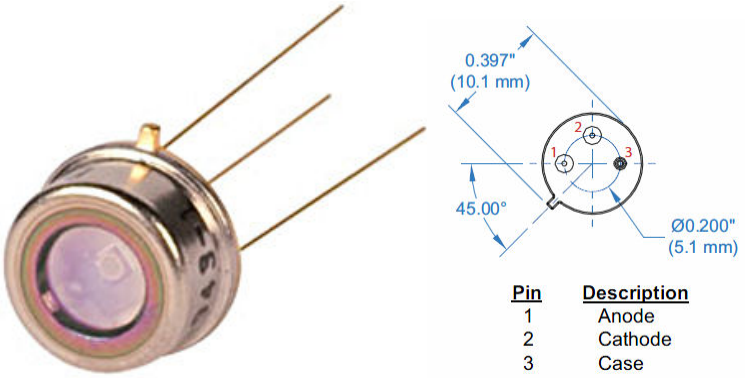

Figure 3.7: FGA 10 photodiode with connection nodes

Current is produced at photodiode anode, which is a function of incident light power (P) and wavelength (λ). Amount of expected current can be estimated from responsivity graph of the photodiode which is a function of wavelength. This photodiode is chosen specifically for the reason it meets the demand of observing the laser in the IR zone wavelength. In addition, it has good responsivity (R(λ)) at 1064 nm amongst the FGA series of Thorlabs photodiodes as can be seen from the specification chart of the manufacturer's below.

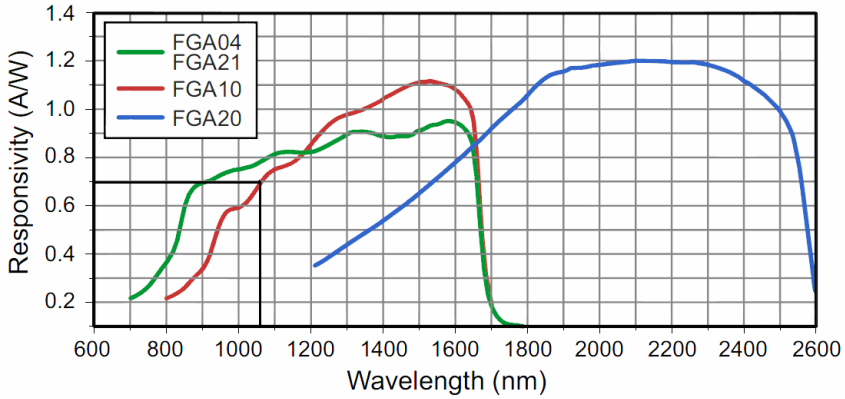

Figure 3.8: Thorlabs FGA series photodiodes responsivity

The current produced is converted to voltage reading by simply placing a load resistor (R_l) from the photodiode anode to the circuit ground which in our case is located inside an oscilloscope device.

$$Output\ Voltage\ (V_o) = P * R(\lambda) * R_l$$

Other performance parameters of photodiode and values for FGA 10 are discussed in the next portion of this sub title. One of the tricky challenges in using optical detectors for measurement of laser pulse, especially pulsed type is its capability to avoid saturation. Also the dark current value also such a significative value defining accuracy of results obtained.

- *Responsivity (R)*: is the ratio between generated photocurrent to incident light power. Unit of responsivity is [Amp/Watt]. Responsivity is observed to be 0.7 A/W at laser wavelength 1064 nm.

- *Dark current*: is the amount of current inside photodiode in the absence of light/ saturation current of PN junction. Dark current is a source for noise and needs calibration. Typical dark current value for FGA 10 photodiode is 25 n Amp, and maximum it could reach is 100 n Amp during 5 volt biasing.

- *Noise Equivalent Power (NEP):* is the minimum input optical power to generate photocurrent. It is measured as r.m.s noise current at one Hertz bandwidth. Typical NEP value is around $2.5*10^{-14}$ $W/Hz^{1/2}$, though it is a function of light wavelength.

- *Detective (D):* is the inverse of Noise Equivalent Power

$$D = \frac{1}{NEP}$$

- *Specific detective (D*):*

$$D^* = D.\sqrt{A} \qquad where\ A\ is\ normalized\ area$$

Thorlabs FGA 10 photodiode has an active area of 0.79 mm^2 which is well large enough compared to spot area of laser beam.

- *Modelling photodiode*

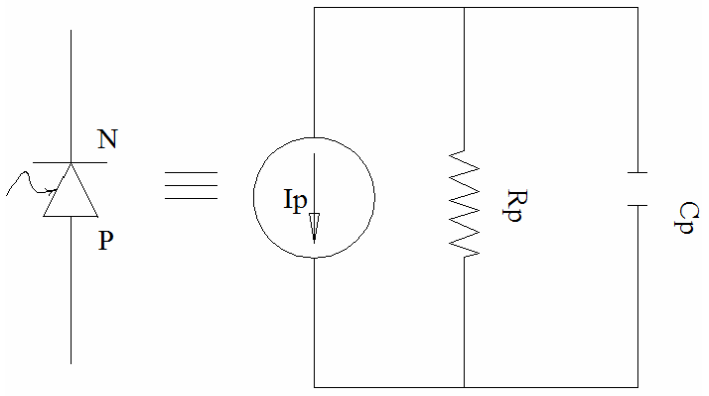

Figure 3.9: conventional representation and equivalent electrical circuit of photodiode

Junction capacitance between P and N ends (C_j) and load resistance (R_l) which comprises both shunt resistance and resistor at oscilloscope determine magnitude of bandwidth of operation. The following relation is valid to compute numerical value of bandwidth (frequency response for 3db fall).

$$f_{BW} = \frac{1}{2\pi(R_l)C_j}$$

The photodiode of interest here FGA 10 of Thorlabs has junction capacitance of 80 pF at zero volt bias condition. An alimentation circuit that is capable of assistance to filter noise and also reverse bias the photodiode is designed. Consequently, bandwidth (f_{BW}) is improved providing a better rise time. The main target of bias voltage of alimentation circuit is to narrow the large gap between P and N junction, which is responsible for a parasitic capacitor. Large parasitic capacitor leads to longer rising time and slows down the circuit considerably.

- *Rise/ fall time and Frequency Response (t_r/ t_f/ f_{3db})*

The rise time and fall time of a photodiode is defined as the time for the signal to rise or fall from 10% to 90% or 90% to 10% of the final value respectively. This parameter can be also expressed as frequency response, which is the frequency at which the photodiode output decreases by 3dB. It is roughly approximated by:

$$t_r \approx \frac{0.35}{f_{BW}} \approx 2.2 * R * C$$

There are three factors defining the response time of a photodiode:

1. t_{DRIFT}, the charge collection time of the carriers in the depleted region of the photodiode.
2. $t_{DIFFUSED}$, the charge collection time of the carriers in the un depleted region of the photodiode.
3. t_{RC}, the R_C (contact resistance) time constant of the diode-circuit combination.

The above approximation for rise time considers t_{RC} only which is computed as:

$$t_{RC} = 2.2 * R * C$$
$$Where\ R = (R_l + R_s),\ sum\ of\ load\ and\ shunt\ resisance$$
$$C = (C_j + C_s),\ sum\ of\ junction\ and\ stray\ capaciance$$

Actual value of rise time is computed using the relation,

$$t_r = \sqrt{t_{drift}^{\ 2} + t_{diffused}^{\ 2} + t_{RC}^{\ 2}}$$

3.1.4 Alimentation circuit for photodiode

The above section 3.1.3 discussion justifies the need of alimentation circuit to improve performance of photodiode. Main parameter influenced with reverse bias voltage supply is junction capacitance which is inversely related with increase in magnitude of bias voltage.

The 5 volt reverse bias decreases the 80 pF junction capacitance of FGA 10 photodiode to 40 pF. The rough but reasonable approximation of rise time is calculated to be 5nsec. Note the design consider total load resistor, set on oscilloscope as 50 ohm.

$$t_r \approx t_{RC} = 2.2 * C_j * R_l = 2.2 * 40 * 10^{-12} * 50 = 4.4\,ns$$

The result consent with typical 7 ns rise time indicated by Thorlabs which considers t_{drift} and $t_{diffused}$ in addition to t_{RC}.

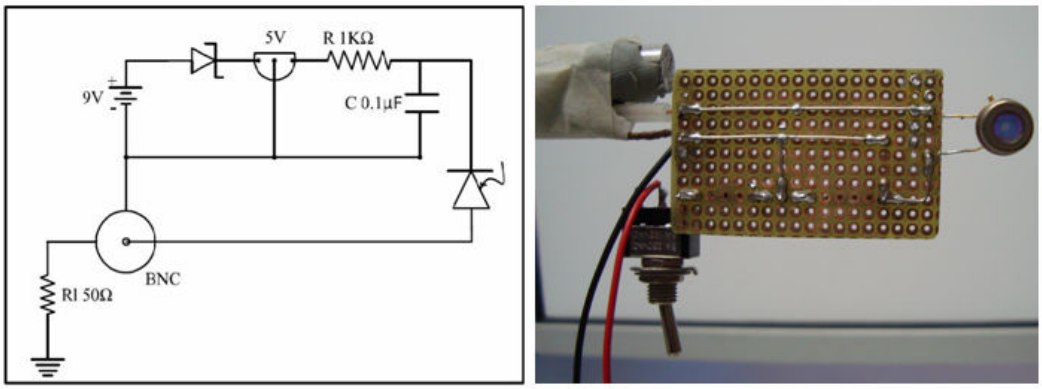

Figure 3.10: Alimentation circuit with reverse biases

3.1.5 Digital oscilloscope

Tektronics TDS-5000B digital oscilloscope characterized with bandwidth 350 MHz capable up to 5Gs/s sampling rate is used to acquire the signal from photodiode.

Bandwidth	350 MHz
Channels	4
Sample Rate	Up to 5 GS/s
Record Length	Up to 16 M
Waveform capture rate	100000 wfms/s

Table 3.3 Tektronics TDS5000B digital oscilloscope basic specification

3.1.6 Copper mirror surface

In both on focus and off focus configuration to detect the laser beam radiation on the photodiodes, a well polished copper mirror is used. Copper is chosen for its low absorption property and ability to act as a reflecting surface.

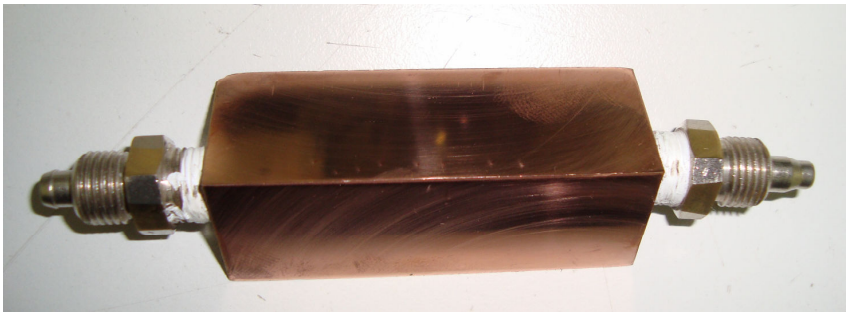

Figure 3.11 copper mirror surface to reflect incident laser beam

3.2 Experimental setup for drilling time measurement

Drilling time measurement setup is performed with a fast responding photodiode capable to measure the laser emission time, and a digital oscilloscope. Like the characterization of the pulsed laser source, the Thorlabs FGA 10 InGaAs photodiode with a combination of alimentation circuit to improve its rise time is implemented. Tektronics TDS 5034B digital oscilloscope with high sampling frequency is implemented to acquire the signal from the photodiode. Measurement time is computed measuring the time difference from laser beam emission to the moment photodiode receive the signal from bottom surface of the titanium material. The transient behaviour of the laser and the formation of through hole is kept under consideration.

In performing drilling process, the laser source is controlled with Tektronix AFG310-Arbitirary Function signal Generator. The photodiode is positioned below the work piece in such a way to receive laser beam after passing through hole.

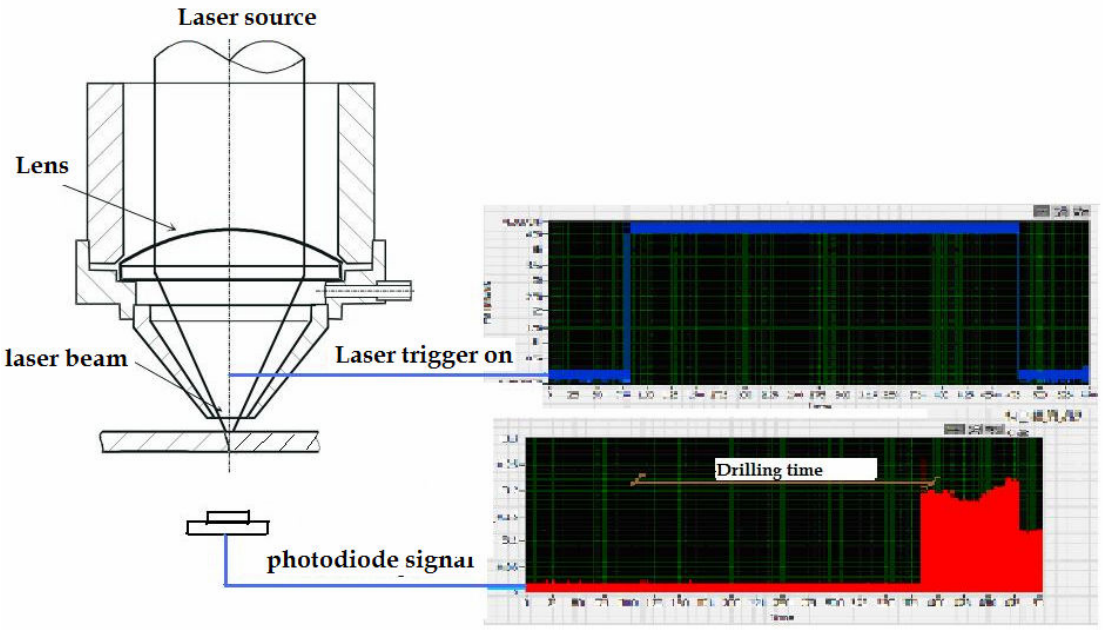

Figure 3.12: measuring drilling time using photodiode and laser emission.

3.3 Experimental setup for OES

3.3.1 Introduction to the OES setup

Figure 3.13 below demonstrated the experimental setup and components utilized for OES during micro drilling process of cp titanium. IPG Photonics YLP-50 fiber laser source emits laser beam at 1064 nm. Collimator is used to directly collect light reflecting out from the process and is connected with a standard SMA fiber cable to transport to spectrometer. The spectrometer is in parallel connection with both the laser source trigger and personal computer used to acquire resulting emission signal.

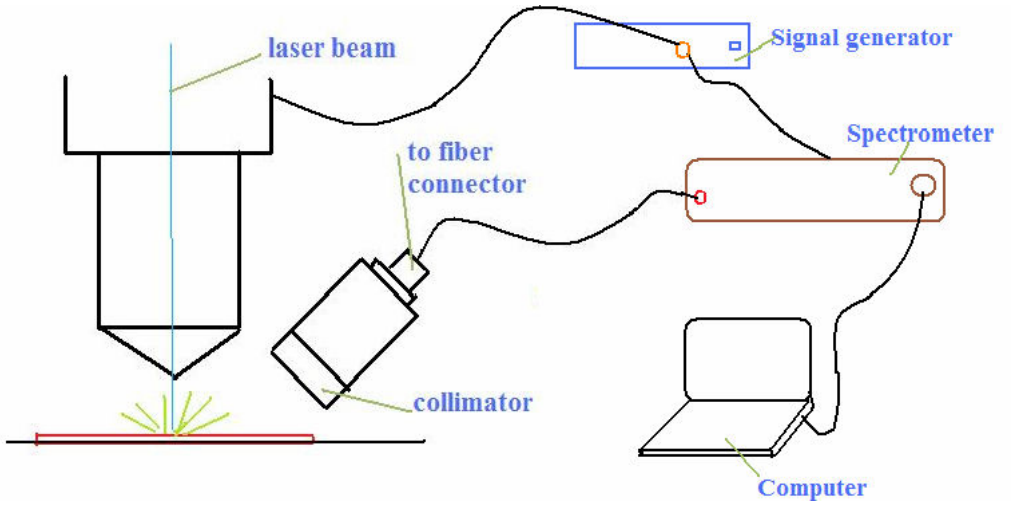

Figure 3.13 Experimental set up OES

3.3.2 The Spectrometer

The LIP spectrum is collected with fiber connected to high resolution Avantes CCD spectrometer 2048 (2048 pixels), which enables fast scanning of the spectrum. It is possible to observe spectral range of UV, visible and NIR with Avantes 2048 with grating of 1200 lines/mm and 300nm blaze. With this grating, the optical resolution (the minimum difference that the spectrometer can separate spectral lines) is in the order of 0.578nm. Table 3.3 summarizes the main specification for the spectrometer in use.

Spectrometer	**Avantes 2048 USB-2**
Wavelength range	200 to 1100 [nm]
Focal length	75 [mm]
Gratting [grooves/mm]	1200 [lines/mm]
Slit width	50 [µm]
Resolution	0.586 [nm]
Signal to noise ratio	200:1
Integration time	1.1 ms to 10 min
Sampling speed with Onboard averaging	1.11 [msec/scan]
Data transfer speed	1.8 [msec/scan]

Table 3.3: specification of Avantes 2048 USB-2 spectrometer

Figure 3.14: Avantes 2048 USB-2 spectrometer

3.3.3 Fiber optic cable

The direct collection of emission light by optical fiber is an advantage because this method prevents problems related to the dependence of focusing on wavelength, which arise when focusing a very large spectral range.

Avantes FC –UV 200-1 fiber cable is used in this experiment covering the wavelength range from UV to NIR range. It is composed of 7 fibers of 200µm with 6 light fibers and 1 read fiber having a numerical aperture of 0.22 and length of 2 meters. The standard SMA-905 connector is supported by the cable to connect to UV to infrared light wavelength collimator which is used to gather reflected light directly from the process at one end and Avantes 2048 spectrometer at the other.

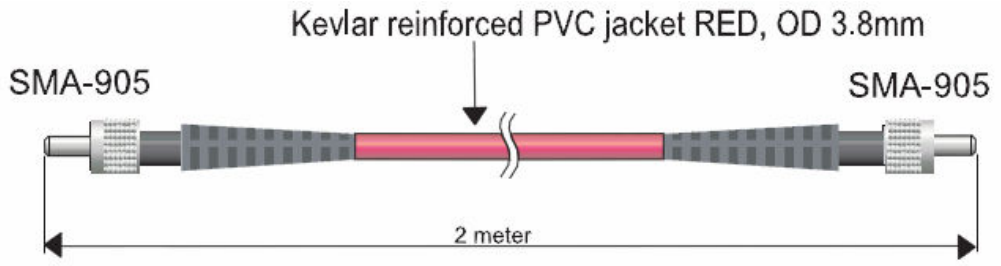

Figure 3.15: Avantes fiber optics cable

A shorter length of fiber is used to avoid the increase in intrinsic delay of light wave propagating from collimation point to spectrometer which is normally in the order of µs. Thus, it is a guarantee there is no delay in between the beginning of drilling process and spectroscopy scan due to measurement setup and instrumentation used.

Fiber cable	**Avantes FC –UV 200-1**
Numerical aperture	0.22
Standard connection	SMA-905
Number of fibers	7 (6 light and 1 read fiber)
Fiber diameter	200µm

Table 3.4: specification of Avantes FC-UV 200 1 fiber cable

Chapter 4: Experimental Design

4.1 Experimental design for laser beam characterisation

This section is dedicated to experimental design in order to study the response behaviour of the pulsed fiber laser source under study. Transient behaviour of laser beam when triggered externally with signal generator (amount of time to reach a nominal peak power, and number of pulses until this nominal peak power is reached) and full width at half maximum pulse duration are the main target response behaviours of interest.

Investigated process parameters/ factors as a predictor for rise time of laser beam, number of pulses and pulse duration are pumping current I [%] and pulse repetition rate. Three levels for each factor (20%, 60% and 100% pump current and 20 KHz, 50 KHz and 80 KHz pulse repetition rate) are considered for each experimental factor with five times of replicates to confirm the repeatability of the measurement.

The laser head calibration to achieve on focus position is 1 mm up from nozzle head mirror surface contact.

FACTORS (F)	LEVEL (L)	REPLICATES (n)
Pumping current I [%]	20, 60, 100	5 replicates each
Pulse repetition rate ,PRR [KHz]	20, 50, 80	5 replicates each

Table 4.1: variable factors and their levels

The number of experiments (NE) required conducting for the selected DOE (design of experiment) is:

$$NE = n.L^F = 45 \ \ for\ off\ axis\ ON\ \ focus\ measurement$$
$$= 45 \ \ for\ off\ \ axis\ \ OFF\ \ focus\ measurement$$

Experimental design decisions and fixed process parameters are presented in the following sub sections. This includes the laser source mainly and the copper material in use as a mirror.

Table 4.2 below summarizes basic specification of laser source and chooses parameters for transient behaviour characterization and pulse width measurement.

Fixed parameters		
Average power	50	Watt
Emission wave length	1064	mm
M^2	1.7	-
Length of fiber	2	m
Focalizing lens	60	mm
Collimated beam diameter	5.9	mm
Focus condition	ON	-
Shield gas (Argon)	7	bar
Variable parameters		
Pumping energy	20, 60, 100	%
Pulse repetition rate	20, 50, 80	KHz

Table 4.2: main characteristics of the laser machine

Waist diameter of laser beam is computed from the relation:

$$\theta.\phi = k.\lambda = consant$$

For Gaussian distributed beam:

$$k = k_G = \frac{4}{\pi} \approx 1.27$$

Beam propagation factor:

$$K = \frac{\theta_G}{\theta} = \frac{k_G}{k} = \frac{4}{\pi.k}$$

Beam propagation ratio:

$$M^2 = \frac{1}{K} = \frac{\pi.k}{4}$$

Where:

$\theta - exit\ angle\ from\ collamation\ lens$

$\lambda - laser\ beam\ wave length$

$d_f - collamated\ laser\ beam\ diameter$

Combining the above equations, the minimum (waist) diameter Φ of the laser beam can be computed as follows.

$$\phi = M^2.\frac{4}{\pi}.\frac{\lambda.f}{d_f} = 1.7.\left(\frac{4}{\pi}\right).\frac{1064*10^{-9}*60*10^{-3}}{5.9*10^{-3}} = 23.42\,\mu m$$

Experimental design for digital oscilloscope is setup with trigger level of 1 volt, at sampling frequency 2ns/point, and scale of 400 μs magnification with $500*10^6$ samples/sec real time sampling rate is used to observe laser pulse profile in both OFF axis ON focus and OFF axis OFF focus arrangement. Channel 1 is dedicated for

trigger signal source cable with 5 volt amplitude, and channel 2 connects BNC cable from alimentation circuit exit to oscilloscope with 200 mill volt amplitude.

Shielding gas used in all the experimentation is Argon gas at a pressure of 7 bar ensuring reliable blowing away of removed material and shielding titanium well from oxidation by surrounding.

As it has been mentioned in the aim of the work, characterization of the laser beam to understand the transient behaviour when triggered externally is studied first. The amount of time the laser pulse require before reaching nominal peak power, which is consider 90 % of intensity value measured, is given the name rise time for the laser beam emission. During this period of time the laser is not emitting with full power and its fluence is below capacity.

The signal acquired by digital oscilloscope is saved as .wfm file format so as to be late processed. The result is later analysed using both Matlab and Labview 8.9 in order to observe the laser pulse shape width, and rise time. Figures below (example from extreme combination of factors with 20% I, 20 KHz PRR and 100% I, 80 KHz PRR respectively) shows the trend from the measurement and it can be deduced based on the stability of the intensity amplitude that rise time is the one to reach to reach 90 % of the peak during emission time. Accordingly the shape of the pulse and nominal intensity of pulse is obtained leading to the identification of rise time.

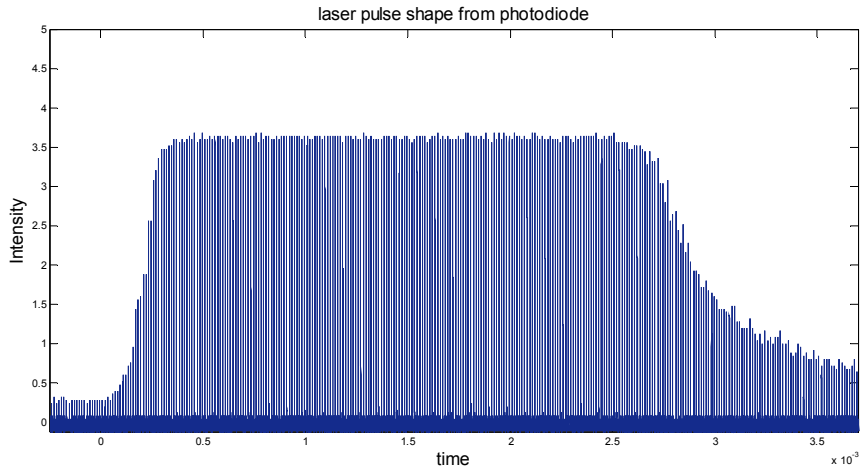

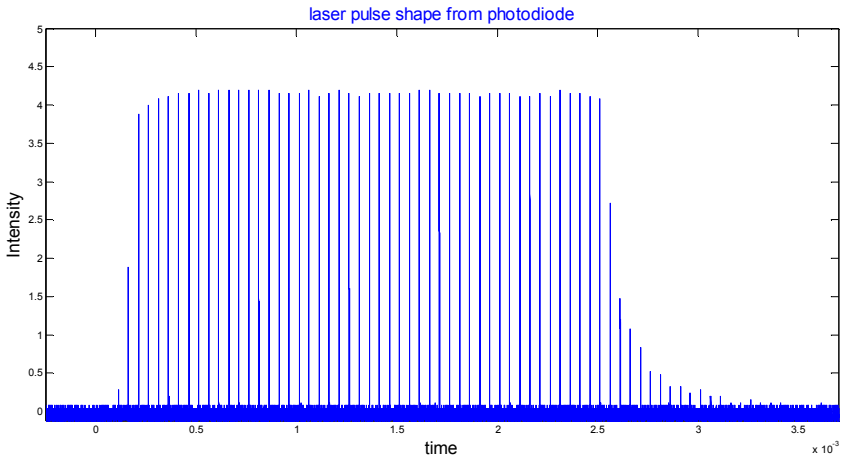

Figure 4.1 laser pulse shape acquired from oscilloscope a): pulse shape at 20% I, 80 KHz; b) Pulse shape at 100% I, 20 KHz

It is possible to measure exact value of rise time plotting the graph in Labview and computing the duration from the trigger start. Also the number of pulses emitted until the rise time reach is counted.

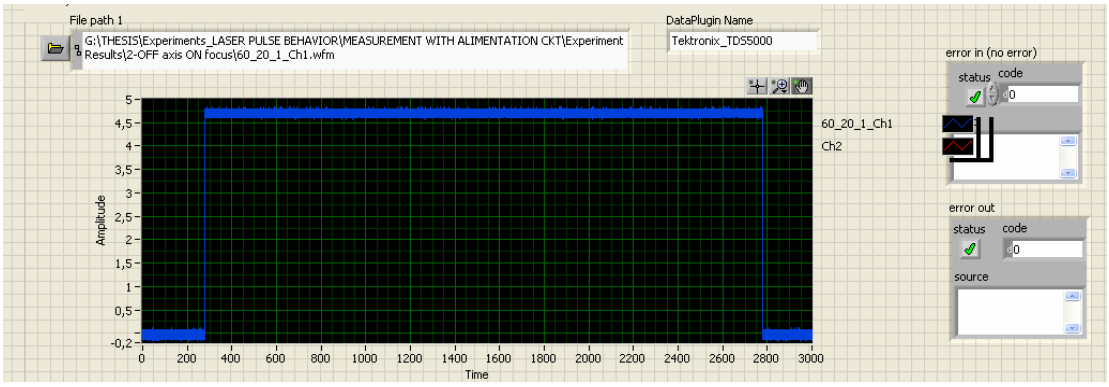

a) trigger signal

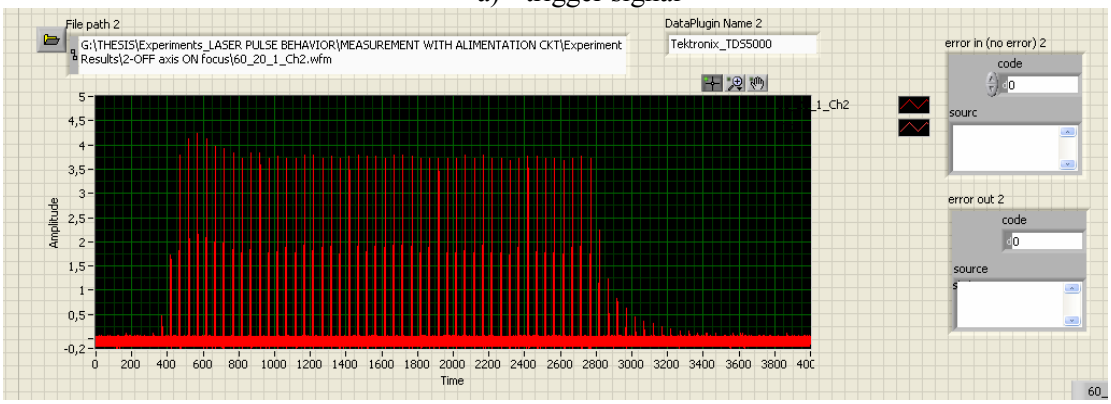

b) laser pulse shape from photodiode

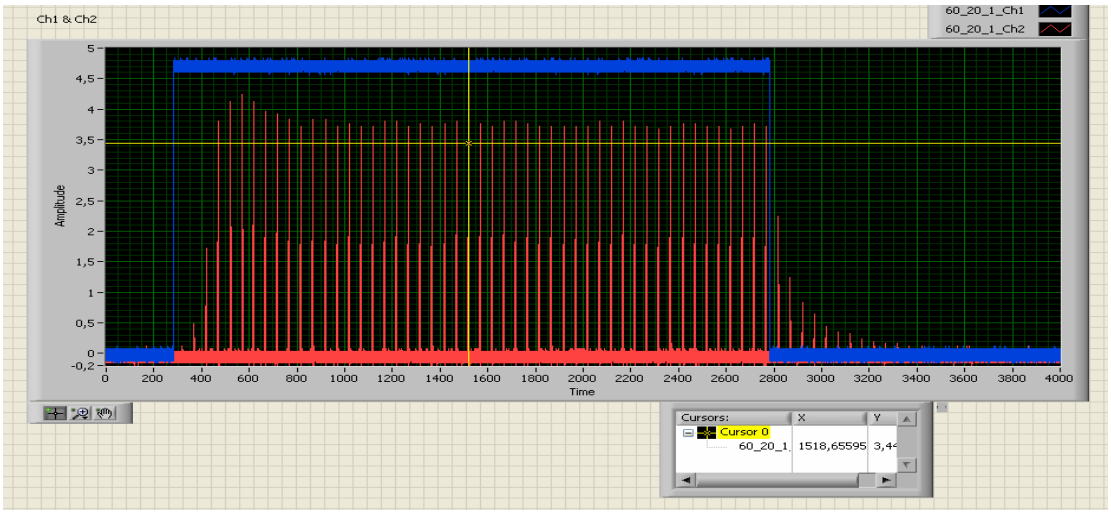

c) Trigger and laser pulse together

Figure 4.2: measuring rise time using Labview

The effect of photodiode positioning, if there is checked measuring rise time at four variable positions with laser process parameters altered. The following table indicates the various positions chosen randomly as sample and parameters in use.

Pump current [%]	60, 100
Pulse frequency [KHz]	20, 50, 80
Photo diode position	80 mm on focus, 80 mm off focus 130 mm off focus, 180 mm off focus

4.2 Experimental design for drilling time measurement

In order to achieve a good spectra intensity (relative) while maintaining the time of evolution for the drilling process, a proper experimental design is performed. The higher gate width or integration time (duration which CCD detector of spectrometer is open and active to acquire emitted light intensity) used, the better will it be in terms of relative intensity (counts corresponding to emission wavelength) and wider dynamic range of spectrometer is used.

There should be a means to know the acquired spectra belongs to the micro drilling process only but not other source of emission or noise. Accordingly, the process time (drilling time of the specified thickness) and integration time of spectroscopy need to be set in a same order.

The work piece is kept stationary perpendicular to laser emission line, successive pulsed laser beam with waist diameter being of focused on top on the surface is ejected. The drilling process is performed at full power and 50 KHz pulse repletion rate for the reason through hole can be obtained in guarantee and previous works suggest the parameter combination [Carlo Alberto Biffi 2009]. Argon shield gas is used using coaxial nozzle on the drilling head during the entire drilling process time and it helps to protect the specimen from atmospheric reaction and facilitates material removal rate. It also protect the optics from damage by reflected beam irradiation.
Table 4.3 below summarizes fixed parameters during drilling time measurement.

Material	1.5 mm CP titanium grade II
Laser source	IPG Photonics YLP 50 (50 watt)
Pump power	100%
Pulse repetition rate	50KHz
Irradiance	$1.68*10^{9}Wcm^{-2}$
Focus condition (working distance)	On focus (0.5 mm)
Shielding gas	Argon at 7 bar
Replicates	10 holes

Table 4.3: Fixed process parameters during micro drilling

A sampling frequency of 5Msamples/second, at 200ns/point in 100 ms resolution is setup for oscilloscope.

Specimen preparation for commercial pure titanium is performed by first well polishing with SiC 1200 number followed by 800 fined grain sand papers before drilling to ensure surface cleanness from oxidation. Polishing with 800 fines numbered fined paper needs a longer polishing time.

In statistics 95 rule or two sigma empirical rule for a normal distribution, nearly all values lie within 2 standard deviations of the mean. About 95% of the values lie within 2 standard deviations of the mean. This is between the mean minus 2 times the standard deviation and the mean plus 1.96 times the standard deviation. The statistical notation for this is $\mu \pm 1.96\sigma$. Here $\mu \pm 2\sigma$ and is used as experimental decision in drilling time computation. It ensures the inclusion of more data values in the confidence interval, is easy from industrial application point of view, and guarantee the formation of through hole.

4.3 Experimental design for OES

Acquisition of laser induced plasma (LIP) spectrum during micro drilling of 1.5 mm cp-titanium is performed with fiber connected high resolution Avantes CCD spectrometer 2048 (2048 pixels), which enables fast scanning of spectrum.

Beam is set at ON focus condition at surface of commercial pure titanium with 23µm waist diameter and a pulse repetition rate of 50 KHz. All the experiments are performed in argon shielding gas medium at 7 bar pressure.

Gate width (Integration time) of spectrometer is set carefully both to meet the criteria of observing maximum spectral intensity, maintaining the temporal resolution of the process at the same time. It has been discussed in the drilling time measurement section, for 1.5mm thick Titanium the process time is in the order of 350 ms. This is taken in to consideration and integration time is chosen to observe the temporal behavior only in this duration avoiding external noise.

As part of the experimental design for OES, a number of attempts have been made to identify a gate width time that can deliver good intensity of spectra. The higher the gate width, results with good dynamic range but permits only lesser number of spectrum during the process time. Compromising these two situations, acquisition of five spectrum was found optimum delivering good dynamic range of spectra with in

the 350 ms process time. Accordingly, an integration time of 87.5 ms (process time divided for the five spectra) is used to acquire five spectrums during the process.

Laser Source	**YLP-50 pulsed laser**
Pumping power	100%
Pulse frequency	50 KHz
Beam focus condition	ON focus
Spectrometer	**Avantes 2048 USB-2**
Wavelength range	200 to 1100 [nm]
Gate width	87.5 ms
Number of scans	5
Replicates	5 holes

Table 4.4 summery of laser and spectrometer fixed variables

In order to determine the LIP physical parameters, a list of spectral lines are selected. Their spectroscopic data is taken from NIST Atomic Spectra Database Lines Form (2009).

For accurate measurements of the atomic excitation temperature, spectral line as isolated as possible and emitted in optically thin conditions are selected. Due to less wavelength resolution of the spectrometer (0.586nm) at densely populated spectral lines such as 429.576nm, identification of precise intensity corresponding to selected emission wavelength will be difficult. To avoid such restraint the discrete wavelength versus count data is transformed to Lorentzian fitted curve so that a better resolution of wavelength is used.

The selected spectra lines used for Boltzmann plot method (BPM) are reported in table 4.5.

Wavelength[nm]	A_{ik} $[10^8 s^{-1}]$	E_k $[cm^{-1}]$	g_k
429.576	1.3	29829.097	1
439.392	0.33	41039.874	11
503.995	0.0389	20006.032	5

Table 4.5: selected Titanium I spectra lines and corresponding physical quantities for BPM (A_{ik}-transition probability, E_k- upper energy level, g_k- upper level)

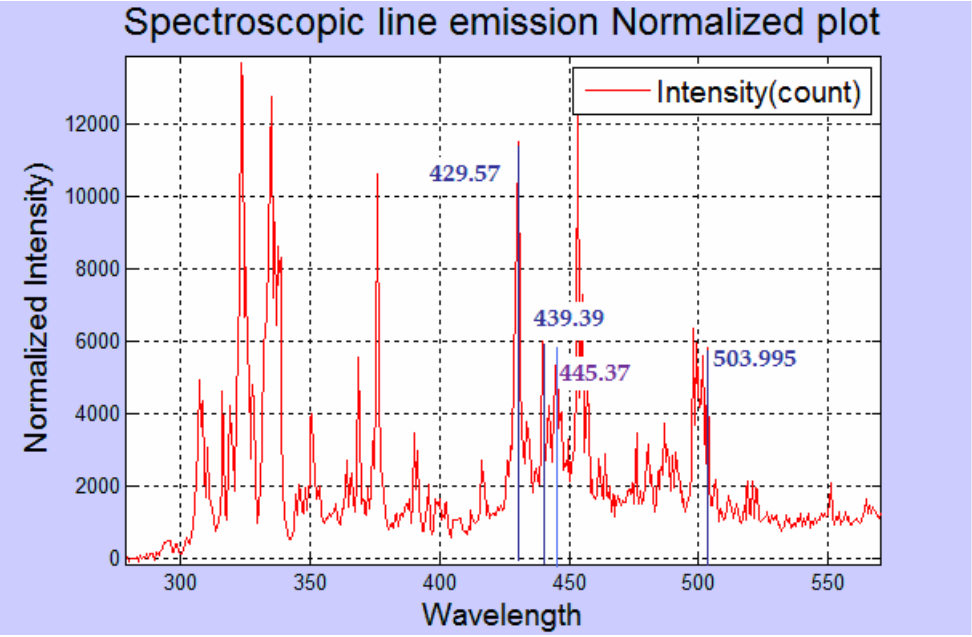

Figure 4.3: sample emission spectra in micro drilling titanium with Ti I spectra line

In spectroscopy, Lorentzian fit distribution is the description for the shape of spectral lines which are subjected to homogeneous broadening in which all atoms interact in the same way with the frequency range contained in the line shape [C. Aragon, J.A. Aguilera 2008 and A. De Giacomo 2000]. With this in mind spectral emission at 429.576nm is transformed to Lorentzian fit for all number of scans during drilling process, and subsequent intensity is pinpointed. While the other selected emission wavelength are quite separable and are clearly distinct by large margin in relative intensity from other emission intensities, there is no need to perform curve fitting and modelling with an equation. The equation below represents the general Lorentzian fit form and the coefficients for curve fitting are computed using IGOR- Pro statistical software for individual scans. All data points in the vicinity of the emission spectra are used in the curve fitting procedure.

$$Intensity_{(fitting)} = y_o + \frac{A}{(wavelength - x_o)^2 + B}$$

Once the coefficients of the Lorentzian function for each spectra is found the general equation representing the form of the emission line is modelled and can be used for any wavelength independent of the resolution of spectrometer in use.

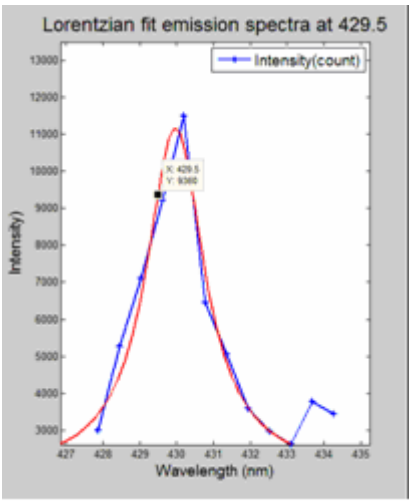

Figure 4.4: acquired Ti I spectra line (close to 429.575 nm) and its Lorentzian fit

Atomic excitation temperature of the process is computed using the Boltzmann plot method (BPM). A Matlab m-file (Refer Appendix for code) is prepared to facilitate the cumbersome mathematical computation and avoid patience error implementing section Boltzmann plot method described in state of the art. It also helps a lot in identify and select peak intensities, summarize the result, check well fitness between linear fit and calculated values, plotting both spectrum and BPM graphs.

For electron density characterization of LIP, the Boltzmann-Saha electron density method is chosen amongst methodological approaches discussed in state of the art, because of its applicability for stark broadened spectra of atoms [Sang-Ho Nam and Young Jo Kim 2001] and its simplicity. Clearly identifiable titanium I and titanium II emission lines are selected to avoid computational errors and uncertainty. Atomic spectra of titanium at 429.576 nm and Ionic spectra at 376.132 nm are those chosen for the analysis. Equation shown below with constant physical parameters m_e, h, and k_b introduced in state of the art will be used to compute electron density.

$$N_e = \left(\frac{I_a}{I_i}\right) .2\left(\frac{2\pi m_e k_b}{h^2}\right)^{\frac{3}{2}} \frac{g_i A_i \lambda_a}{g_a A_a \lambda_i} T^{\frac{3}{2}} \exp\left(\frac{-E^i + \Delta E_i}{K_b T}\right).\exp\left(\frac{E^a - E_i}{K_b T}\right)$$

Spectra	Wavelength	E_k	A_{ik} (10^8)	g_k
Ti I	429.576	29829.097	1.3	1
Ti II	376.132	31207.42	0.99	6

Table 4.6: Selected Ti I and Ti II spectra for Saha Boltzman method N_e

4.4 Use of Analysis of Variance (ANOVA)

Statistical model Analysis of Variance (ANOVA) in which the observed variance of response is partitioned into components (variable parameters) due to laser process parameter variation is used to study behavior and characteristics of transient behavior and pulse width of he laser source. In its simplest form ANOVA provides a statistical test of whether or not the means of several groups are equal, and therefore generalizes sample tests in to multiple groups. The use of ANOVA is helpful to detect if there is a large variance between mean of response due to different of treatment groups, and also the measured difference with is each group variance that is how much variability is there in each of our treatment group. Thus variability between groups and with in groups variability of response is studied using ANOVA. Statistical software MINITAB 15 is used for to perform ANOVA analysis. In all the analysis a confidence interval of 95 % (family alpha value of 0.05) for the means is used.

Chapter 5: Results and Discussions

5.1 Introduction

Chapter 5 aims the presentation , analysis and interpretation results of the whole thesis work experimentations. Coherently flowing the first section is devoted to the characterization of the fiber laser source transient behaviour and pulse width. Section two deals with result and discussion for drilling time measurement of 1.5 mm CP titanium specimen. Finally the optical emission spectroscopy approach results with discussion and explanation is presented.

5.2 Result and discussion laser beam characterization

In the experimental design, it is explained that the amount of time the laser pulse require before reaching nominal peak power is given the name rise time for the laser beam emission. Laser emission in this duration is below full power at the process parameter preset. The larger this duration of time is, the worst is the expected performance of the laser. Accordingly, it is studied in this section, the relation between process parameters and rise time needed to reach peak nominal pulse power. Later on, a more convenient and familiar approach for pulsed laser source, is used correlating this parameter with number of pulse and pulse frequency. Afterwards, with the aid of the experimental result and tools developed, duration of pulse width which is expected in nano seconds regime from the Q-switched laser source is investigated and analysed.

5.2.1 Rise Time

Result of Analysis of Variance enabled to study the impact of variable factors pulse frequency and laser power on change in response of rise time behavior. This helped to identify effect of the variable factors, pump current and PRR on rise time, and if yes, how significant are they. Later, in section 5.2.2, a more frequently used and familiar parameter in pulsed laser technology, number of pulses, is used to analyze rise time. In view of that, the number of pulses counted before rise time is observed. A simple dot plot from figure 5.1 shows the repeatability of rise time when replicates of experiments is performed. Standard deviation calculated at each level reveals high repeatability is observed at high pump current and pulse frequency, and lower repeatability the other way. For instance, 2.59 μs is calculated at 100% pump current and 80 KHz, and 42.61 μs at 20% pump current and 20 KHz PRR.

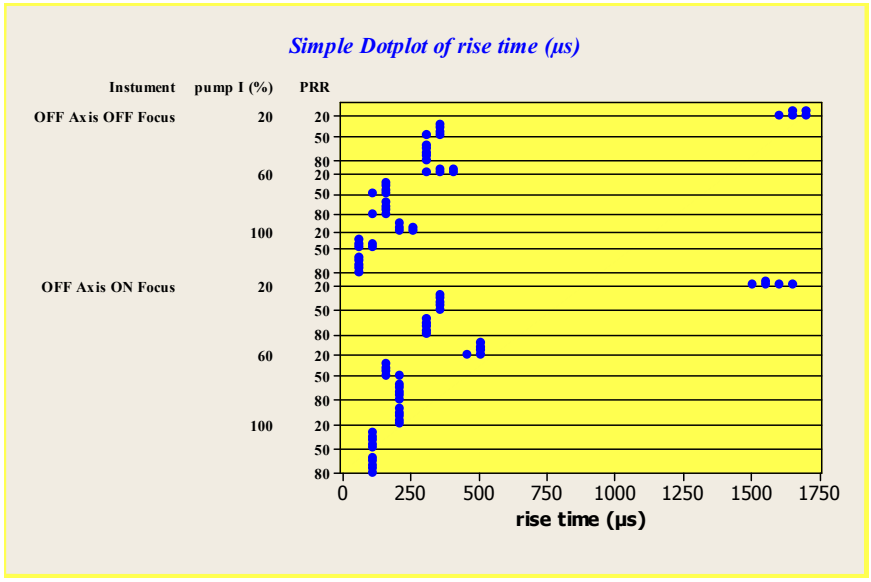

Figure 5.1: dot plot for rise time as a function of PRR and pump current %

The factorial experiment design here consists of more than one variable and it is worth to know the variation followed by the response (rise time) produced by changing the level of the factor. The main effect plot is capable of delivering this imperative observation so as to decide which of the factors selected in the experimental design are influential. The result from analysis in this case shows (figure 5.2) that the pump current and pulse frequency showed a significant variation on the rise time with in level of treatment. The significance of laser focusing condition, on copper mirror surface, or not, is identified after ANOVA is performed.

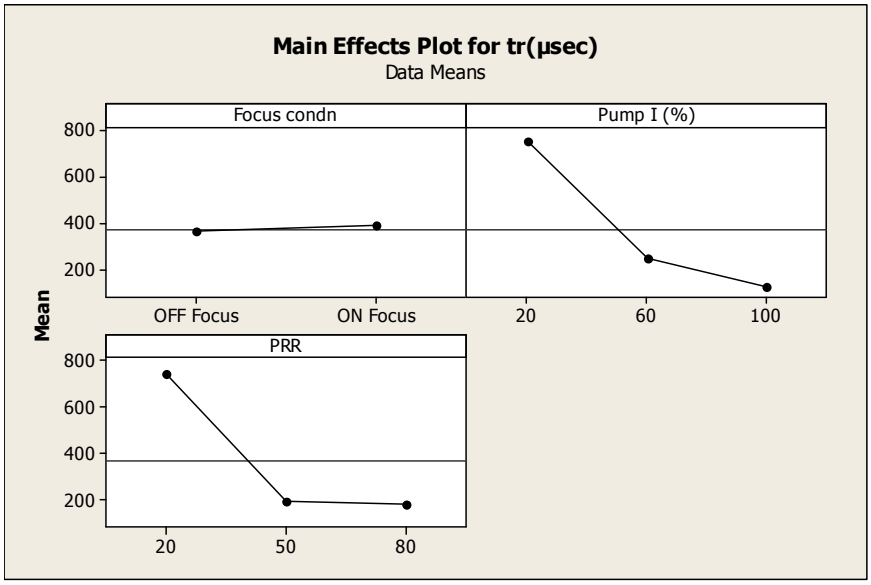

Figure 5.2: Main effects plot t_r three level power and frequency

Another interesting observation from the conducted experiment is the interaction plot showing the response between levels of a factor (pump current or pulse frequency) on levels of the other factor. For instance at 20% pump current, the rise time varies from approximately 1600 µs to 350 µs if pulse frequency changes from 20 to 80 KHz. Contrarily at higher pump current (100%), the rise time response changes slightly for a variation by pulse frequency. This suggests, pulse frequency is influential in monitoring rise time at low pump current.

Moreover, rise time response behaviour in the first zone of laser beam (20 to 50 KHz) is momentous in comparison to the rest of the zone. This observation agrees with the fact the laser characteristics and main energetic features are spontaneous inside technological zone operation.

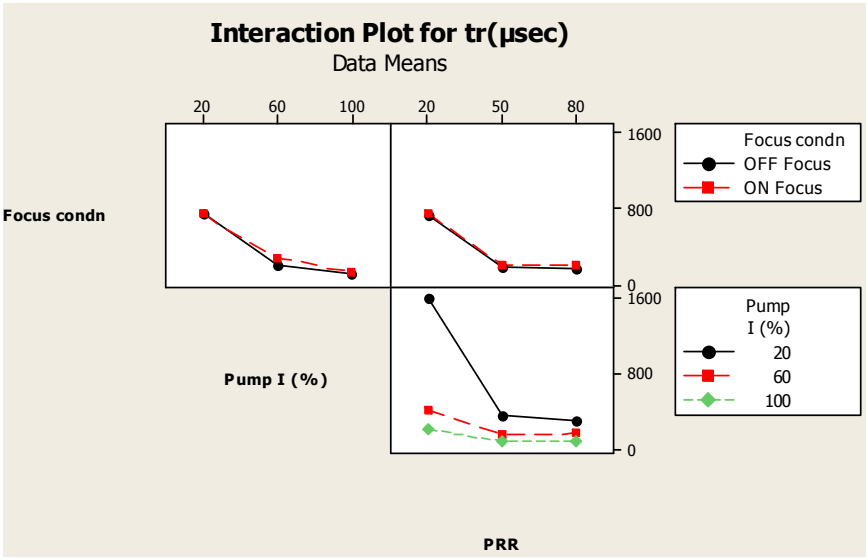

Figure 5.3: Interaction plot between pump current and PRR tr

The result indicates there is a strongly positive expected result observed all in all, but the possible interaction between pump current and pulse frequency at lower value of pump current is an indication pump current has a little practical meaning at this condition. Also, the lower right element of figure 5.3 acquaint with the fact at higher value pulse frequency is significant well enough that change in pump current does not matter most.

Factors	**type**	**levels**	**values**
Pump I (%)	Fixed	3	20,60,100
PRR (KHz)	Fixed	3	20, 50, 100
Focus condition	Fixed	2	On focus, Off focus

Table 5.1: process parameters used for rise time modelling

	Pump I	PRR	Focus	Pump I*PRR	Pump I*Focus	PRR*Focus	Pump I*PRR*Focus
P	0.000	0.000	0.000	0.000	0.000	0.147	0.000
F	7368.72	6759.27	32.26	2991.61	38.23	1.97	17.26
S = 21.3287				R-Sq = 99.82 %		R-Sq (adj) = 99.87 %	

Table 5.2: result of ANOVA for rise time with three levels of power and three levels of pulse frequency

In this test the null hypothesis Ho is the difference between the means of the response is zero. This is tested against the alternative hypothesis that the difference between the means is not equal to zero. The null hypothesis is rejected if p-value is less than 0.05 divided by the number of treatments at 95 % confidence interval. Accordingly, p- test reveal only the interaction between pulse repetition rate and focus condition is insignificant with 5% family confidence interval which is 0.71% for each treatment considered above. In all the other model conditions, the probability that we would be wrong when we reject the null hypothesis with at least one pair of treatment mean is equal to p = 0.000. The p- test only tells a difference is significant but it says nothing about its magnitude or precision. A clearer observation for identification of parameter significance can be seen from F test result. Pump current, pulse repetition rate and interaction in between them by far dominate the significance test for the response (rise time) with f-value 7368.72, 6759.27 and 2991.61 respectively. The larger the f statistics, the more useful the model is since similar confidence interval and degree of freedom is in use. In contrary, the other modelling parameters, focus condition, interaction between pump current and focus, and interaction between focus condition pump current and pulse rate have f-statistics value of 32.26, 38.23 and 17.26. This by far differs from the more imperative model parameters and it could be reasonable to trim them out from modelling. Uncertainty of experimental measurement, and use of copper surface as mirror, need to be considered in addition.

The Residual Plot which displays the response variable (rise time) on the horizontal axis versus the residuals from fit on the vertical axis is an appealing method for our ANOVA result interpretation. Below shows residual plot for the above analysed analysis of variance, and couple of interesting conclusions have been deduced based on it.

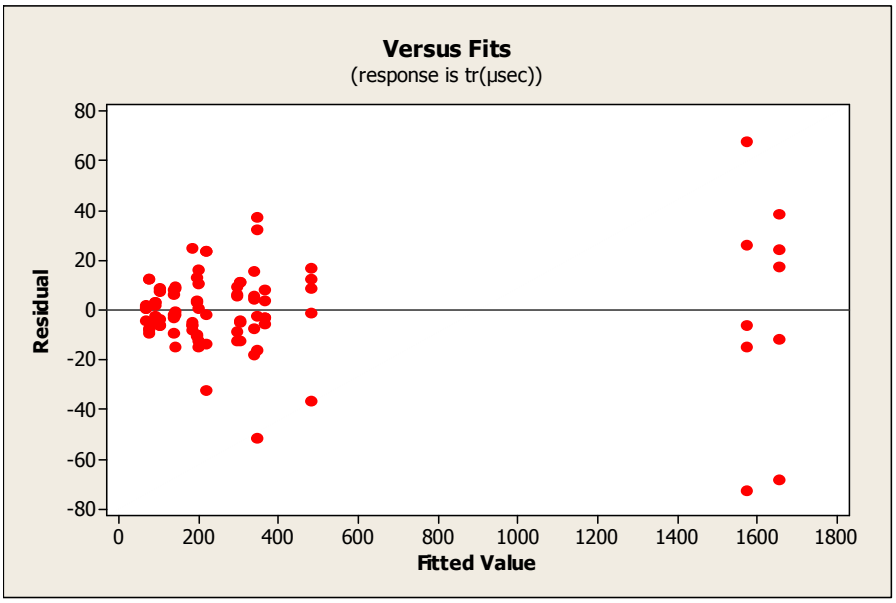

Figure 5.4: residual plot for ANOVA test; rise time 3 level of power and frequency

The residuals plot is an ANOVA diagnostic plot that helps diagnose the suitability of the assumptions underlying ANOVA for the data being analyzed. Here residual plot is used to detect non normal error distributions, non constant error variance, nonlinearity and outliers.

- The normality test could merely be acceptable as most of the points in the plot are normally distributed about the zero line within each source level.
- On the other hand, the assumption of linearity seems to be violated since it is observed some of the residual points form a systematic pattern at low pump current response 20% pump current(rise time values close to 1600 µs).
- There is also a strong indication that the model is subjected to outliner with the observation there are residuals that are much larger than the rest of the residual values at 20% pump current once again.

Based on the above observations, and the fact 20% pump current is too low power which is not in regime. In fact [Biffi C.A. 2009] describer it is difficult to drill at this power condition. Accordingly, it has been decided to discard the level and model the response with the other two levels of pump current, 60% and 100%, and the three levels of pulse repetition rates 20, 50 and 80 KHz. The following section discusses the result with this consideration.

tr (µsec)		Method (Instrument)							
		ON Focus				OFF Focus			
		Pump I (%)				Pump I (%)			
		60		100		60		100	
PRR	20	488.498	479.5	213.642	197.7	340.162	342.7	182.068	214.5
		442.696		198.216		380.256		212.78	
		492.164		182.83		375.096		200.862	
		496.326		208.432		291.324		238.496	
		478.008		185.34		326.738		238.496	
	50	204.264	179.4	92.8	89.6	131.824	133.4	84.894	72.3
		171.412		83.71		141.678		84.89	
		173.36		91.592		139.666		64.658	
		173.364		87.078		130.07		62.726	
		174.692		92.8		123.846		64.278	
	80	181.036	191.7	108.282	99.6	135.654	137.4	66.39	64.4
		182.022		95.678		146.584		59.83	
		204.67		93.56		145.848		65.054	
		195.074		93.37		122.312		65.5	
		195.704		107.156		136.578		65.064	

Table 5.3: rise time with 20% pump current level cut-off

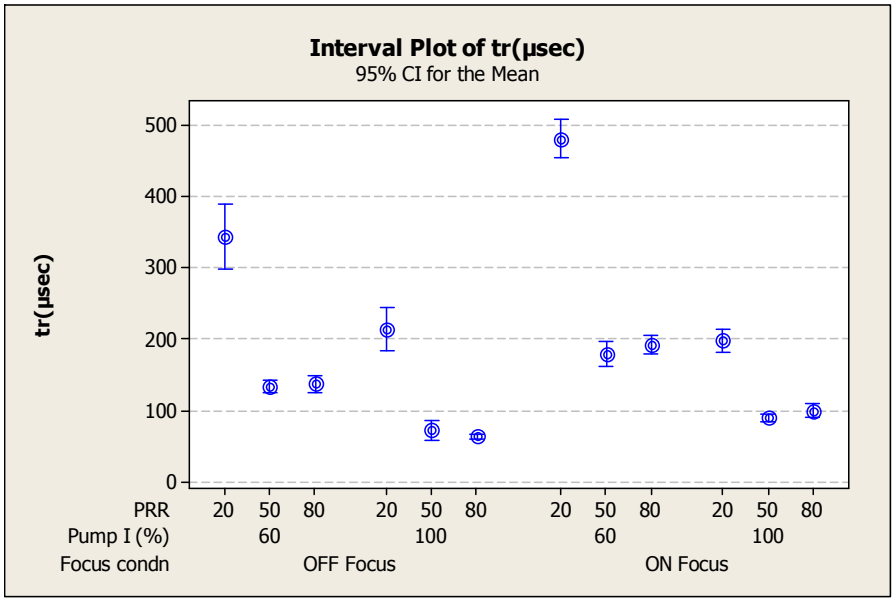

Figure 5.5: Interval plot of rise time for both ON and OFF focus measurement with two level of power and three level pulse frequencies

It is interesting to observe the response follow almost an identical trend for change in pump current both in on focus and off focus measurement. Increase in pulse frequency reduces the rise time; in other words laser reaches peak power faster at first until 50 KHz; and then keeps the same value with slight increase for further frequency step up.

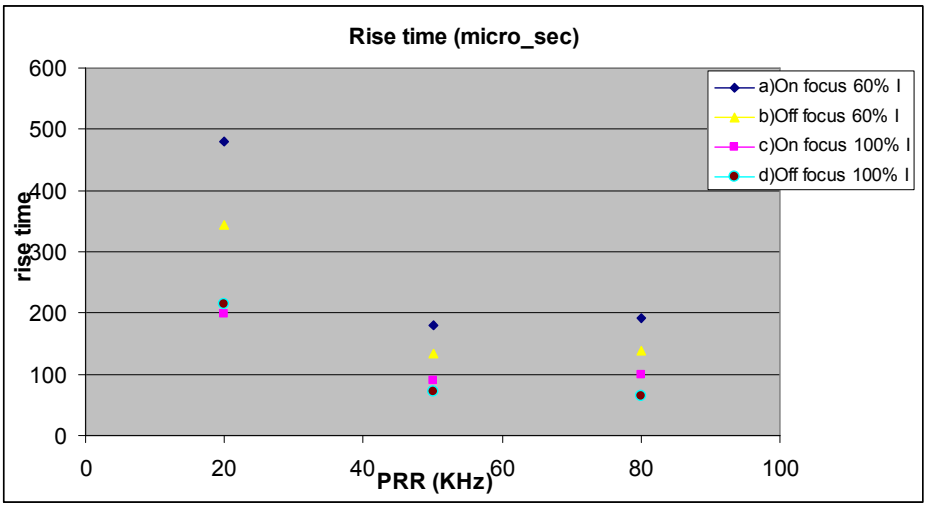

Figure 5.6: trend of rise time for different configuration and power as a function of pulse frequency: a) On focus and 60% I, b) Off focus and 60% I, c) On focus and 100% I, d) Off focus and 100% I

The main effect and interaction plots are once again implemented to observe the broad-spectrum behaviour of the response in rise time as a function of the factors.

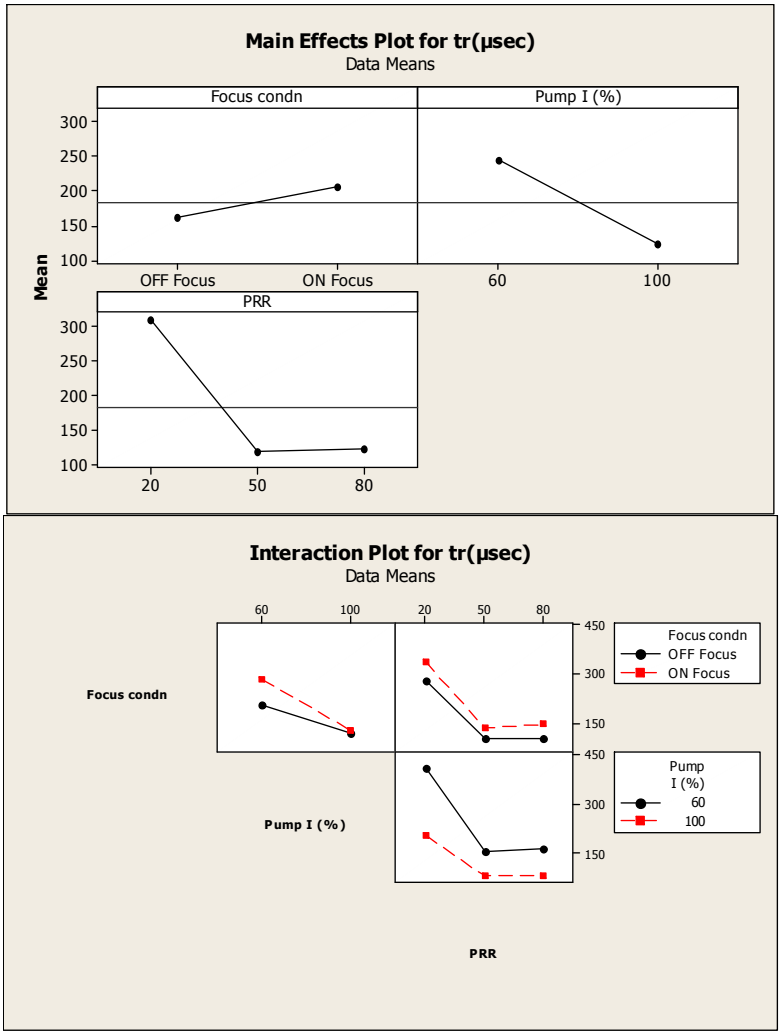

Figure 5.7: main effect and interaction plot with two level of pump current

Factors	type	levels	values
Pump I (%)	Fixed	2	60,100
PRR (KHz)	Fixed	3	20, 50, 100
Focus condition	Fixed	2	On focus, Off focus

Table 5.4: process parameters used for rise time modelling

	Pump I [%]	PRR [kHz]	Focus	Pump I*PRR	Pump I*Focus	PRR* Focus	Pump I*PRR* Focus	Error	Total
DF	1	2	1	2	1	2	2	48	59
SS	219670	469697	31015	53040	16906	2011	0.233	13005	819440
MS	219670	234849	31015	26520	16906	1005	5.85	271	
P	0.000	0.000	0.000	0.000	0.000	0.032	0.000		
F	810.8	866.82	114.5	97.88	62.40	3.71	26.01		
S = 16.46				R-Sq = 98.41 %		R-Sq (adj) = 98.05 %			

Table 5.5: result of ANOVA for rise time with two levels of power and three levels of PRR

ANOVA result indicates pump current (power); pulse frequency, focus condition, and interaction between pump current and frequency are the most significant modelling parameters governing rise time behaviour of laser source studied. Significant improvement in reduction of rise time is observed for increase in pulse frequency in the region of 20 to 50 KHz, but further increment results un-appreciable change. Laser power and rise time has also an inversely relation like pulse frequency; with continuous decrease while laser power increases up to 100 %.

Another thing that attract attention is the observation of the focus condition of the laser (measurement approach) being found significant even though not like laser power and frequency (the f-statistics order point out). Off focus condition results with lower mean value of rise time in comparison with laser on focus condition of copper surface (refer figure 5.7 on main effect plot). The rationale could be, on focus condition leads to laser material interaction with the copper material since it become difficult for copper to act as a perfect mirror. With this understanding and know-how, it is wise to consider the off focus condition measurement that is performed with no observation of spark is the more likely and true value of response behaviour.

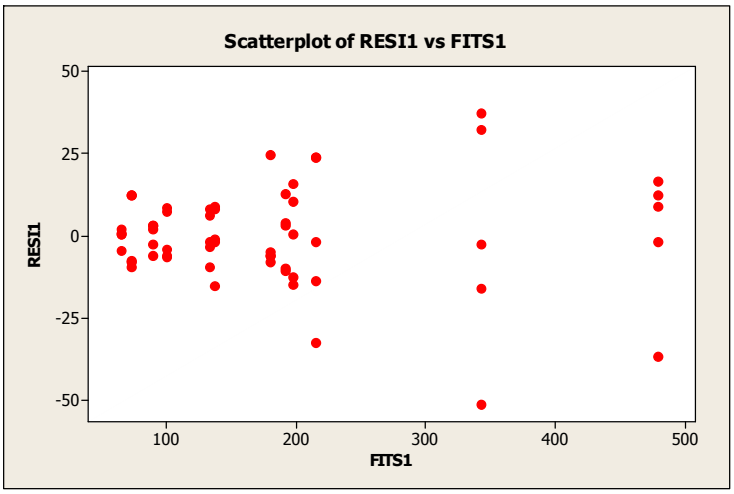

Figure 5.8: residual plot for ANOVA test; rise time 2 level of power and 3 level of frequency

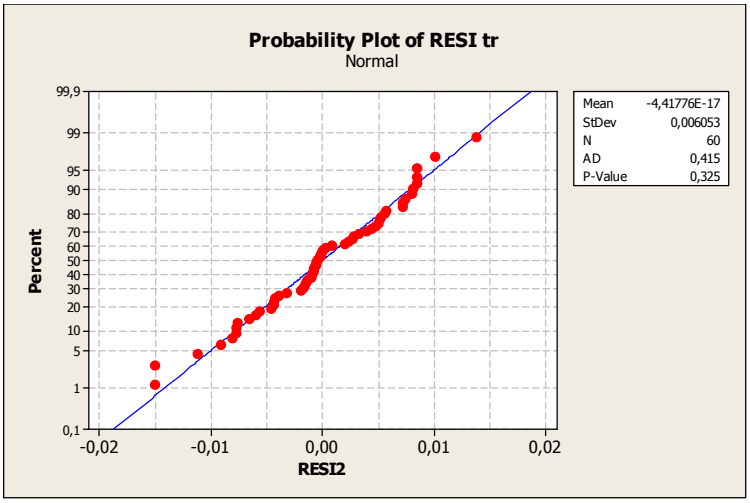

Figure 5.9: Normality test for ANOVA test; rise time 2 level of power and 3 level of frequency

Results has proved both laser power and pulse frequency play a major role in controlling the rise time of the YLP-50 fiber laser source. Increase in laser power at constant frequency, results in reducing the rise time continuously.

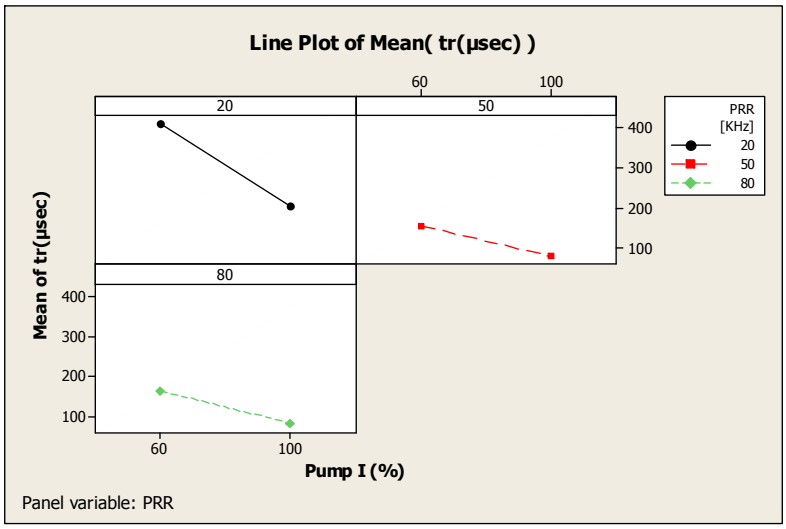

Figure 5.10: constant frequency curves indicating response of rise time with variable power

Since the laser source is pulsed in nature, the main governing phenomenon is associated with the mechanism of pulsation; in this case AOM Q-switching. Accordingly, it is important to understand it can be the reason for variation in rise time with process parameters. At lower pumping power, the amount of power reaching to the resonator is slower and below the saturation energy inside, leading to a slower rise and decay of the laser emission. Increase in pumping power continuously improves rise time because of the improvement in gain, increase in peak power delivered, and a total loss inside the resonator is lesser. This concept is discussed in section 2.2 of state of the art, and in accordance with previous studies [M. Delgado-Pinar et.al 2006, C. Cuadrado Laborde 2007].

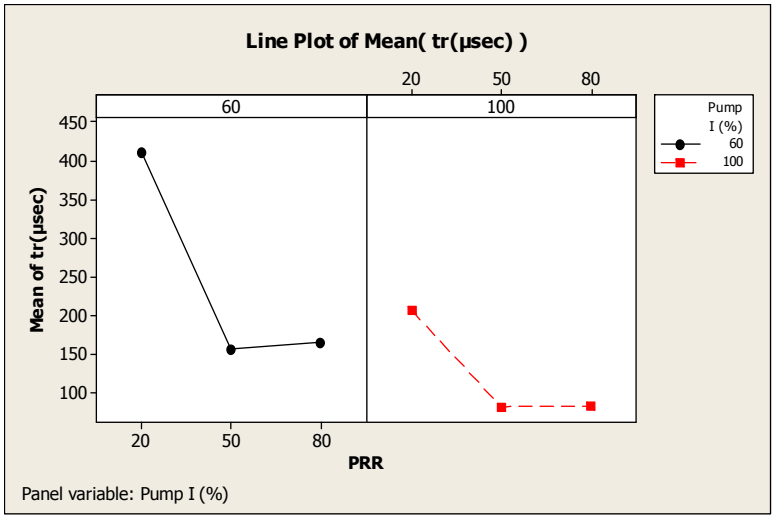

Figure 5.11: constant power curves indicating response of rise time with variable PRR

It is also noticed the response corresponding to alteration in power is rapid in comparison to pulse frequency. On the other hand variation in pulse frequency with laser power kept at constant level results with improvement from 20 to 50 KHz and a more or less constant effect afterwards. At lower pulse frequency (lower frequency of AOM and thus central frequency of oscillator), the number of resonation inside resonator is higher so that the amount of time it takes to reach peak power increases. As a consequence the rise time of laser pulse measured is gradual. When the pulse repetition rate of an actively Q-switched laser falls just below the inverse upper-state lifetime τ_c of doping element Yb^{3+} (refer chapter 2), the maximum gain and pulse energy is achieved. Here it is observed at 50 KHz.

In conclusion, the emission behaviour (rise time to full power) of IPG Photonics YLP 50 fiber laser source is presented in numerical value, and the trend followed in response to change fundamental laser parameters is observed. Both process parameters under consideration (laser power and pulse frequency) were found significant. In a typical micro drilling process parameter condition, the rise time required for the laser source was found to be in the order of 150 μs, which could be considered significant in comparison with a ms drilling time.

Measurement stability in terms of photodiode position:

In order to validate the experimental result in measurement of rise time, measuring the response was performed positioning photodiodes in different configuration and distance. It is proved this factor has no impact on measurement result and observation confirming the corroboration of the previous approach.

Here, the effect of position of the photodiode on rise time, if there, is studied arranging random location for the photodiode as described in the experimental design before. The result is scrutinized with the outcome from previous section. Table below summarizes measured rise time at the selected positions of photodiode in micro second (μs).

Factor (I%)_PRR	On focus PD 80mm (ONF_80)	Off focus PD 80mm(OFF_80)	Off focus PD 130mm(OFF_130)	Off focus PD 180mm(OFF_180)
60_20	479,54	342,72	349,89	386,706
60_50	179,42	133,42	138,66	167,51
60_80	191,7	137,4	165,916	171,298
100-20	197,69	214,54	216,126	219,928
100-50	89,6	72,29	75,448	76,508
100-80	99,61	64,37	67,314	74,172

Table 5.6: sample levels selected for studying measurement stability of photodiode position in rise time

Graph below shows scatter plot of the four different positions of photodiode and respective measured rise time. The On focus at 80mm and off focus 80 mm far photodiode are those measurement results performed with factorial design of three level and five times replicates. Here as a convenient with target of this section, the mean value of rise time at the respective pump current and pulse frequency is used to compare with two additional positions of photodiode considered here; 130 mm and 180 mm far from laser incident on mirror.

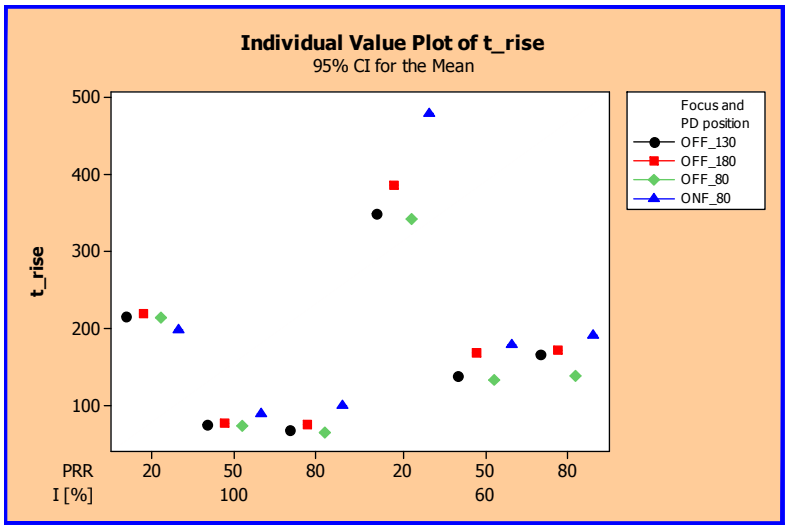

Figure 5.12: Effect of photodiode position on measurement of Laser rise time

Observation of the graph reveal the on focus configuration result in a slight deviation of rise time compared to the other three positions. One good reason and justification for this circumstance might be the ignition of spark observed during laser firing (reported on Appendix) on the copper mirror. Accordingly, there is a possibility for copper surface-laser interaction persuading our initial target to differ.

Analysis of variance is performed to observe the significance of the process parameters and position of photodiode on rise time. Both pump current and PRR, and their interaction are found significant; while Focus and PD position on the other hand is insignificant according to p- value test with family confidence interval of 5%. It is observed focus and photodiode position has 0.029 value of which is larger than the 0.0125 critical values for the four treatments. Also, according to F-test, calculated F_o value which is the ratio between mean square of treatment and mean square error is 3.98. But the critical range for F probability distribution function with degree of freedom 3 for treatment and 15 for error with α of 0.05 is 3.29. Since F_o is not large enough than critical F value, indicating once again we confirm the non significance of the factor (focus and photodiode position) on rise time measurement.

Another observation from the ANOVA result is the unusual response for the rise time during ON focus measurement. These values are observed during ON focus condition, and with pump current and pulse frequency magnitudes that corresponds to maximum power and pulse energy. Thus, as it had bean mentioned before, the fact and the observation of spark during the experiment can lead to a conclusion: there might be material drilling during ON focus setup at high power and frequency.

Factors	**type**	**levels**	**values**
Pump I (%)	Fixed	2	60,100
PRR (KHz)	Fixed	3	20, 50, 100
Focus and PD position	Fixed	4	Off_130;Off_180,Off_80;On_80

	Pump I [%]	**PRR [KHz]**	**Focus & PD position**	**Pump I*PRR**	**Error**	**Total**
DF	1	2	3	2	15	23
SS	78958	176470	7132	12073	8967	283601
MS	78958	88235	2377	6037	598	
P	0.000	0.000	0.029	0.002		
F	132.08	147.60	3.98	10.10		
S = 24.45			R-Sq = 96.84 %	R-Sq (adj) = 95.15 %		

Table 5.7: result of ANOVA for investigation of effect of photodiode positioning on measurement of rise time

Generally speaking the photodiode position in reference to the mirror has no effect on measurement of rise time. It is observed, only the intensity of laser beam received by the photodiode vary as a function of distance; the more far from incident, the lesser the amplitude.

5.2.2 Number of pulses before rise time

As a continuation from section 5.1.1, here the number of pulses required, in other words number of pulses emitted by the laser machine before reaching its nominal peak amplitude is studied. It is common to represent laser micro drilling performance in terms of number of pulses it takes to complete through hole of a definite sample thickness. Researches by [S. Dòring, et. al 2009] and [A. Acona 2007] use number of pulses required to drill through hole as a performance measure in laser parametric study as a value for drilling efficiency. The lower the number of pulses applied before the breakthrough the higher is the corresponding drilling efficiency. Similarly in this section the number of pulses before rise time is count to correlate laser behaviour response as a function of process parameters.

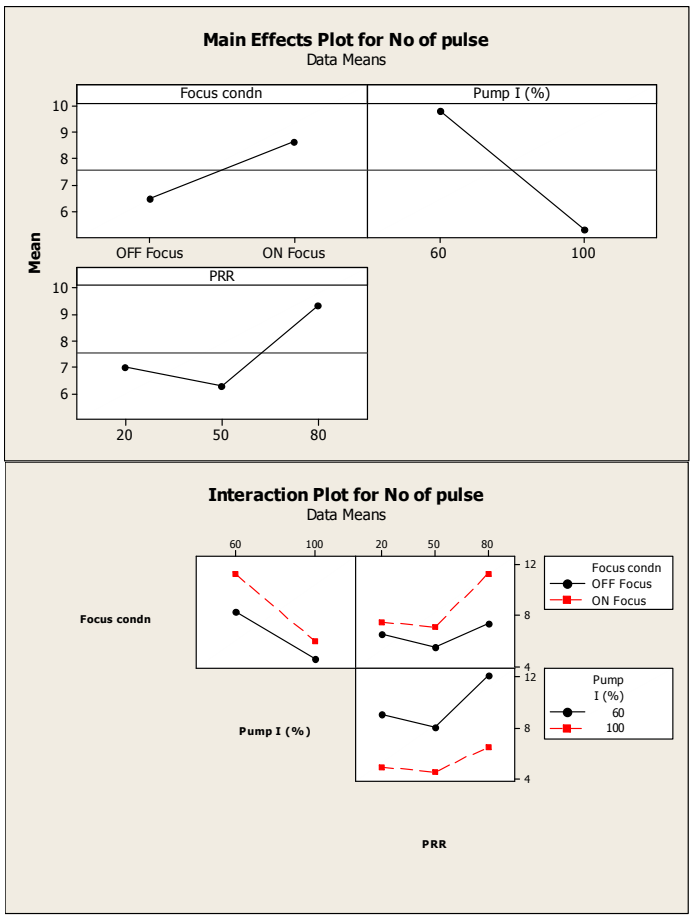

Figure 5.13: Main effect and interaction plots of number of pulses before peak power reached

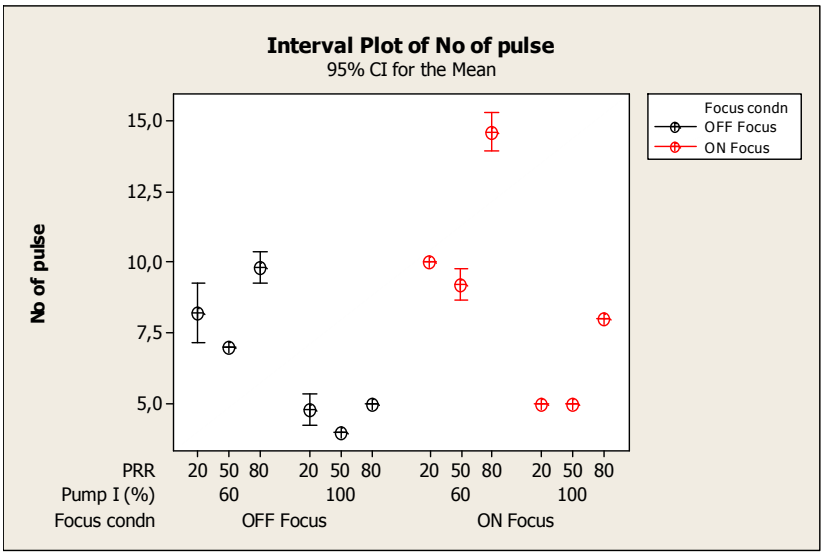

Figure 5.14: Interval plot, number of pulses before rise time reached for two levels power and three levels pulse frequency measurement in both focus conditions.

In agreement with the result obtained in rise time behaviour study of the fiber laser, the number of pulses before peak power efficiency is improved directly with laser pumping power. Both the on focus and off focus configuration had proved the rigorousness of the experiment delivering the same trend. Considering the effect of pulse frequency (at constant power) on number of pulses before peak power, it is observed a slight decrease at first (between 20 to 50 KHz) and increase (between 50 to 80 KHz) The decrease inside the first zone is associated with the improvement of rise time (in micro second). While in the second zone, no improvement was observed and justified in terms of rise time. But the increase in frequency results with more number of pulses in time domain. This leads to increase in number of pulses before rise time between 50 to 80 KHz.

It is interesting to notice an increase in pulse frequency is efficient only up to 50 KHz. Further increase results with no more improvement in terms of rise time and even negative from number of pulses before rise time point of view.

Factors	type	levels	values
Pump I (%)	Fixed	2	60,100
PRR (KHz)	Fixed	3	20, 50, 100
Focus condition	Fixed	2	On focus, Off focus

Table 5.8: process parameters used for number of pulses before rise time modelling

	Pump I [%]	PRR [KHz]	Focus	Pump I*PRR	Pump I*Focus	PRR* Focus	Pump I*PRR* Focus	Error	Total
DF	1	2	1	2	1	2	2	48	59
SS	303.75	102.1	70.42	11.7	8.82	23.433	0.233	6.4	526.8
MS	303.75	51.05	70.42	5.85	8.82	11.72	5.85	0.133	
P	0.000	0.000	0.000	0.000	0.000	0.000	0.423		
F	2278.12	382.87	528.1	43.87	66.12	87.87	0.88		
S = 0.365148				R-Sq = 98.79 %		R-Sq (adj) = 98.51 %			

Table 5.9: result of ANOVA for number of pulses before rise time, with two levels of power and three levels of pulse frequency

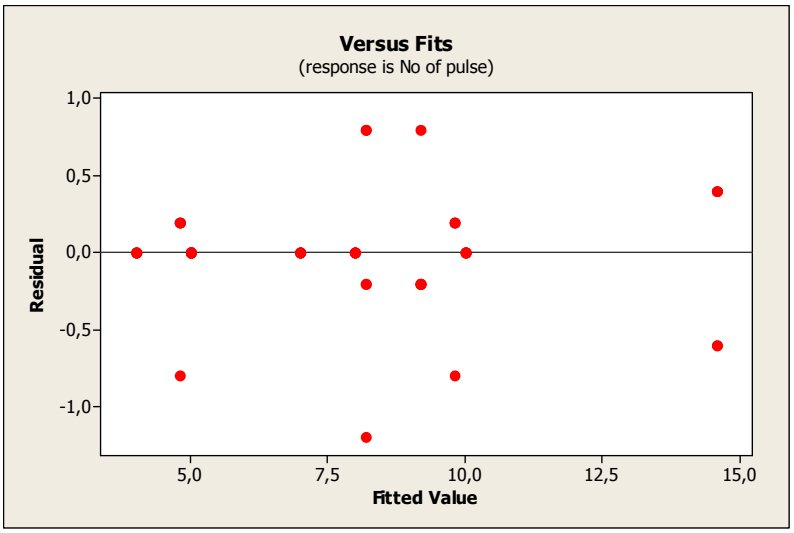

Figure 5.15: Residual plot for number of pulses before rise time indication distribution along mean value

Once again ANOVA result indicates laser power; pulse frequency, focus condition, and interaction between pump current and frequency are the most significant modelling parameters governing number of pulses before rise time is reached. All the observations and conclusions discussed in the analysis of rise time holds true here again with off focus condition resulting lower mean value of number of pulses in comparison with laser on focus condition of copper surface. The rationale could be on focus condition leads to laser material interaction with the copper material since it become difficult for copper to act as a perfect mirror. With this understanding and know-how, it is wise to consider the off focus condition measurement that is performed with no observation of spark is the more likely and true value of response behaviour.

5.2.3 Laser pulse shape

In this section the pulse shape and width acquired from the experimentation are analyzed. Distribution of laser power in time domain and measurement of full width at half maximum (FWHM) is obtained at different process parameter.

Below from figure 5.16 to 5.24 is reported sample pulse shapes acquired at each level of pump current and pulse frequency. The result consents again with the argument conducted both in previous sections of this work and referred studies.

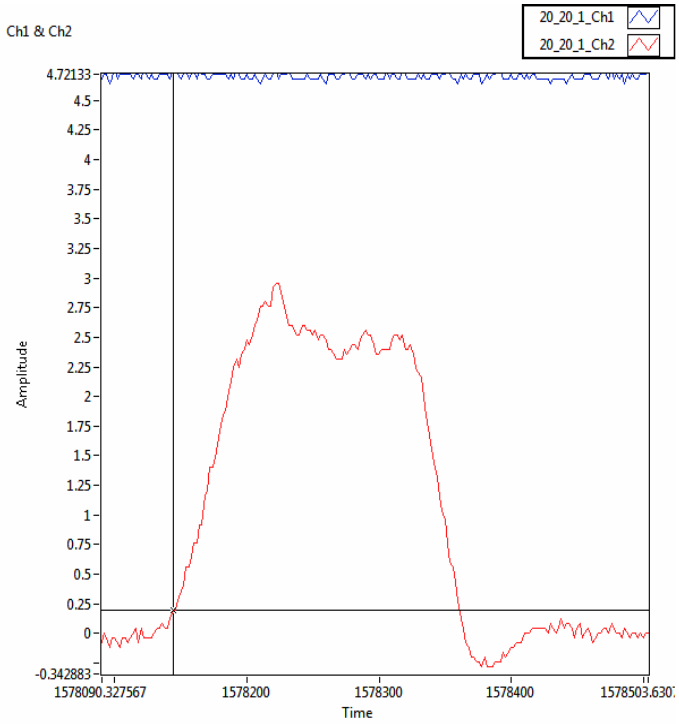

Figure 5.16: pulse shape 20% pump current 20 KHz frequency

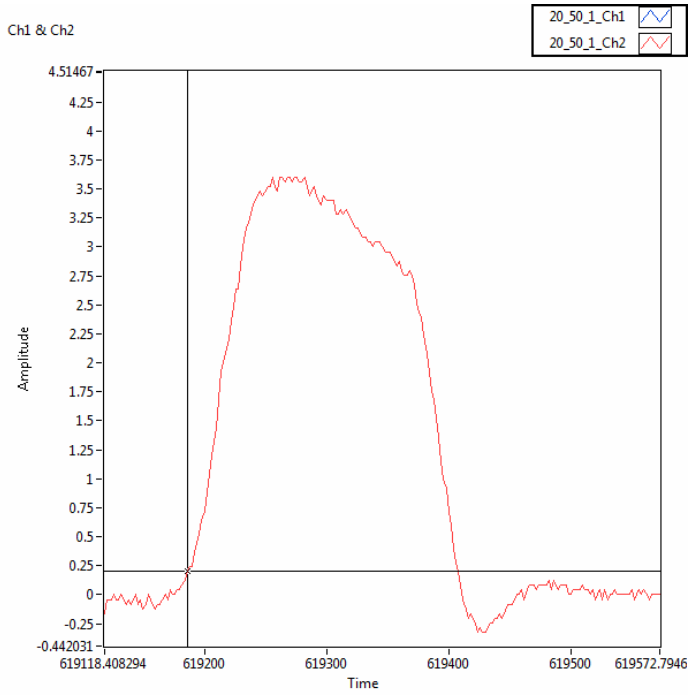

Figure 5.17: pulse shape 20% pump current 50 KHz frequency

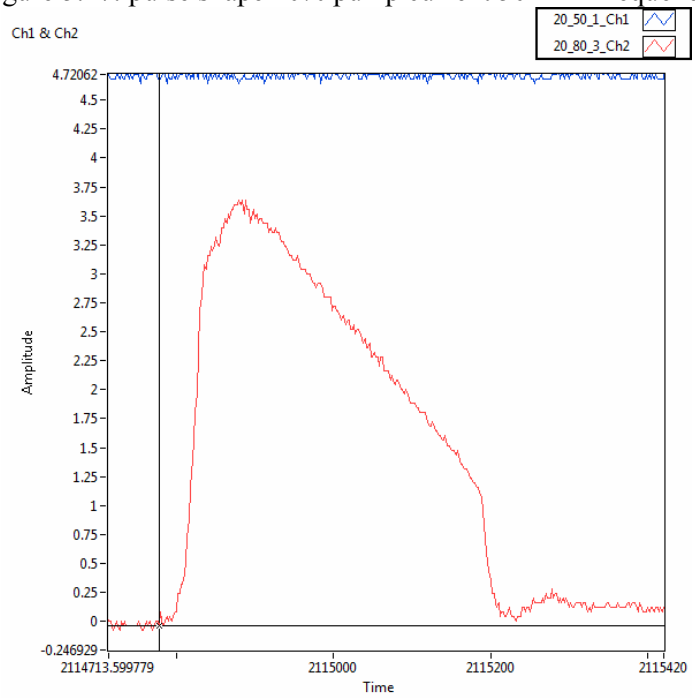

Figure 5.18: pulse shape 20% pump current 80 KHz frequency

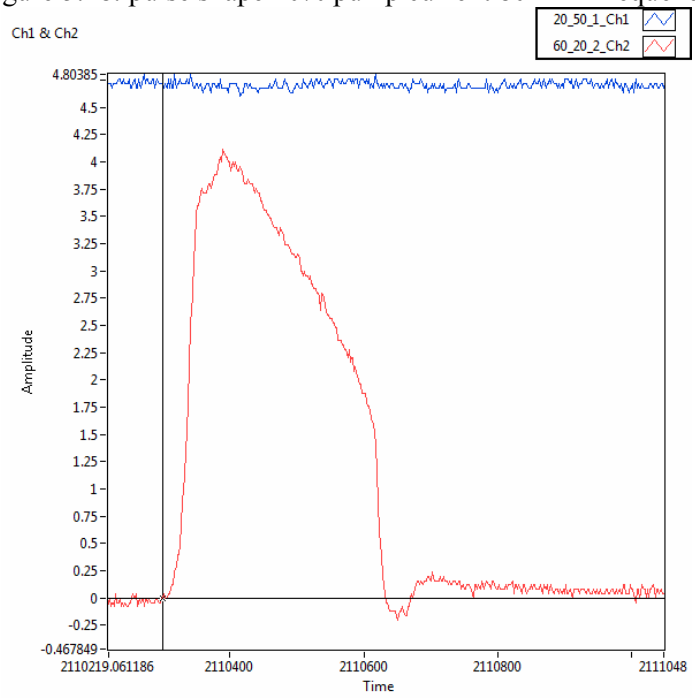

Figure 5.19: pulse shape 60% pump current 20 KHz frequency

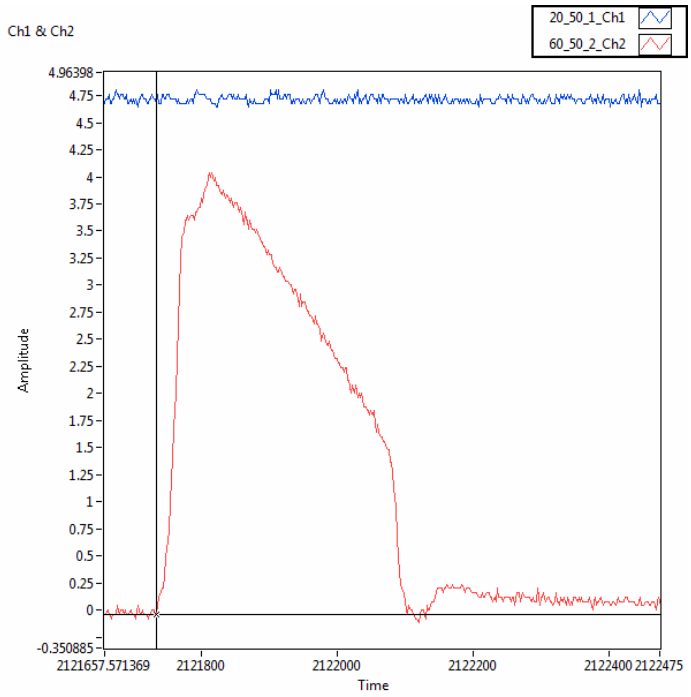

Figure 5.20: pulse shape 60% pump current 50 KHz frequency

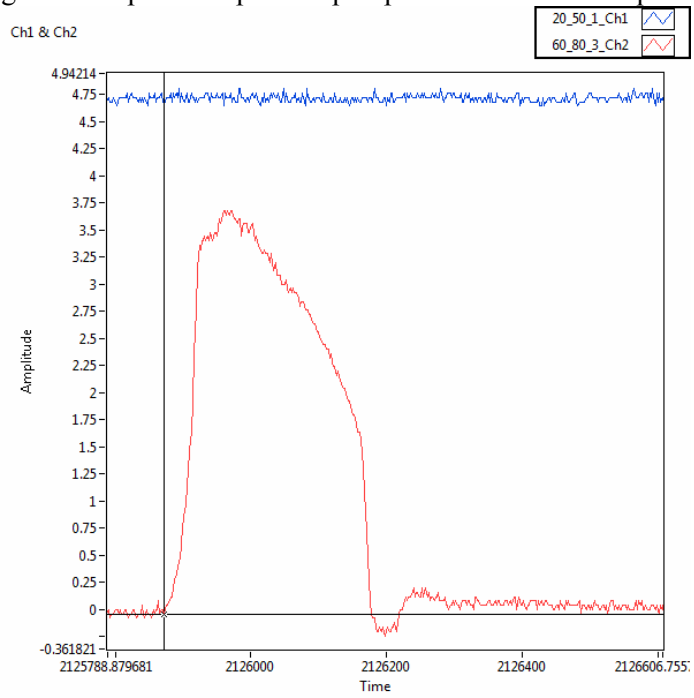

Figure 5.21: pulse shape 60% pump current 80 KHz frequency

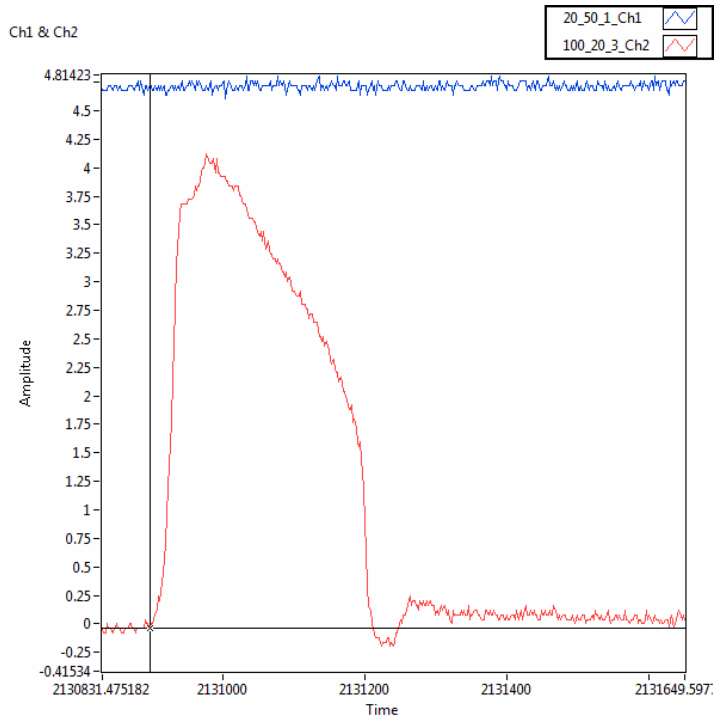

Figure 5.22: pulse shape 100% pump current 20 KHz frequency

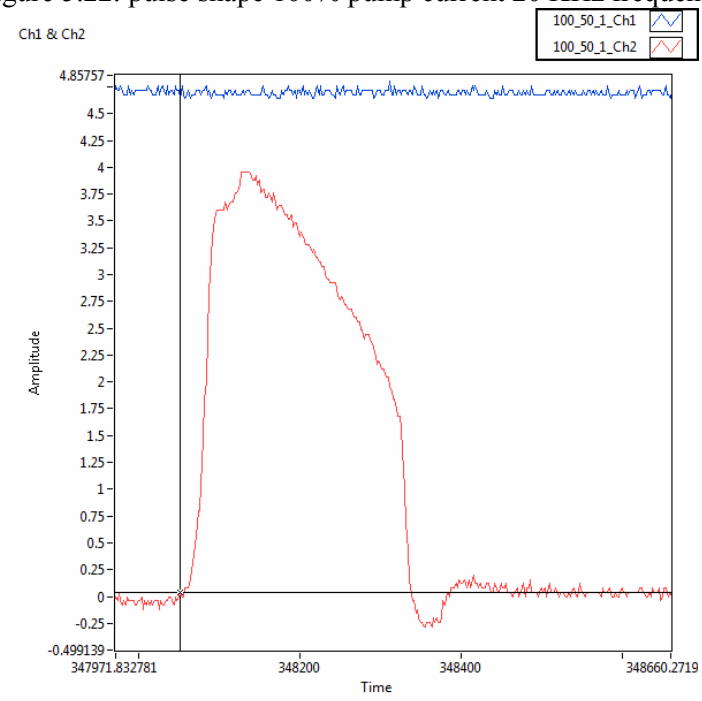

Figure 5.23: pulse shape 100% pump current 50 KHz frequency

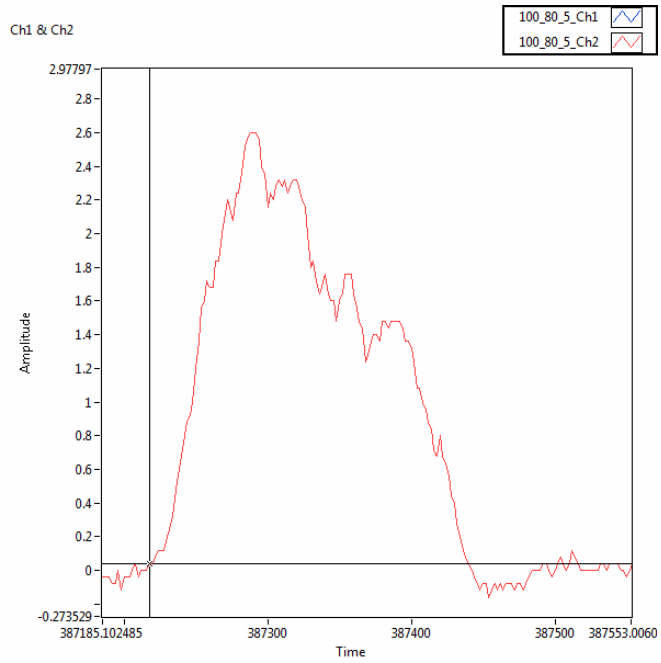

Figure 5.24: pulse shape 100% pump current 80 KHz frequency

Pulse width(ns) FWHM		Method (Instrument)					
		ON Focus			OFF Focus		
		Pump I [%]			Pump I [%]		
		20	60	100	20	60	100
PRR	20	159	173	131	163	156	134
		166	169	128	170	158	132
		161	165	138	172	156	128
		152	162	131	176	164	138
		160	166	136	172	167	134
	50	164	160	153	161	156	142
		164	157	137	173	160	146
		178	153	135	175	152	141
		160	154	133	171	149	148
		176	157	132	168	152	140
	80	144	160	126	153	160	128
		152	166	116	156	165	127
		138	165	130	149	164	123
		142	167	118	145	164	122
		139	168	124	148	165	125

Table 5.10: summary of laser pulse width measures as Full width at half maximum (FWHM) with ON and OFF focus measurement

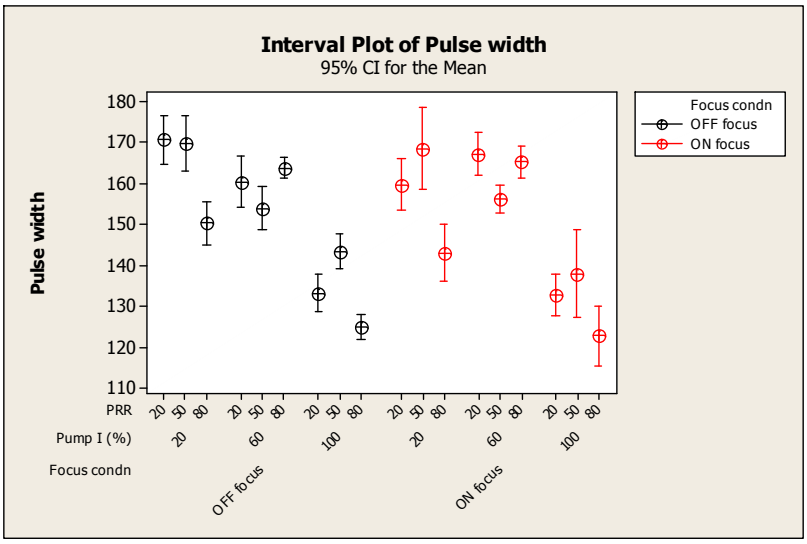

Figure 5.25: Interval plot for pulse width with three levels of laser power and three levels pulse frequency.

It is well known and once again proved the fiber laser source YLP 50 is in nano second regime. Nanosecond pulses are typically longer than the electron phonon relaxation time of metals. Thus, the thermal load to the material is governed by the pulse duration. In case of short pico-second or femto-second pulses, the heating process is determined by the material-dependent relaxation time that now is comparable to or even longer than the pulse duration.

At lower pump current and frequency, laser pulse shape follows a trend with both slow rise and fall slope. Moreover the intensity is too weak with a rectangular profile attained lacking energy concentration with in short pulse width and high peak. Effect could be longer drilling time with poor quality or even inability at all for through hole. Increase in laser power improves pulse shape with better rise slope and energy concentration achievable. For laser drilling process, this phenomenon or behaviour is crucial as a matter of fact, since rapid energy deposition and a nearly direct solid - vapour transition of the ablated material is a primary step.

Single pulse peak energy available in each pulse is the area under the pulse intensity versus time graph. Graphs below show result of ‘Full Width at Half Maximum’ as a function of process parameters.

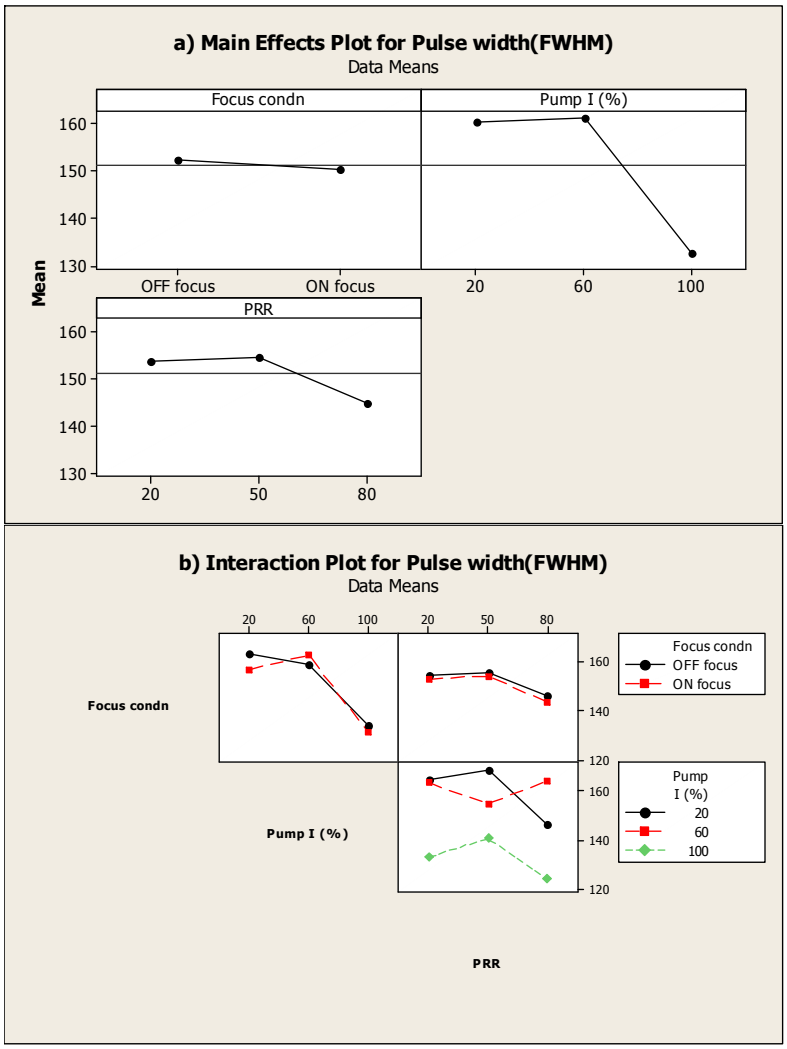

Figure 5.26: laser pulse width (FWHM) behaviour a) main effect plot b) interaction plot with three level of process parameters power and pulse frequency

Factors	**type**	**levels**	**values**
Pump I (%)	Fixed	3	20,60,100
PRR (KHz)	Fixed	3	20, 50, 100
Focus condition	Fixed	2	On focus, Off focus

Table 5.11: process parameter factors used for laser pulse width modelling

	Pump I [%]	**PRR [KHz]**	**Focus**	**Pump I*PRR**	**Pump I*Focus**	**PRR* Focus**	**Pump I*PRR* Focus**	**Error**	**Total**
DF	2	2	1	4	2	2	4	72	89
SS	15782.3	1794.8	76.5	3027	387.6	6.5	186.8	1721	22983
MS	7891.1	897.4	76.5	756.5	193.8	3.2	46.7	23.9	
P	0.000	0.000	0,078	0.000	0,001	0,873	0,111		
F	330,02	37,53	3,20	31,65	8,11	0,14	1,95		
S = 4,88990				R-Sq = 92,51%		R-Sq (adj) = 90,74%			

Table 5.12: result of ANOVA for laser pulse width, with three levels of power and three levels of pulse frequency

Observation of p-distribution test result with 5% family confidence interval for the seven treatments shows laser power, frequency, interaction between power and frequency, and interaction between power and focus condition of measurement are the only significant factors. Though the interaction between power and focus condition seems close significant level from the p-test, its F-test indicates a slightly larger F_o value (8.11) compared to F-value (≈ 3.1) with α value of 0.05 and degree of freedom 2 and 72 for treatment and error respectively. It leads to conclusion interaction in between is not as such significant and can be neglected.

The Residual Plot exhibits pulse width against the residuals from fit on the vertical axis is an appealing method for our ANOVA result interpretation. Below shows residual plot for pulse width analysis of variance and couple of interesting conclusions have been deduced based on it.

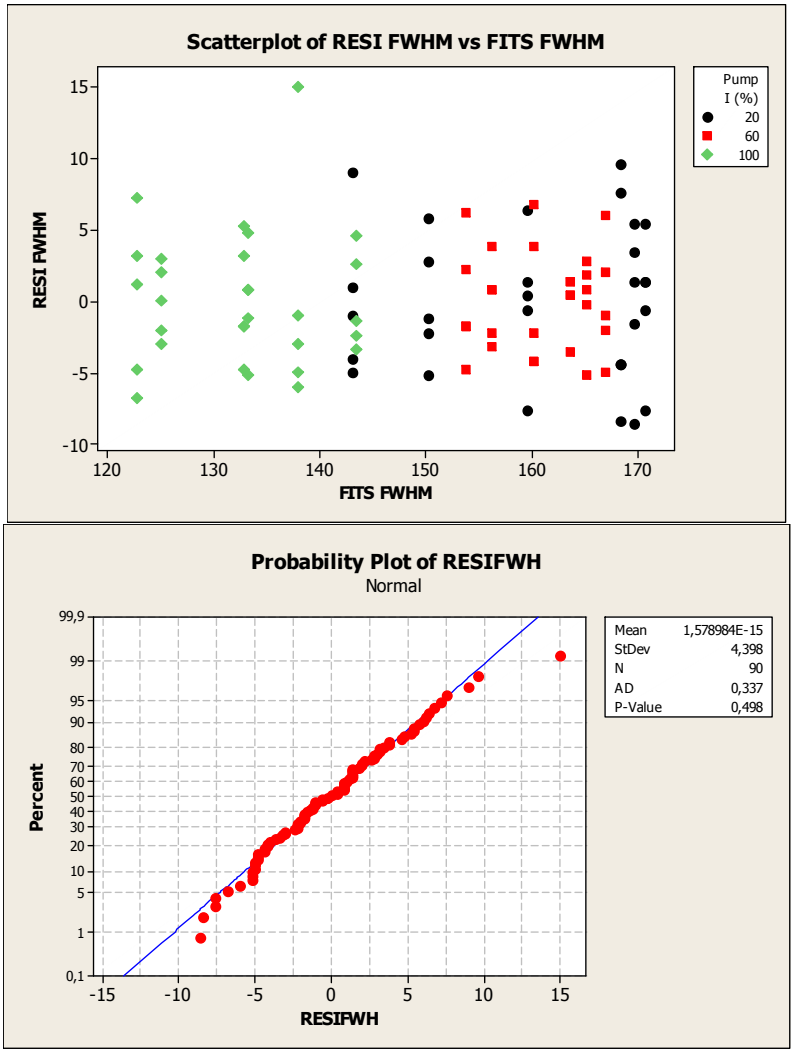

Figure 5.27: residual and normality plot for ANOVA test; pulse width (FWHM) 3 level of power and frequency

The residuals plot connote non normal error distributions is not observed and most of the points lie near zero value above and below.

It is also observed the IPG Photonics YLP-50 fiber laser source posses pulse width in the region of 120ns which is in agreement with the specification by the manufacturers. It should also be reminded the uncertainty of measurement and copper 'mirror' used.

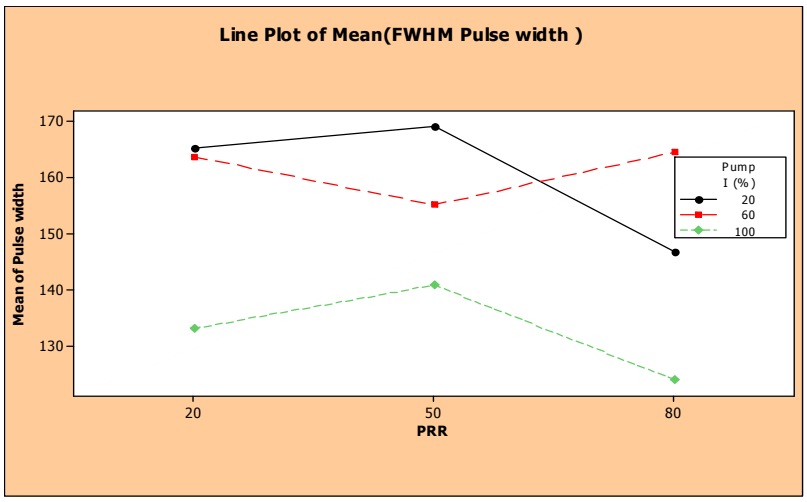

Figure 5.28: calibration curves for laser pulse FWHM

It is important to remember the behavior study is performed for solid state diode pumped fiber laser where pulsing is defined by an intra-cavity Q-switch element that is acusto optic controlled. In this case, pulse duration, pulse frequency and pulse energy are governed by a carefully tuned and balanced switching system and consequently, adjusting one of the pulse parameters often impacts other parameters. For example, changing PRR or pulse width would unavoidably lead to changes in pulse peak power (Single pulse average power, $P_H = {P_{av}}/{(PRR * \tau_H)}$) or pulse shape.

Increase in pumping power results average power of the pulses becomes higher in directly proportional way, and shorter pulse is achieved due to less number of resonation, if the effect of pulse repetition rate is not considered or assumed constant. But repetition rate has a significant roll to play in determining single pulse average power and pulse duration. At lower repetition rate, average pulse power becomes peaking because the pump has enough time between pulses to replenish the population inversion. Thus pulse width value is result of a combined effect between the reduced pulse repetition rate and the improved pulse average power. It is thereby

difficult to perform a concise study to evaluate and distinguish the effects of the pulse shape, peak power, and pulse energy on the process at hand.

Finally, the linear response behaviour and short rise time of the photodiode used for the experimentation could confirm well the measurement validity. One point worth to mention regarding the measurement of pulse width is the sensitivity of photodiode saturation and fast energy dissipation capability when pulsed laser source is measured. The detail performance measure and specification of Thorlabs FGA 10 is discussed in experimental setup chapter of this paper. It is worth mentioning that rise time of the photodiode in use FGA 10 is about 7 ns. It is important to remember the inherent 7 ns rise and fall time of the photodiode used especially from measurement of pulse width point of view where the variation in response to pulse frequency alteration is in the same range at constant power. Also dark current is one of the performance measures that concerns here since the pulse width is highly dependent of the fall time of the photodiode. Typical dark current value for FGA 10 photodiode is 25 nA as reported before which is quite low. But the use of alimentation circuit with 5 volt biasing can noise and push dark current up to 100 nA.

5.3 Drilling time

In this section result of the drilling time for commercial pure titanium with 1.5mm thickness is investigated with experimental approach. With 1.5mm thickness, it is both possible to obtain through hole and drilling time that enables spectroscopic record that matches well good relative intensity and integration time. The resulting signal from photodiode is processed and drilling time was computed for ten sample holes performed at 100% pump current and 50 kHz pulse repetition rate. As It has been mentioned in the experimental setup chapter, drilling time is the difference between the time photodiode begin to receive laser beam and the laser source begin to emit beam. Transient delay of trigger and rise time for laser power at 100% current and 50 kHz is considered during calculation.

The signal from photodiode proves the laser beam passes out through hole and it is proved it is actually the laser beam by checking the pulse frequency exactly matches with the presetted laser one. It is possible to observe the temporal behavior of the signal indicating a gradually increasing intensity of laser power measured by photodiode. This is due to the fact a complete through hole formation takes a couple of more pulses after breakthrough. Consequently as bottom diameter of the drilled hole increases it exposes wider area of the photodiode that leads to uniform and normal laser pulse acqusition.

Hole	1	2	3	4	5	6	7	8	9	10
t_d (ms)	306.7	331.8	334.9	330.0	327.3	313.9	335.4	296.7	301.6	298.66
Mean						317.7				
Stdv						15.82761				
Mean + 2*Stdv						349.4				

Table 5.13: Summery of drilling time for 1.5 mm CP Titanium at 100% current and 50 KHz

The drilling time result for measurement of cp titanium which is 1.5 mm thickness considering the ten samples with mean plus two times of standard deviation is found to be 350 ms.

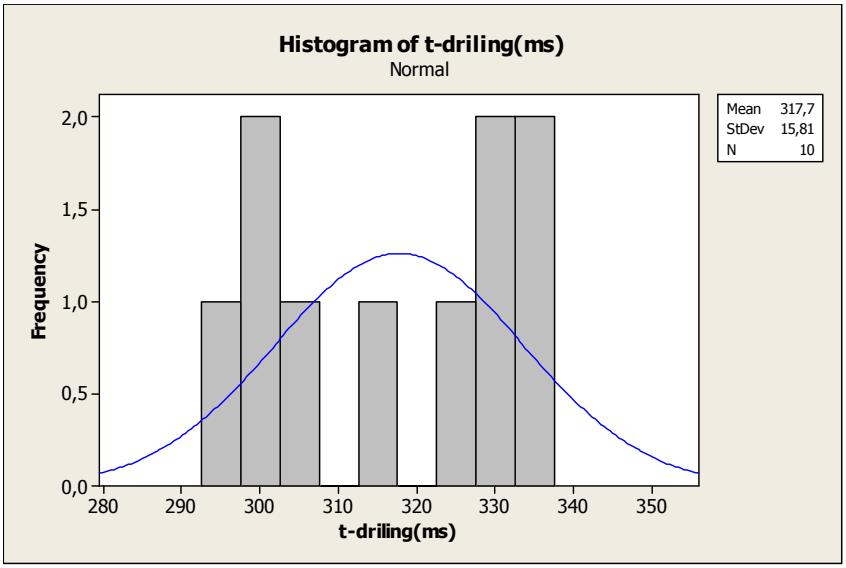

Figure 5.29: Drilling time for 1.5 mm cp Titanium at 100% current and 50 kHz

5.4 Optical emission spectroscopy

5.4.1 Temporal evolution of LIP

The physical characterization of LIP is performed on five spectra for every micro drilled hole and is repeated for the five times. Each of the five spectra belongs to a different portion of the LIP temporal distribution and represents time evolution. The maximum intensity of the spectral lines represents the most populated section of the LIP. It is observed that as consequence of the high ionization degree, for the most part of spectra the ionic lines are proportionally more intense than those of the atoms. At the tails of the temporal distribution of the LIP line intensities, which corresponds to the colder part of the plasma, it is possible to observe the disappearance of ionic lines, and the fact most of titanium emission lines are congested near UV wavelength.

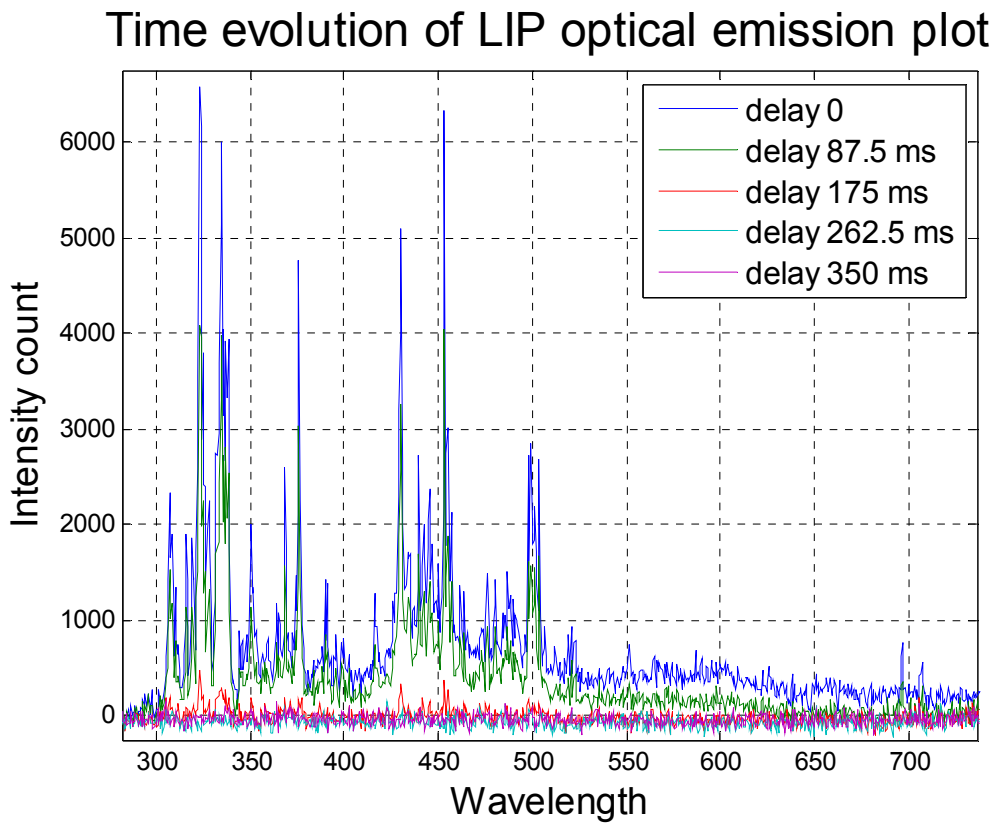

Figure 5.30: Temporal evolution of portion of LIP spectra of Ti in Argon medial with time resolution of 87.5ms (gate width)

A number of characteristic titanium lines are observed and interpreted as emission from the excited neutral atoms and from single-charged ions Ti I and Ti II. It is observed there is continues fall down in amplitude of relative intensity indicating the decrease in population density of emission. This is associated to the amount of light intensity reaching collimator and heading to spectrometer. As the process of drilling

keeps moving down through the thickness of the specimen, it gets more difficult to reflect on the inside wall of the hole and get out to be collected by collimator. Afterwards, continues decrease in intensity is end up with almost non emission of spectra at the delay time of 350ms. This is interesting point to note down because it is in perfect agreement with the drilling time measurement performed in the previous section 2.3. Once the drilling process is finished and there is a through hole, there is no optical emission of Titanium from specimen.

Schematic 3D- plot (wavelength, count, time) for temporal evolution in figure 5.31 and a 2D-plot (count vs. time) at selected wavelength 325.6nm (emission spectra with relatively large intensity) agree with the above statements.

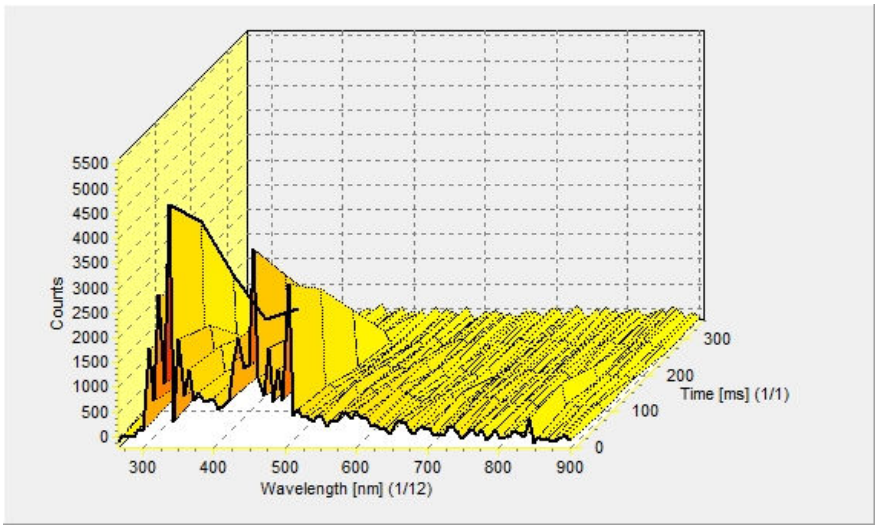

Figure 5.31: Schematic 3D- plot (wavelength, intensity, time) for temporal evolution LIP spectra of Ti in UV to Visible range

A substantially low intensity of emission is observed during the tail end of the drilling process in comparison to the beginning of the process. The lack of strength by emission lines after mid way of the drilling process is an indication for population density drop of the plume formed reaching spectrometer's collimator. Light which comes out from inside of the hole especially as drilling closes down to bottom surface of specimen gets lesser and lesser. Though it has been observed after Boltzmann plot method approach though that atomic temperature computed is at similar level in all the drilling process.

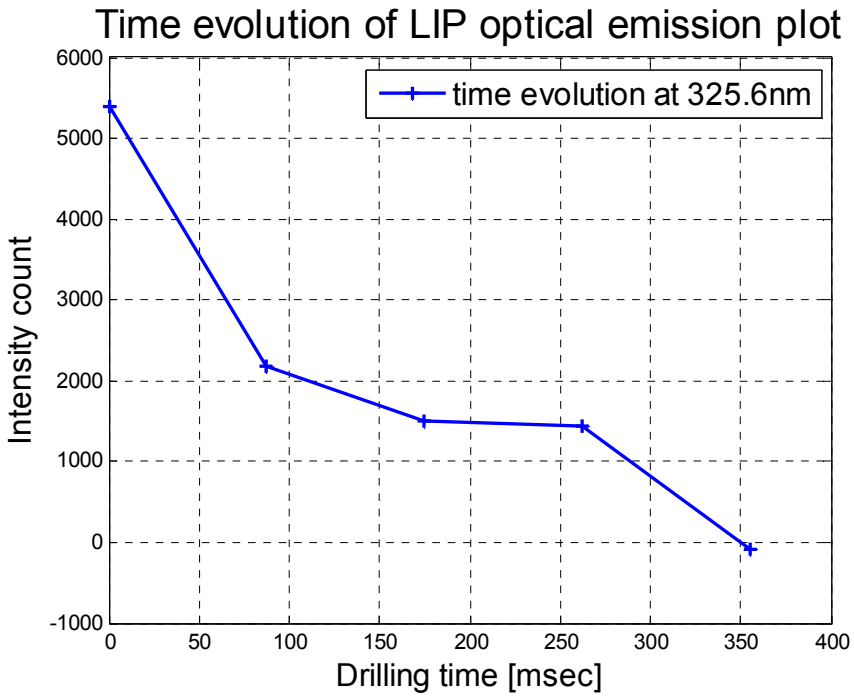

Figure 5.32a): Sample Schematic 2D- plot (time, intensity) for temporal evolution LIP spectra of Ti at 325.6 nm

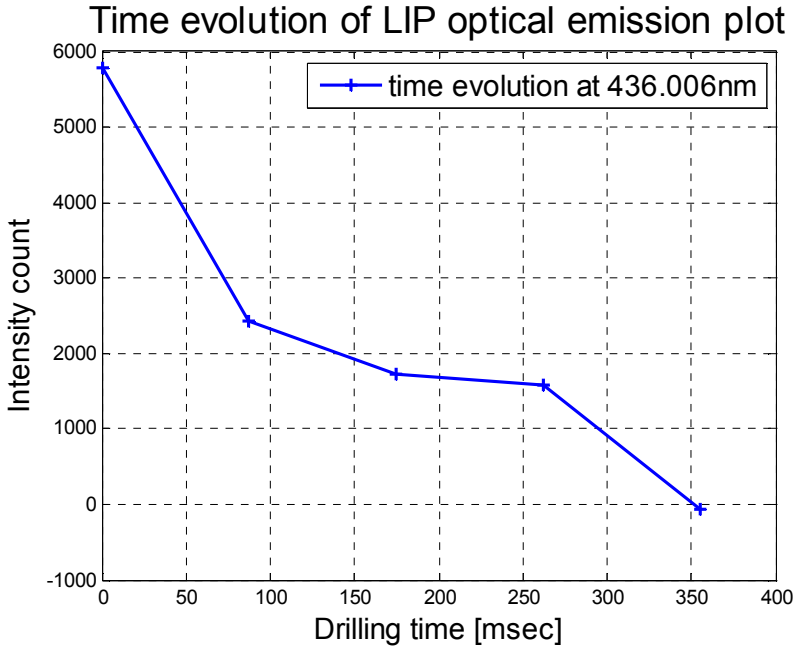

Figure 5.32 b): Sample Schematic 2D- plot (time, intensity) for temporal evolution LIP spectra of Ti at 436.006 nm

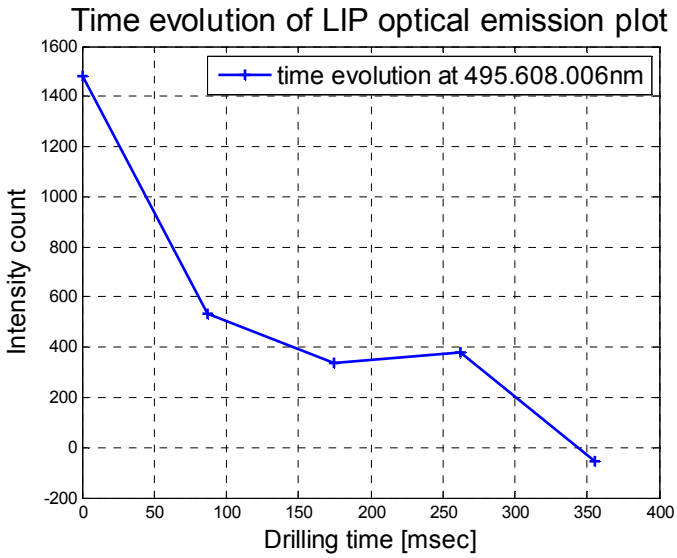

Figure 5.32.c): Sample Schematic 2D- plot (time, intensity) for temporal evolution LIP spectra of Ti at 495.608 nm

Justification for identical temporal behaviour of drilling process and measurement setup is shown with the graphs shown from 'a' to 'c' of figure 5.32. The trend is more or less the same independent of the wavelength observed.

5.4.2 LIP temperature

In this section analysis of acquired spectroscopic spectra for the determination of atomic temperature of LIP is presented. The first part focuses on result of Lorentzian fitted TI I spectra which are chosen and presented in experimental design section. Afterwards result of BPM computation is followed for each temporal evolution zone (scan) of micro drilling. The method is repeated for the five holes drilled during the experiment.

It is discussed in the experimental design section for OES that the Lorentzian fit modelling is needed for Ti I emission at 429.576 nm only with the others clearly pin-point able with no resolution problem. The result for Lorentzian curve fitting coefficients at this wavelength is tabulated on table 5.14.

	y_o	A	x_o	B	*Intensity (count)*
Scan 1	1827.3	8600.7	429.97	0.92081	9360
Scan 2	822.49	2691.2	429.99	0.643	3870
Scan 3	513.2	2677.6	429.97	0.9064	2888
Scan 4	684.92	1500.7	429.97	0.508	2744

Table 5.14: Lorentzian fit coefficients and intensity count at 429.576 nm

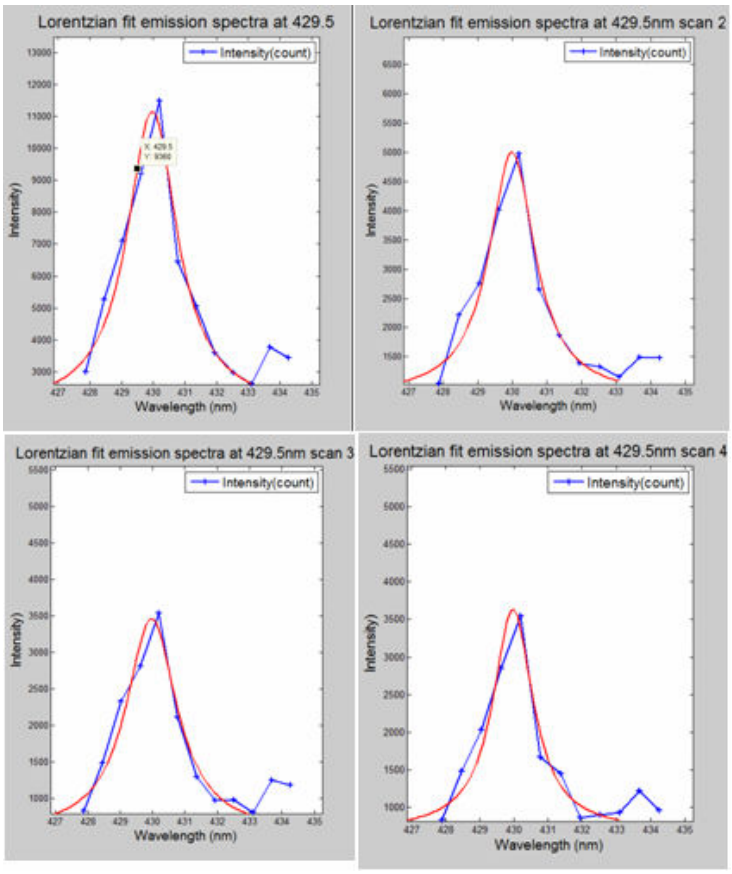

Figure 5.33: comparison between the raw data from spectrometer with resolution of 0.586 with a Lorentzian fit equivalent plot

It is shown in figure 5.32 and discussed that the evolution of intensity with time is continuously falling down. It is also observed at the fifth spectra the intensity is too low that makes the identification of emission lines difficult. For this reason , it is not included in computation of BPM method for atomic excitation temperature.

With a careful implementation utilizing the largest upper energy level and clearly spaced spectral lines, the graphical method (BPM) deliver excellent result with R^2 value of 98.1% for four spectrum of Ti I in use. Below is compiled summary of result for atomic excitation temperature computation for one of the five sample holes .

	Ek [cm^{-1}]	*Y_calculated*	*Y_best fit*	*Error*	*slope*	*Atomic T [K^0]*
Scan 1	29829.1	-23.9934	-24.131	-0.137547	-0.000156	4018.65
	41039.9	-25.659	-25.8745	-0.215495		
	37555.02	-25.6678	-25.3325	0.33528		
	20006	-22.621	-22.6032	0.017762		
Scan 2	29829.1	-24.8331	-24.9944	-0.16135	-0.000162	3865.27
	41039.9	-26.6362	-26.8072	-0.170911		
	37555.02	26.5388	-26.2437	0.295166		
	20006	-23.4432	-23.4061	0.0370949		
Scan 3	29829.1	-25.1716	-25.3096	-0.138066	-0.000166	3766.69
	41039.9	-26.9004	-27.1698	-0.269378		
	37555.02	-26.9917	-26.5916	0.400154		
	20006	-23.687	-23.6797	0.00729056		
Scan 4	29829.1	-25.1713	-25.3286	-0.157253	-0.000163	3838.21
	41039.9	-26.9358	-27.1541	-0.218345		
	37555.02	-26.9364	-26.5866	0.349727		
	20006	-23.7549	-23.729	0.0258718		

Table 5.15: summary for BPM sample hole physical parameters and atomic temperature of LIP with time (four Ti I spectra in use)

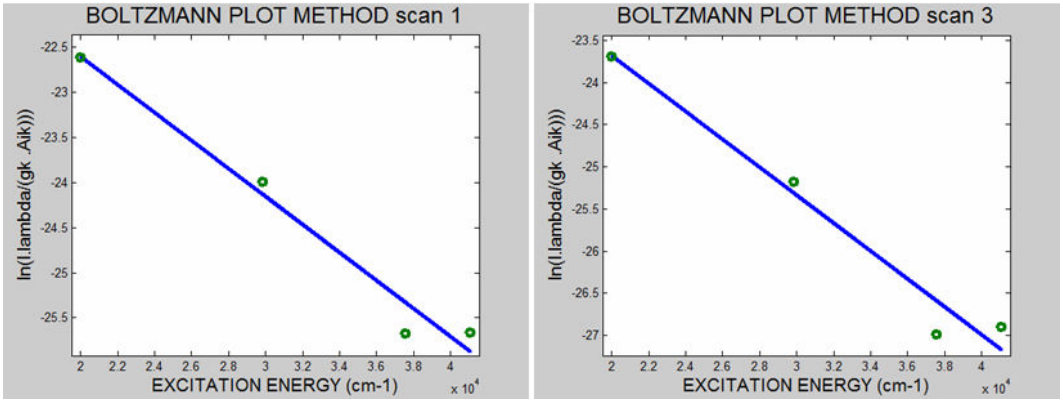

Figure 5.34: BPM result for graphical estimation of temperature from three Ti I emission spectra (note only BPM plot for scan 1 and scan 3 are presented here)

It is inferred from the obtained atomic excitation temperature that the mean process temperature during micro drilling of titanium with the fiber laser source under study (Fiber laser YLP-50, nominal power 50 watt with pulse duration in nano second regime) is in the order of 4000 K. As it has been mentioned in section 2.2.2 complete ionization of plasma plume can not exist at this condition of temperature which is less that 5000 ^{0}C. Rather, partially ionized plasma is formed.

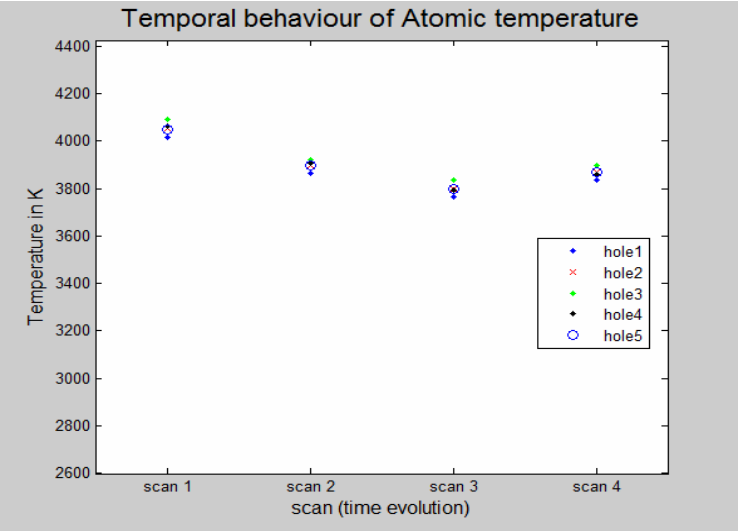

Figure 5.35: temporal behaviour of atomic temperature during drilling process using four Ti I spectra for the five micro drilled holes

Table 5.16 summarizes BPM atomic excitation temperature result computed for the five sample micro holes drilled. The five times replicates of the experiment indicated the result is consistent and the experiment is rigorous. Average value of excitation temperature is also reported in the table.

	Temperature in K			
	Scan 1	Scan 2	Scan 3	Scan 4
Hole 1	4018.65	3865.27	3766.69	3838.21
Hole 2	4054.55	3897.35	3798.52	3871.26
Hole 3	4092.98	3921.45	3836.74	3897.52
Hole 4	4061.88	3909.15	3795.72	3859.6
Hole 5	4049.33	3896.15	3799.22	3870.49
Average	4055.478	3897.874	3799.378	3867.416

Table 5.16: Summary of atomic excitation temperature for the five holes with four Ti I

It has been discussed in experimental design section of OES that the four spectra lines are chosen based on the criteria they have a clear emission spectra free from delusion or recombination with other lines. The four of them have also delivered an excellent linear fitting for BPM for excitation temperature computation. Justifiably, the result obtained with three emission spectra is considered as the pre-eminent value to take as process temperature during micro drilling.

Characterizing the LIP and determination of atomic temperature during the drilling process reveal there exist a slightly higher temperature at the beginning of the drilling process followed by a more or less constant temperature distribution in other temporal zones. The higher temperature obtained at the beginning of the process is an indication for formation more LIP on top surface of the specimen. Accordingly, formation of spatter is eminent and expected. More plasma means higher temperature and effectiveness of drilling process mitigated. It is well stated at the state of the art part of this work in laser micro drilling laser material interaction results with heating of the surface, increase local temperature and even form vaporization and LIP depending on process parameters irradiance and pulse width. The observation here agree with the fact that there exist maximum irradiance at the top surface of target material and nature of laser source pulse (in this case nano second regime). Generally speaking it can be understood from the physical property characterization result there is a uniform behavioural response during micro drilling titanium at the preset process parameters and the effectiveness of laser micro drilling is encouraging .

5.4.3 Electron density

Experimental results for electron density computation during micro drilling process are presented here. In agreement with the LTE assumption for the validity of the Boltzmann equation and atomic excitation temperature determination, the electronic density measured during the time evolution of the process is in higher order of $10^{16}cm^{-3}$. It is also observed that there is a drop in electron density from the beginning of plasma formation which leads to the conclusion of weakened excitation of ionic elements after the first laser material interaction process at the surface of specimen. The decrease of laser irradiance with thickness of titanium together with material behaviour is also a crucial factor.

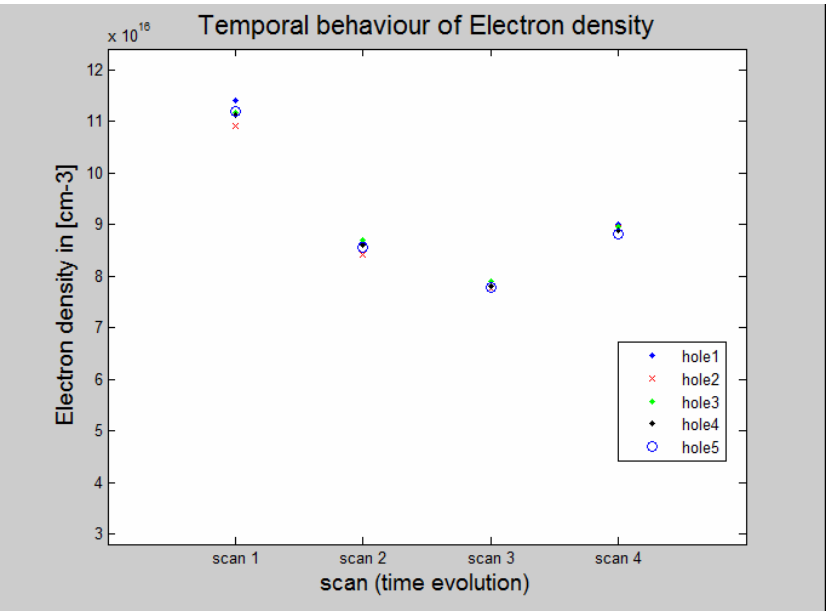

Figure 5.39: temporal behaviour of electron density drilling process

Average	Scan 1	Scan 2	Scan 3	Scan 4
N_e [cm^{-3}]	$1.1156*10^{17}$	$8.5852*10^{16}$	$7.807*10^{16}$	$8.91196*10^{16}$

The result for thermodynamic physical parameter electron density of LIP investigated during micro drilling of cp titanium reveal there is significantly large temporal change in electron density especially comparing the beginning of drilling and other portion of the process in the afore mentioned working condition. During the early stage of the drilling process, the electron density computed from Boltzmann Saha relation confirms the immediate reach of LTE which is well above $10^{16}cm^{-3}$. Later the effect of ionization and recombination of atomic and ionic spectra, together with variation in intensity with material thickness results to slight reduction in temperature as discussed above and a sudden drop in electron density from scan 1 to scan 2 indicating the expansion of laser induced plasma. Afterwards a distribution of electron density in the order of $10^{16}cm^{-3}$ with stable plasma density is observed.

Conclusions

The fiber laser source at SITEC lab of Politecnico Di Milano, YLP 50 IPG Photonics was implemented for the investigation of characterizing LIP using OES in this thesis work. The first part of the work focused on characterizing laser source and process parameters such as pulse width, rise time to nominal power (transient behaviour of power) and relation between process parameters pump current and pulse frequency is studied. A nano second regime minimum pulse width of the order 120 ns is obtained after rigorous experimental procedure. The result agrees very well with the theoretical knowledge and previous works on Q-switched short pulse laser sources. Performance of photodiodes to detect the laser beam using a copper surface as a mirror is tried to be as best as possible with the implementation of built alimentation circuit for better rise and fall time. With this configuration the Thorlabs FGA 10 photodiode performance is improved up to 7 ns rise and fall time. All the acquired signals are processed extensively with the help of Labview plotting and time axis identification technique for excellent accuracy of result. The transient behaviour is also investigated with the same technique of acquiring laser pulse from oscilloscope and processing using Labview and Matlab with results obtained in hundreds of micro second depending on laser processing parameter. Higher pumping current and pulse repetition rate resulted with better transient behaviour with a continuous improvement. It is understood micro drilling of thin sheet metals could substantially be affected with the slow transient behavior of the laser source especially during the beginning of the process.

Once the behaviour of the laser source is studied and drilling process time for specific thickness of the specimen is carried out, development of configuration for process characterization which suits with the characteristics of the system is carried out. As a result, optical emission spectroscopy (OES) that evaluate light emitted from laser source with specimen interaction was proposed as a solution which is suitable to characterise micro drilling physical parameters such as temperature and electron density for laser induced plasma.

With 1.5 mm thick specimen drilling time in the order of 350 ms was measured and this suited the possibility of measuring up to five spectra with reasonable emission intensity. The result show for laser process parameter at full power and technological

pulse frequency of 50 KHz, average process temperature is in the order of 4000 K using the Boltzmann plot method (BPM). The temporal distribution of temperature over the drilling process is also determined to observe thermodynamic physical characteristics of micro drilling titanium at the specified laser process parameters. It is found a slightly higher temperature is scrutinized at the beginning of the process and a nearly constant distribution over the other entire drilling. This is associated to availability of highest irradiance on top of surface and commencement of laser material interaction with no shielding effect of ionization for the laser beam. Accordingly, it is expected to have formation of spatter on top surface of specimen. All in all it is generalized the computation of atomic excitation temperature could led to understanding of good effectiveness of micro drilling at the experimental designed process parameters on titanium. In addition, analysis of emission spectra using the Boltzmann Saha relation revealed the assumption and implementation of equation with the basis of local thermodynamic equilibrium holds true thanks to the computed higher electron density value above 10^{16} cm^{-3} the agree with the literature review. OES method which is based on the formation of plasma or at least partial ionization state of excitation has delivered a good result; but still there is a challenge from laser-process brightness point of view which was a challenge in acquiring spectra for large delay time after drilling began especially towards end of the process.

At last, it is the suggestion of this thesis paper for further work to use the experimental setup and technique of evaluating physical parameters at various working condition, so that a correlation analysis can be designed to understand the system response of micro drilled hole quality at various process parameters of laser beam and drilling setup.

References

A. De Giacomo, M. Dell'Aglio, O. De Pascale, M. Capitelli (2007), From single pulse to double pulse ns-Laser Induced Breakdown Spectroscopy under water: Elemental analysis of aqueous solutions and submerged solid simples, Spectrochim.

A. De Giacomo (2002), Experimental characterization of metallic titanium-laser induced plasma by time and space resolved optical emission spectroscopy.

A. Ancona, D. Nodop , J. Limpert , S. Nolte, A. Tünnermann (2008) , Microdrilling of metals with an inexpensive and compact ultra-short-pulse fiber amplified microchip laser.

A. Semerok , C. Chaleard , V. Detalle, J.L. Lacour , P. Mauchien, P. Meynadier , C. Nouvellon , B. Salle, P. Palianov, M. Perdrix, G. Petite (2000), Experimental investigations of laser ablation efficiency of pure metals with femto, pico and nanosecond pulses.

Ancona, S. Döring, C. Jauregui, F. Röser, J. Limpert,1 S. Nolte, and A. Tünnermann (2009). Femtosecond and picosecond laser drilling of metals at high repetition rates and average powers.

Alexey M.Rodin, Joseph Callaghan and Niall Brennan. High Throughput Low CoO Industrial Laser Drilling Tool.

Annemie Bogaerts, Zhaoyang Chen (2005), Effect of laser parameters on laser ablation and laser induced plasma formation: A numerical modelling investigation.

B.S. Yilbas (2001), Parametric study for laser hole drilling of Inconel 617 alloy

C. Aragon, J.A. Aguilera (2008). Characterization of laser induced plasmas by optical emission spectroscopy: A review of experiments and methods.

C. Cuadrado-Laborde, M. Delgado-Pinar, S. Torres-Peiro, A. Dı´ez, M.V. Andre´s (2007). Q-switched all-fibre laser using a fibre-optic resonant acousto-optic modulator.

C.Y. Chien and M.C. Gupta (2004), Pulse width effect in ultra fast laser processing of materials.

Biffi C.A (2009), Micro drilling of Titanium with pulsed fiber laser: characterization of process and reduction of spatter, PhD thesis, Politecnico di Milano.

Chengde Li, S. R. Vatsya, and S. K. Nikumb (2006), Effect of plasma on ultra short pulse laser material processing

Collin E. Webb (2005). Hand book of laser technology and applications, Book.

D.K.Y. Low, L. Li, A.G. Corfe, P.J. Byrd (2000) Spatter-free laser percussion drilling of closely spaced array holes.

Ferrara M, Ancona A, Lugara PM, Sibilano M (2000), On-line quality monitoring of welding processes by means of plasma optical spectroscopy.

G.P. Pinho, H. Schittenhelm,W.W. Duley, S.A. Schlueter, H.R. Jahani, R.E. Mueller (1999), Energy distributions in the laser ablation of metals and polymers.

Griem HR.(1997) Principles of plasma spectroscopy. Cambridge: Cambridge University Press.

H.C. Man, Q.Wang, X.Guo (2009). Laser surface micro drilling of Ti and laser gas nitrided Ti for enhancing fixation of dental implants.

H.R. Griem (1997), Plasma Spectroscopy.

http://physics.nist.gov/PhysRefData/ASD/lines_form.html,NIST Atomic Spectra Data base Lines Form 2009 (last visited October 4,2010)

http://www.thorlabs.us, home page of Thorlabs optics (last visited October 4, 2010)

J. Hermann, C. Boulmer-Leborgne, D. Hong (1998), Diagnostics of the early phase of an ultraviolet laser induced plasma by spectral line analysis considering self absorption.

J. Limpert, N. Deguil-Robin, S. Petit , I. Manek-Ho¨ nninger, F. Salin, P. Rigail, C. Ho nninger, E. Mottay (2005). High power Q-switched Yb-doped photonic crystal fiber laser producing sub-10 ns pulses.

J. Meijer, K. Du, A. Gillner, D. Hoffmann, V.S. Kovalenko, T. Masuzawa, A. Ostendorf, R. Poprawe, W. Schulz , Laser Machining by short and ultra short pulses, state of the art and new opportunities in the age of the photons.

J. Mirapeix , A. Cobo, O.M. Conde , C. Jau´regui, J.M. Lopez-Higuera (2005), Real-time arc welding defect detection technique by means of plasma spectrum optical analysis.

James T. Luxon, David E. Parker (1985). Industrial Lasers and Their Applications, Book

K. F. Kleine and K. G. Watkins (2004). Pulse Shaping for Micro Cutting Applications of Metals with Fiber Lasers.

L.Li, D.K.Y.Low and M.Ghoreshi (2007) . Hole Taper Characterization and Control in Laser Percussion Drilling.

M. Capitelli, A. Casavola, G. Colonna, A. De Giacomo (2003), Laser-induced plasma expansion: theoretical and experimental aspects.

M. Delgado-Pinar, D. Zalvidea, A. Díez, P. Pérez-Millán and M. V. Andrés (2006). Q-switching of an all-fiber laser by acousto-optic modulation of a fiber Bragg grating.

M. Keith Hudson, Robert B. Shanks, Dallas H. Snider. UV, visible, and infrared spectral emissions in hybrid rocket plumes.

M. Peters, J. Hemptenmacher, J. umpfert and C. Leyens (2003), Structure and Properties of Titanium and Titanium Alloys

Nikolai V. Tkachenko (2005), Optical Spectroscopy Methods and Instrumentations [Book].

P. Bassani, E. Capello, C. Gallus, E. Gariboldi, L. Longoni, B. Previtali (2004). Relevant geometric features in the percussion laser micro drilling of different alloys.

P W French, D P Hand, C Peters, G J Shannon, P Byrd, W M Steen (1999), Investigation of the Nd:YAG laser percussion drilling process using high speed filming

R. Biswas, A.S.Kuar, S.Sarkar, S.Mitra (2009). A parametric study of pulsed Nd:YAG laser micro-drilling of gamma-titanium aluminide.

Rudiger Paschotta (2008). Encyclopedia of laser physics and technology, Book.

S. Conesa, S. Palanco and J. J. Laserna (2004), Acoustic and optical emission during laser-induced plasma formation

S. Döring, A. Ancona, S. Hädrich, J. Limpert, S. Nolte A. Tünnermann (2010). Micro drilling of metals using Femto second laser pulses and high average powers at 515 nm and 1030 nm.

Sang-Ho Nam and Young Jo Kim (2001), Excitation temperature and electron number density measured for end-on-view inductively coupled plasma discharge.

S. Pandhija and A.K. Rai (2008), In situ multi elemental monitoring in coral skeleton by CF-LIBS.

S. Petzoldt, J. Reif, E. Matthias 1995, Laser plasma threshold of metals.

Sami T. Hendow and Sami A. Shakir (2010). Structuring materials with nanosecond laser pulses.

T. Sibillano, A. Ancona, V. Berardi , P.M. Lugara (2004), Correlation analysis in laser welding plasma.

Taras V Kononenko, D Walter, Vitalii I Konov and F Dausinger (2009). Interaction of laser radiation with matter laser plasma.

Valentin Gapontsev and William Krupke (2002), Laser Focus World.

W. Sdorra, K. Niemax (1992), Basic investigations for laser micro analysis: III. Application of different buffer gases for laser-produced sample plumes.

William F. Krupke (2000). Ytterbium Solid-State Lasers—the First Decade.

X. Zhu, A.Yu. Naumov, D.M. Villeneuve, P.B. Corkum (1999). Influence of laser parameters and material properties on micro drilling with Femto second laser pulses.

APENDIX I: OFF-axis ON focus measurement rise time and number of pulses before t_r results

FACTOR		time to trigger (micros)	max signal Amp (Volt)	time to reach max(μs)	Rise time*	No of pulses	Remark
Pump current	PRR						
20	20	280,1359921	3,4920	1.778,2020	1498,07	31	
20	20	280,1359921	3,4200	1.844,9639	1564,83	31	
20	20	280,1359921	3,4200	1.877,0399	1596,90	32	
20	20	280,1359921	3,4920	1.836,4499	1556,31	31	
20	20	280,1359921	3,4920	1.918,9239	1638,79	32	
20	50	280,1359921	3,6360	639,3140	359,18	18	
20	50	280,1359921	3,6360	641,7100	361,57	18	
20	50	280,1359921	3,6360	648,7300	368,59	19	
20	50	280,1359921	3,6720	641,5140	361,38	18	
20	50	280,1359921	3,6360	652,7080	372,57	19	
20	80	280,1359921	3,3840	576,9380	296,80	24	
20	80	280,1359921	3,3480	577,3080	297,17	24	
20	80	280,1359921	3,3480	582,069984	288,97	24	
20	80	280,1359921	3,3480	569,1040	312,73	24	
20	80	280,1359921	3,3480	592,8700	312,73	25	
60	20	280,1359921	3,8160	768,6340	488,50	10	
60	20	280,1359921	3,4200	722,8320	442,70	10	
60	20	280,1359921	3,4200	772,3000	492,16	10	
60	20	280,1359921	3,4920	776,4620	496,33	10	
60	20	280,1359921	3,4920	758,1440	478,01	10	
60	50	280,1359921	3,4200	484,4000	204,26	10	
60	50	280,1359921	3,4200	451,5480	171,41	9	
60	50	280,1359921	3,3840	453,4960	173,36	9	
60	50	280,1359921	3,3840	453,5000	173,36	9	
60	50	280,1359921	3,3480	454,8280	174,69	9	
60	80	280,1359921	2,2500	461,1720	181,04	14	*
60	80	280,1359921	2,2500	462,1580	182,02	14	
60	80	280,1359921	2,2500	484,8060	204,67	15	
60	80	280,1359921	2,2500	475,2100	195,07	15	
60	80	280,1359921	2,2500	475,8400	195,70	15	
100	20	280,1359921	3,6720	493,7780	213,64	5	**
100	20	280,1359921	3,6360	478,3520	198,22	5	
100	20	280,1359921	3,6360	462,9660	182,83	5	
100	20	280,1359921	3,6360	488,5680	208,43	5	
100	20	280,1359921	3,6360	465,4760	185,34	5	
100	50	280,1359921	3,7080	372,9360	92,80	5	
100	50	280,1359921	3,7440	363,8460	83,71	5	
100	50	280,1359921	3,6000	371,7280	91,59	5	
100	50	280,1359921	3,5280	367,2140	87,08	5	
100	50	280,1359921	3,4920	372,9360	92,80	5	
100	80	280,1359921	2,5000	388,4180	108,28	8	***
100	80	280,1359921	3,1680	375,8140	95,68	8	
100	80	280,1359921	3,1680	373,6960	93,56	8	
100	80	280,1359921	3,0960	373,5060	93,37	8	
100	80	280,1359921	3,2400	387,2920	107,16	8	

Remark: * Spark observed, signal speak, PD position tilted approximately 15 degree horizontally
** Spark observed
*** A very pronounced spark with considerable pulse amplitude variation, material drilled

APENDIX II:OFF-axis OFF focus measurement rise time and number of pulses before t_r results

FACTOR		time to trigger (µs)	max signal Amp (Volt)	time to reach max(µs)	Rise time(µs)*	No of pulses	Remark
Pump current	PRR						
20	20	280,1359921	3,4560	1.863,3199	1583,18	32	
20	20	280,1359921	3,4920	1.970,8319	1690,70	33	
20	20	280,1359921	3,4560	1.956,4439	1676,31	33	
20	20	280,1359921	3,4560	1.920,4119	1640,28	32	
20	20	280,1359921	3,4560	1.949,5159	1669,38	33	
20	50	280,1359921	3,6720	622,2560	342,12	17	
20	50	280,1359921	3,6720	608,8880	328,75	17	
20	50	280,1359921	3,6720	598,3580	318,22	17	
20	50	280,1359921	3,6720	632,2780	352,14	17	
20	50	280,1359921	3,6720	620,6240	340,49	17	
20	80	280,1359921	3,3120	563,3380	283,20	23	
20	80	280,1359921	3,3480	578,2780	298,14	23	
20	80	280,1359921	3,3120	577,4240	297,29	23	
20	80	280,1359921	3,3120	581,5960	301,46	23	
20	80	280,1359921	3,3480	559,9260	279,79	23	
60	20	280,1359921	3,7440	620,2980	340,16	8	
60	20	280,1359921	3,7080	660,3920	380,26	9	
60	20	280,1359921	3,7080	655,2320	375,10	9	
60	20	280,1359921	3,7440	571,4600	291,32	7	
60	20	280,1359921	3,7440	606,8740	326,74	8	
60	50	280,1359921	3,6360	411,9600	131,82	7	
60	50	280,1359921	3,6360	421,8140	141,68	7	
60	50	280,1359921	3,6720	419,8020	139,67	7	
60	50	280,1359921	3,6360	410,2060	130,07	7	
60	50	280,1359921	3,6720	403,9820	123,85	7	
60	80	280,1359921	3,3840	415,7900	135,65	10	*
60	80	280,1359921	3,3840	426,7200	146,58	10	
60	80	280,1359921	3,3480	425,9840	145,85	10	
60	80	280,1359921	3,3480	402,4480	122,31	9	
60	80	280,1359921	3,3480	416,7140	136,58	10	
100	20	280,1359921	3,8160	462,2040	182,07	4	**
100	20	280,1359921	3,7800	492,9160	212,78	5	
100	20	280,1359921	3,7440	480,9980	200,86	5	
100	20	280,1359921	3,8160	518,6320	238,50	5	
100	20	280,1359921	3,8160	487,1920	238,50	5	
100	50	280,1359921	3,7440	365,0300	84,89	4	
100	50	280,1359921	3,7440	365,0260	84,89	4	
100	50	280,1359921	3,7440	344,7940	64,66	4	
100	50	280,1359921	3,7440	342,8620	62,73	4	
100	50	280,1359921	3,7080	344,4140	64,28	4	
100	80	280,1359921	3,3840	346,5260	66,39	5	***
100	80	280,1359921	3,3840	339,9660	59,83	5	
100	80	280,1359921	3,3840	345,1900	65,05	5	
100	80	280,1359921	3,3840	345,6360	65,50	5	
100	80	280,1359921	3,3840	345,2000	65,06	5	

Remark: * Spark observed, signal speak, PD position tilted approximately 15 degree horizontally
** Spark observed
*** A very pronounced spark with considerable pulse amplitude variation, material drilled

APENDIX III …Matlab m-file Boltzmann plot method

```
%%%%%%%%%%%%%%%%%%%%%%%%%%%%%%%%%%%%%%%%%%%%%%%%%%%%%%%%%%%%%%%%%%%%%%%%%%%%
%this program analyses spectroscopic emission data for the
determination of
%     *  visualizing the spectral emission wavelenght Vs Intensity
count plot
%     *  Indentify the relative peak amplitude wavelength and their
%        corresponding intensity
%     *  determination of atomic excitation temperature, and IONIC
excitation temp using BOLTZMANN
%        method
%     *  Compute Electron number density using Saha equation


close all;
clear all;
clc;

fn1= 'xls hole.xls';
a= xlsread(fn1);

wave_length = a(7:1640,1); %%load wavelength range observed with the
spectrometer resolution
Intensity_count= a(7:1460,2); %%%load corresponding intensity


%%%%Normalization for row spectrum
summ=sum(Intensity_count*0.586);
for i=1:length(wave_length)
    normal_intensity(i)=Intensity_count(i)*0.586/summ;
end

%%%%%%%%%%%%%%%%%%%%%%%%%%%%%%%%%%%%%%%%%%%%%%%%%%%%%%%%%%%%%%%%%%%%%%%%%%%%

        plot(wave_length,Intensity_count,'-r')
        h_legend = legend('Intensity(count)');
        h_title = title('Spectroscopic line emission Normalized
plot');
        h_xlabel = xlabel('Wavelength');
        h_ylabel = ylabel('Normalized Intensity)');
        set(h_legend,'FontSize',14);
        set(h_title,'FontSize',18);
        set(h_xlabel,'FontSize',14);
        set(h_ylabel,'FontSize',14);
        grid
        h = findobj(gcf,'type','line');
        set(h,'linewidth',1);

display('Selected emission spectral lines with peak intensity')
[wavelength,intensity] = ginput2

%%%%%%%%%%%%%%%%%%%%%%%%%%%%%%%%%%%%%%%%%%%%%%%%%%%%%%%%%%%%%%%%%%%%%%%%%%%%
%%%%
nI=3; %number of considered Titanium I spectra

wl_I= 10^-9*[429.576  439.392 503.995]; %%%wavelength in nano meters
g_I= [1 11 5];
```

```
Aij_I=10^8*[1.3 0.33  0.0389];
Ej_I= [29829.097 41039.874 20006.032]; % upper ionization energy in
[cm-1]

for k=1:nI
Y1(k)=log((intensity(k)*wl_I(k))/(g_I(k)*Aij_I(k)));
end

fprintf('   Observed ATOMIC transition spectral lines are %2.0f \n',
nI');
fprintf('\n');
fprintf('\n');



%PART FOR LINEAR FITTING, PLOTTING AND EXCITATION TEMPERATURE
COMPUTATION
coef1 = polyfit(Ej_I,Y1,1); % Least-squares fit for a linear model
m1 = coef1(1); % m1 = the slope of the curve: y = mx + b
b1 = coef1(2); % b1 = the intercept on y-axis
ybest1 = m1*Ej_I + b1; % m1 and b1 are used to compute the best fit
line
fprintf('\n');
M = 2; % Number of fit parameters (M=2 is a linear curve)
sum_sq = sum((Y1 - ybest1).^2); % The sum of squares of deviations
fprintf('\n'); fprintf('\n');
fprintf('Summary of Experimental Data ATOMIC spectra : \n\n');
for i=1:length(wl_I)
fprintf('       Ionization Energy = %g cm-1,  ln((I*lamda)/gi*Aij) =
%g [], \n',Ej_I(i),Y1(i));
end
fprintf('\n');
fprintf('       Summary of Best Fit ATOMIC line (Least Squares):
\n\n');

for i=1:length(wl_I)
fprintf('       ln((I*lamda)/gi*Aij)best = %g [],
ln((I*lamda)/gi*Aij) = %g [],  ln((I*lamda)/gi*Aij)best -
ln((I*lamda)/gi*Aij) = %g [] \n',ybest1(i),Y1(i),ybest1(i)-Y1(i));
end

fprintf('\n');
fprintf('       The slope from ATOMIC spectra line is:    = %10.6f
\n', m1);
T_exi = fprintf('       corresponding Temperature = %10.6f \n', -
0.625/m1);
```

```
%%%%%%%%%%%%%%%%%%%%%%%%%%%%%%%%%%%%%%%%%%%%%%%%
% Statistical summary:
fprintf('\n');
fprintf('N = number of data points: %3.0f\n',nI);
fprintf('\n');
fprintf('\n');
fprintf('\n');

disp ('Strike any key to display BOLTZMANN plot METHOD ATOMIC...')
pause
fprintf('\n'); fprintf('\n');

% h = findobj(gcf,'type','line');
% set(h,'linewidth',2);

figure(2)

        plot(Ej_I,ybest1,Ej_I,Y1,'o')

        h_title = title('BOLTZMANN PLOT METHOD scan 4');
        h_xlabel = xlabel('EXCITATION ENERGY (cm-1)');
        h_ylabel = ylabel('ln(I.lambda/(gk .Aik))');
        set(h_title,'FontSize',18);
        set(h_xlabel,'FontSize',14);
        set(h_ylabel,'FontSize',14);
        axis([min(Ej_I)-500,max(Ej_I)+500,min(Y1)-0.25,max(Y1)+0.25])
h = findobj(gcf,'type','line');
set(h,'linewidth',3);
```

APENDIX IV …Matlab m-file Saha -Boltzmann electron density method

```
%%%%%%%%%%%%%%%%%%%%%%%%%%%%%%%%%%%%%%%%%%%%%%%%%%%%%%%%%%%%%%%%%%%%%%%%%%%%
%%%%%%%%%%%%
%this program analyses spectroscopic emission data for the
determination of
%     *  visualizing the spectral emission wavelenght Vs Intensity
count plot
%     *  Indentify the relative peak amplitude wavelength and their
%        corresponding intensity
%     *  determination of atomic excitation temperature, and IONIC
excitation temp using BOLTZMANN
%        method
%     *  Compute Electron number density using Saha equation
close all;
clear all;
clc;

fn1= 'xls hole.xls';
a= xlsread(fn1);

wave_length = a(100:454,1); %%load wavelength range observed with
the spectrometer resolution
Intensity_count= a(100:454,17); %%%load corresponding intensity

summ=sum(Intensity_count*0.586);
for i=1:length(wave_length)
    normal_intensity(i)=Intensity_count(i)*0.586/summ;
end
        plot(wave_length,Intensity_count,'-r')
        h_legend = legend('Intensity(count)');
        h_title = title('Spectroscopic line emission Normalized
plot');
        h_xlabel = xlabel('Wavelength');
        h_ylabel = ylabel('Normalized Intensity)');
        set(h_legend,'FontSize',14);
        set(h_title,'FontSize',18);
        set(h_xlabel,'FontSize',14);
        set(h_ylabel,'FontSize',14);
        grid
        h = findobj(gcf,'type','line');
        set(h,'linewidth',1);



display('Selected ATOMIC then IONIC emission spectral lines with
Intensity')
[wavelength,intensity] = ginput2

wl= 10^-9*[429.576  376.132]; %%%wavelength in nano meters
g= [1 6];
Aij=10^8*[1.3 0.99];
Ej= [29829.097 31207.42]; % upper ionization energy in [cm-1]
```

```
me=0.51099891*10^6/(2.9*10^8)^2; %%mass of electron in [eV]
h=4.13566733*10^(-15); %% planks constant [eVs]
Kb= 8.61743*10^(-5); %% Boltzmann constant [eVk-1]
AA=2*pi*me*Kb/h^2;
I_ratio = (Intensity_count(1)/Intensity_count(1)); % ratio between
ATOMIC and IONIC intensity at selected wavelenghts
C1=(2*pi*me*Kb/h^2)^(3/2); %inverse of Thermal de Broglie wavelength
C2 = ((g(2)*Aij(2)*wl(2))/(g(1)*Aij(1)*wl(1)));
delta_Eion = abs(Ej(2)-Ej(1));

T1=4226.1;
T2=4131.97;
T3=4097.44;
T4=4144.83;

E1 = exp((1/8065.5447)*(delta_Eion-Ej(2))/(Kb*T4));
E2 = exp((1/8065.5447)*(Ej(1)-Ej(2))/(Kb*T4));

ne = I_ratio*2*C1*C2*(T4/11604.505)^(3/2)*E1*E2; % computation of
Electron density

fprintf('\n');
fprintf('ne = Electron Number Density: %3.0f\n',ne);
```

APENDIX VA: Titanium I emission spectra and physical parameters (source: NIST 2009)

Observed Wavelength (nm)	Rel. Int	Aik (10^8)	E_i (cm^{-1})	Ek (cm^{-1})	g_k
320.383	240	7.2e-02	170.132	31 373.801	7
321.424	260	6.5e-02	386.874	31 489.451	9
334.188	5700	6.5e-01	0	29 914.720	7
335.294	120	9.7e-03	170.132	29 986.185	7
335.464	4100	6.9e-01	170.132	29 971.078	9
335.828	290	7.6e-02	0	29 768.655	5
337.044	1100	7.6e-01	0	29 661.232	3
337.145	4300	7.2e-01	386.874	30 039.211	11
337.748	2900bl	6.9e-01	170.132	29 768.655	5
337.922	290	6.2e-02	386.874	29 971.078	9
338.566	170	5.2e-02	386.874	29 914.720	7
338.595	1400	5.0e-01	386.874	29 912.262	7
350.664	120	6.8e-03	386.874	28 896.062	11
363.546	4800	8.04e-01	0	27 498.975	7
363.797	120	9.3e-03	0	27 480.047	7
364.268	6600	7.74e-01	170.132	27 614.667	9
364.620	180	2.6e-02	0	27 418.015	5
365.350	7200	7.54e-01	386.874	27 750.124	11
365.459	290	8.7e-02	0	27 355.042	3
365.810	660	5.83e-02	170.132	27 498.975	7
366.063	380	3.0e-02	170.132	27 480.047	7
366.897	380	5.4e-02	170.132	27 418.015	5
367.167	600	4.59e-02	386.874	27 614.667	9
368.735	95	3.5e-03	386.874	27 498.975	7
368.991	600	3.53e-02	386.874	27 480.047	7
371.740	450	4.3e-02	0	26 892.926	7
372.257	330	3.4e-02	170.132	27 025.652	9
372.457	600	9.1e-01	12 118.394	38 959.499	9
372.516	380	7.3e-01	8 602.340	35 439.228	3
372.982	2900	4.27e-01	0	26 803.417	5
374.106	3300	4.17e-01	170.132	26 892.926	7
375.286	5200	5.04e-01	386.874	27 025.652	9
375.364	600	8.2e-02	170.132	26 803.417	5
377.166	600	6.03e-02	386.874	26 892.926	7
378.604	840	1.4e+00	7 255.369	33 660.671	3
388.995	70	5.1e-03	0	25 699.95	5

389.849	85	3.48e-03	0	25 643.695	7
390.096	180	1.28e-02	170.132	25 797.60	7
391.434	500	2.3e-02	386.874	25 926.771	9
391.474	24	8.3e-03	0	25 537.276	3
392.142	290	2.15e-02	0	25 493.722	5
392.453	1100	7.15e-02	170.132	25 643.695	7
392.988	890	7.52e-02	0	25 438.898	5
393.424	70	4.5e-03	386.874	25 797.60	7
394.778	1100	9.6e-02	170.132	25 493.722	5
394.867	4500	4.85e-01	0	25 317.813	3
395.634	4500	3.00e-01	170.132	25 438.898	5
395.821	5200	4.05e-01	386.874	25 643.695	7
396.285	950	4.13e-02	0	25 227.217	7
396.427	950	3.09e-02	170.132	25 388.334	9
398.176	4800	3.76e-01	0	25 107.417	5
398.248	570	4.5e-02	0	25 102.88	5
398.976	5700	3.79e-01	170.132	25 227.217	7
399.864	7800	4.08e-01	386.874	25 388.334	9
400.893	950	7.03e-02	170.132	25 107.417	5
400.966	190	1.21e-02	170.132	25 102.88	5
402.457	1200	6.14e-02	386.874	25 227.217	7
405.502	290	2.8e-01	8 436.618	33 090.492	3
406.026	410	2.4e-01	8 492.421	33 114.412	5
406.422	200	2.4e-01	8 492.421	33 090.492	3
406.510	200	7.0e-01	8 492.421	33 085.153	1
411.271	220	7.65e-03	386.874	24 694.895	9
418.612	360	2.10e-01	12 118.394	36 000.144	9
426.622	40	3.1e-01	18 525.07	41 958.51	5
428.138	110	3.18e-02	6 556.828	29 907.273	5
428.499	160	3.2e-01	14 028.47	37 359.13	5
428.740	840	1.46e-01	6 742.757	30 060.328	9
428.907	950	3.0e-01	6 598.749	29 907.273	5
429.094	840	4.5e-01	6 556.828	29 855.248	3
429.576	840	1.3e+00	6 556.828	29 829.097	1
439.392	170	3.3e-01	18 287.560	41 039.874	11
441.728	220	3.6e-01	15 220.390	37 852.434	9
444.127	50	6.1e-02	15 108.121	37 617.868	9
444.915	840	9.7e-01	15 220.390	37 690.320	11
445.090	550	9.6e-01	15 156.787	37 617.868	9
445.332	840	5.98e-01	11 531.760	33 980.639	5
445.371	290	4.7e-01	15 108.121	37 555.021	7
445.533	950	4.8e-01	11 639.804	34 078.580	7

445.743	1100	5.6e-01	11 776.806	34 204.971	9
446.209	21	3.72e-04	0	22 404.69	7
446.581	290	3.28e-01	14 028.47	36 414.58	7
448.126	530	5.7e-01	14 105.68	36 414.58	7
449.615	240	4.4e-01	14 105.68	36 340.67	5
451.274	780	9.86e-02	6 742.757	28 896.062	11
451.803	1000	1.72e-01	6 661.003	28 788.372	9
451.870	95	6.5e-02	11 531.760	33 655.853	5
452.280	1000	1.9e-01	6 598.749	28 702.768	7
452.731	780	2.2e-01	6 556.828	28 638.832	5
453.324	6000	8.83e-01	6 842.964	28 896.062	11
453.478	3600	6.87e-01	6 742.757	28 788.372	9
454.469	720	3.3e-01	6 598.749	28 596.293	3
454.877	950	2.85e-01	6 661.003	28 638.832	5
455.246	950	2.1e-01	6 742.757	28 702.768	7
455.549	720	1.16e-01	6 842.964	28 788.372	9
456.263	50	1.41e-03	170.132	22 081.198	5
456.343	35	2.1e-01	19 573.968	41 481.13	11
461.727	950	8.51e-01	14 105.68	35 757.51	9
462.309	480	5.74e-01	14 028.47	35 652.95	7
463.995	190	6.64e-01	13 981.75	35 527.76	3
464.519	140	8.57e-01	13 981.75	35 503.40	1
465.002	120	2.6e-01	14 028.47	35 527.76	3
465.604	24	9.3e-02	14 105.68	35 577.14	5
465.647	720	1.99e-02	0	21 469.494	7
466.759	840	2.18e-02	170.132	21 588.496	9
467.512	70	1.85e-02	8 602.340	29 986.185	7
468.192	950	2.35e-02	386.874	21 739.713	11
469.080	24	4.4e-03	8 602.340	29 914.720	7
469.368	40	8.5e-04	170.132	21 469.494	7
471.530	24	6.9e-04	386.874	21 588.496	9
472.262	65	4.7e-02	8 492.421	29 661.232	3
474.279	170	5.3e-01	18 037.225	39 115.958	9
475.812	310	7.13e-01	18 141.229	39 152.057	11
475.928	310	7.40e-01	18 192.577	39 198.320	13
477.826	65	2.0e-01	18 037.225	38 959.499	9
478.172	45	2.9e-03	6 842.964	27 750.124	11
480.543	110	5.8e-01	18 911.399	39 715.437	7
482.042	200	1.49e-01	12 118.394	32 857.721	7
484.087	470	1.76e-01	7 255.369	27 907.026	5
485.601	290	5.2e-01	18 192.577	38 779.856	15
488.508	400	4.90e-01	15 220.390	35 685.160	13

491.362	320	4.44e-01	15 108.121	35 454.051	9
491.524	55	2.40e-02	15 220.390	35 559.627	11
492.616	30	2.65e-03	6 598.749	26 892.926	7
492.834	150	6.2e-01	17 369.59	37 654.77	5
494.158	30	5.3e-02	17 423.853	37 654.77	5
496.475	55	7.22e-02	15 877.18	36 013.57	5
498.173	5800	6.60e-01	6 842.964	26 910.705	13
498.915	150	3.25e-01	15 975.59	36 013.57	5
499.107	4600	5.84e-01	6 742.757	26 772.965	11
499.710	140	4.07e-03	0	20 006.032	5
499.951	4000	5.27e-01	6 661.003	26 657.409	9
500.101	230	3.52e-01	16 106.08	36 096.47	7
500.721	3600	4.92e-01	6 598.749	26 564.385	7
500.965	120	2.09e-03	170.132	20 126.055	7
501.419	3200bl	5.3e-02	0	19 937.859	3
501.424		6.8e-01	6 556.828	26 494.322	5
501.617	580	6.43e-02	6 842.964	26 772.965	11
502.003	840	1.13e-01	6 742.757	26 657.409	9
502.287	840	1.39e-01	6 661.003	26 564.385	7
502.484	580	1.32e-01	6 598.749	26 494.322	5
503.647	840	3.94e-01	11 639.804	31 489.451	9
503.840	740	3.87e-01	11 531.760	31 373.801	7
503.995	1200	3.89e-02	170.132	20 006.032	5
504.062	75	8.57e-03	6 661.003	26 494.322	5
504.359	85	6.93e-03	6 742.757	26 564.385	7
504.541	55	2.92e-03	6 842.964	26 657.409	9
506.211	110	2.98e-01	17 423.853	37 172.947	3
506.407	35	1.3e-01	21 739.713	41 481.13	11
506.466	1400	3.79e-02	386.874	20 126.055	7
507.148	130	2.49e-02	11 776.806	31 489.451	9
508.707	130	1.4e-01	11 531.760	31 184.021	3
511.344	190	8.41e-02	11 639.804	31 190.631	5
514.547	270	9.60e-02	11 776.806	31 205.985	7
514.748	230	3.50e-03	0	19 421.576	7
515.220	210	2.64e-03	170.132	19 573.968	9
517.375	1100	3.80e-02	0	19 322.988	5
519.298	1300	3.49e-02	170.132	19 421.576	7
519.404	85w	7.6e-02	16 961.42	36 208.92	9
520.110	65	6.28e-02	16 875.19	36 096.47	7
521.039	1400	3.57e-02	386.874	19 573.968	9
521.971	150	2.50e-03	170.132	19 322.988	5
522.269	95	1.95e-01	16 817.19	35 959.07	3

522.364	85	1.35e-01	16 875.19	36 013.57	5
522.432	250	3.6e-01	17 215.44	36 351.43	11
524.731	75	9.08e-02	16 961.42	36 013.57	5
525.211	110	1.23e-03	386.874	19 421.576	7
525.999	55	2.3e-01	22 081.198	41 087.31	7
528.239	40	2.4e-02	8 492.421	27 418.015	5
529.579	65	7.91e-03	8 602.340	27 480.047	7
535.108	75	3.4e-01	22 404.69	41 087.31	7
536.665	26	8.64e-04	6 598.749	25 227.217	7
538.918	40	3.3e-03	6 556.828	25 107.417	5
542.626	40	3.19e-04	170.132	18 593.99	7
543.673	26	1.0e-03	7 255.369	25 643.695	7
544.664	40	2.5e-04	170.132	18 525.07	5
545.365	35	6.1e-03	11 639.804	29 971.078	9
546.051	55	3.90e-04	386.874	18 695.23	9
547.121	75	1.3e-02	11 639.804	29 912.262	7
547.423	85	1.2e-02	11 776.806	30 039.211	11
549.015	150	3.69e-02	11 776.806	29 986.185	7
549.084	26	1.4e-04	386.874	18 593.99	7
550.390	110	2.6e-01	20 795.599	38 959.499	9
564.858	75	1.3e-01	20 126.055	37 824.748	9
566.216	190	1.47e-01	18 695.23	36 351.43	11
567.994	30w	1.1e-01	19 937.859	37 538.804	5
568.947	95	1.00e-01	18 525.07	36 096.47	7
570.268	75	1.1e-01	18 482.86	36 013.57	5
571.648	55	8.1e-02	18 525.07	36 013.57	5
572.048	35	8.6e-02	18 482.86	35 959.07	3
573.951	85	4.6e-02	18 141.229	35 559.627	11
574.002	40	4.8e-02	18 037.225	35 454.051	9
577.405	75w	5.5e-01	26 657.409	43 971.513	11
578.598	75w	6.1e-01	26 772.965	44 051.333	13
580.426	65w,l	6.8e-01	26 910.705	44 134.639	15
586.646	400	4.00e-02	8 602.340	25 643.695	7
588.031	65	3.48e-03	8 492.421	25 493.722	5
589.932	230	2.69e-02	8 492.421	25 438.898	5
590.333	55	4.57e-03	8 602.340	25 537.276	3
591.855	120	1.3e-02	8 602.340	25 493.722	5
592.212	150	2.17e-02	8 436.618	25 317.813	3
593.782	75	4.9e-03	8 602.340	25 438.898	5
594.176	120	1.9e-02	8 492.421	25 317.813	3
595.317	300	6.79e-02	15 220.390	32 013.534	13
596.584	200	6.64e-02	15 156.787	31 914.277	11

597.856	270	6.62e-02	15 108.121	31 829.972	9
606.463	110	6.88e-03	8 436.618	24 921.110	3
609.117	120	6.17e-02	18 287.560	34 700.212	11
609.281	40	6.83e-03	15 220.390	31 628.668	11
609.867	40w	2.5e-01	24 694.895	41 087.31	7
612.622	120	2.23e-02	8 602.340	24 921.110	3
622.049	75w	1.8e-01	21 588.496	37 659.927	7
625.810	380	8.36e-02	11 639.804	27 614.667	9
625.870	380	8.9e-02	11 776.806	27 750.124	11
626.110	300	8.07e-02	11 531.760	27 498.975	7
630.375	65	6.51e-03	11 639.804	27 498.975	7
631.224	55	5.22e-03	11 776.806	27 614.667	9
633.610	30	6.01e-03	11 639.804	27 418.015	5
655.423	65	1.34e-02	11 639.804	26 892.926	7
655.607	75	1.45e-02	11 776.806	27 025.652	9
659.911	35	1.80e-03	7 255.369	22 404.69	7
666.655	18w	3.3e-03	11 776.806	26 772.965	11
674.312	80	6.9e-03	7 255.369	22 081.198	5
686.147	35	3.7e-02	18 287.560	32 857.721	7
713.891	26	4.8e-03	11 639.804	25 643.695	7
720.944	260	5.8e-02	11 776.806	25 643.695	7
721.620	60	1.8e-02	11 639.804	25 493.722	5
724.486	130	3.9e-02	11 639.804	25 438.898	5
725.172	130	7.2e-02	11 531.760	25 317.813	3
726.629	19	1.7e-02	13 981.75	27 740.19	5
734.472	120	1.4e-02	11 776.806	25 388.334	9
735.774	90	1.33e-02	11 639.804	25 227.217	7
736.411	60	1.6e-02	11 531.760	25 107.417	5
744.060	26	2.2e-02	18 192.577	31 628.668	11

APENDIX VB: Titanium II emission spectra and physical parameters (source: NIST 2009)

Observed Wavelength (nm)	Rel. Int	Aik (10^8)	E_i (cm^{-1})	Ek (cm^{-1})	g_k
290.992	30	7.9e-03	393.44	34 748.40	10
301.719	120	3.6e-01	12 774.69	45 908.53	12
302.973	140	3.5e-01	12 676.97	45 673.62	10
304.668	110	2.2e-01	9 395.71	42 208.59	6
305.674	130	3.2e-01	9 363.62	42 068.52	4
305.740	130	2.2e-02	0	32 697.99	6
305.809	170	5.0e-01	9 518.06	42 208.59	6
306.622	1300bl	2.53e-01	94.10	32 697.99	6
306.635		3.3e-01	0	32 602.55	4
307.124	70	3.6e-01	9 518.06	42 068.52	4
307.211	600	2.0e-01	225.73	32 767.07	8
307.297	1100	1.6e+00	0	32 532.21	2
307.522	1600	1.13e+00	94.10	32 602.55	4
307.864	2300	1.09e+00	225.73	32 697.99	6
308.802	3600	1.25e+00	393.44	32 767.07	8
308.940	180	1.3e+00	15 265.62	47 624.88	6
309.719	180	4.4e-01	9 930.69	42 208.59	6
310.380	230	1.1e+00	15 257.43	47 466.54	8
310.508	230	6.3e-01	9 872.73	42 068.52	4
310.623	260	7.8e-01	10 024.73	42 208.59	6
311.067	50	2.7e-01	9 930.69	42 068.52	4
311.767	140	1.1e+00	9 930.69	41 996.57	2
311.980		5.9e-01	10 024.73	42 068.52	4
313.080	240	8.2e-02	94.10	32 025.47	6
314.376	220	6.2e-02	225.73	32 025.47	6
314.804	240	1.1e-01	0	31 756.51	4
315.225	240	9.4e-02	983.89	32 697.99	6
315.420	240	1.1e-01	908.02	32 602.55	4
315.567	240	7.4e-02	1 087.32	32 767.07	8
316.120	500	5.9e-01	908.02	32 532.21	2
316.177	780	4.6e-01	983.89	32 602.55	4
316.257	1000	3.9e-01	1 087.32	32 697.99	6
316.852	1600	4.1e-01	1 215.84	32 767.07	8
319.087	1000	1.3e+00	8 744.25	40 074.52	8
319.752	50	1.1e-02	225.73	31 490.82	8
320.254	780	1.1e+00	8 710.44	39 926.66	6

320.344	50	2.1e-02	0	31 207.42	6
321.314	110	6.1e-03	94.10	31 207.42	6
321.475	190	3.3e-02	393.44	31 490.82	8
321.706	1100	1.69e-01	225.73	31 301.01	10
322.284	1300	2.6e-01	94.10	31 113.65	8
322.424	240	7.0e-01	12 774.69	43 780.79	10
322.860	530	2.0e+00	8 710.44	39 674.66	2
323.132	110	3.4e-02	1 087.32	32 025.47	6
323.228	240	6.0e-01	8 997.71	39 926.66	6
323.452	6600	1.38e+00	393.44	31 301.01	10
323.612	220	7.0e-01	8 710.44	39 602.75	4
323.657	5200	1.11e+00	225.73	31 113.65	8
323.904	4100	9.87e-01	94.10	30 958.50	6
323.966	220	9.4e-01	8 744.25	39 602.75	4
324.199	2600	1.16e+00	0	30 836.32	4
325.191	950	3.38e-01	94.10	30 836.32	4
325.291	1200	3.9e-01	225.73	30 958.50	6
325.425	1200	2.0e-01	393.44	31 113.65	8
327.165	310	2.4e-01	10 024.73	40 581.49	6
327.208	310	3.2e-01	9 872.73	40 425.59	4
327.829	200	9.6e-01	9 930.69	40 425.59	4
328.766	530	1.4e+00	15 265.62	45 673.62	10
330.881	220	4.5e-02	1 087.32	31 301.01	10
331.532	290	3.8e-01	9 872.73	40 027.11	4
331.802	330	6.0e-02	983.89	31 113.65	8
332.170	550	7.2e-01	9 930.69	40 027.11	4
332.294	2900	3.96e-01	1 215.84	31 301.01	10
332.676	380	8.4e-02	908.02	30 958.50	6
332.946	2100	3.25e-01	1 087.32	31 113.65	8
333.211	550	1.1e+00	10 024.73	40 027.11	4
333.520	1800	2.93e-01	983.89	30 958.50	6
334.034	1100	3.6e-01	908.02	30 836.32	4
334.377	260	4.0e-02	1 215.84	31 113.65	8
334.673	330	7.9e-02	1 087.32	30 958.50	6
336.121	7200	1.1e+00	225.73	29 968.30	10
337.221	140	7.3e-02	4 897.65	34 543.26	8
337.280	5700	1.11e+00	94.10	29 734.54	8
337.435	60	1.6e-01	9 975.92	39 602.75	4
338.028	1400	1.6e-01	393.44	29 968.30	10
338.376	5700	1.09e+00	0	29 544.37	6
338.784	1400	2.18e-01	225.73	29 734.54	8
338.876	60	9.0e-02	9 975.92	39 476.80	6

339.458	1100	2.5e-01	94.10	29 544.37	6
340.720	60	7.2e-03	393.44	29 734.54	8
340.981	95	1.2e-02	225.73	29 544.37	6
344.431	890	7.3e-02	1 215.84	30 240.88	12
345.247	60	7.7e-01	16 515.86	45 472.27	2
345.639	180	8.2e-01	16 625.11	45 548.76	4
346.150	600	6.27e-02	1 087.32	29 968.30	10
347.718	600	6.05e-02	983.89	29 734.54	8
348.974	60	8.2e-03	1 087.32	29 734.54	8
350.489	890	8.2e-01	15 257.43	43 780.79	10
351.084	600	9.3e-01	15 265.62	43 740.65	8
352.025	60	4.8e-01	16 515.86	44 914.70	4
353.541	310	5.5e-01	16 625.11	44 902.29	6
357.374	120	2.8e-02	4 628.58	32 602.55	4
358.713	60	1.1e-02	4 897.65	32 767.07	8
359.605	240	5.2e-02	4 897.65	32 697.99	6
362.482	190	2.9e-01	9 850.90	37 430.58	2
364.133	190	4.9e-01	9 975.92	37 430.58	2
365.976	120	1.1e-01	12 758.11	40 074.52	8
366.224	190	1.4e-01	12 628.73	39 926.66	6
370.623	140	3.1e-01	12 628.73	39 602.75	4
372.164	140	3.9e-02	4 628.58	31 490.82	8
374.164	330	6.2e-01	12 758.11	39 476.80	6
375.930	3300	9.4e-01	4 897.65	31 490.82	8
376.132	2900	9.9e-01	4 628.58	31 207.42	6
376.189	50	1.4e-01	20 891.66	47 466.54	8
390.054	530	1.6e-01	9 118.26	34 748.40	10
391.346	500	1.6e-01	8 997.71	34 543.26	8
393.202	35	8.9e-03	9 118.26	34 543.26	8
401.239	70	1.7e-02	4 628.58	29 544.37	6
402.514	40	5.4e-03	4 897.65	29 734.54	8
402.834	40	5.1e-02	15 257.43	40 074.52	8
416.365	70	2.6e-01	20 891.66	44 902.29	6
417.190	40	2.6e-01	20 951.62	44 914.70	4
429.023	120	4.6e-02	9 395.71	32 697.99	6
429.412	140	4.7e-02	8 744.25	32 025.47	6
430.005	200	7.7e-02	9 518.06	32 767.07	8
430.193	85	6.2e-02	9 363.62	32 602.55	4
430.790	180	4.6e-02	9 395.71	32 602.55	4
431.287	85	4.1e-02	9 518.06	32 697.99	6
433.792	160	6.6e-02	8 710.44	31 756.51	4
434.429	24	7.2e-03	8 744.25	31 756.51	4

439.504	330	9.4e-02	8 744.25	31 490.82	8
439.977	60	3.1e-02	9 975.92	32 697.99	6
441.772	60	2.1e-02	9 395.71	32 025.47	6
444.380	230	1.1e-01	8 710.44	31 207.42	6
445.049	30	2.0e-02	8 744.25	31 207.42	6
446.850	240	1.0e-01	9 118.26	31 490.82	8
448.832	19	6.3e-02	25 192.79	47 466.54	8
450.127	200	9.8e-02	8 997.71	31 207.42	6
453.397	240	9.2e-02	9 975.92	32 025.47	6
454.963	240	1.1e-01	12 774.69	34 748.40	10
456.377	110	8.8e-02	9 850.90	31 756.51	4
457.198	240	1.2e-01	12 676.97	34 543.26	8
458.995	24	1.3e-02	9 975.92	31 756.51	4
480.510	28	1.1e-01	16 625.11	37 430.58	2
512.915	30	1.0e-02	15 257.43	34 748.40	10
518.870	85	2.5e-02	12 758.11	32 025.47	6
522.656	65	3.1e-02	12 628.73	31 756.51	4
533.681	26	5.8e-03	12 758.11	31 490.82	8

APPENDIX VI: Optical Emission Plot Spectroscopic Results

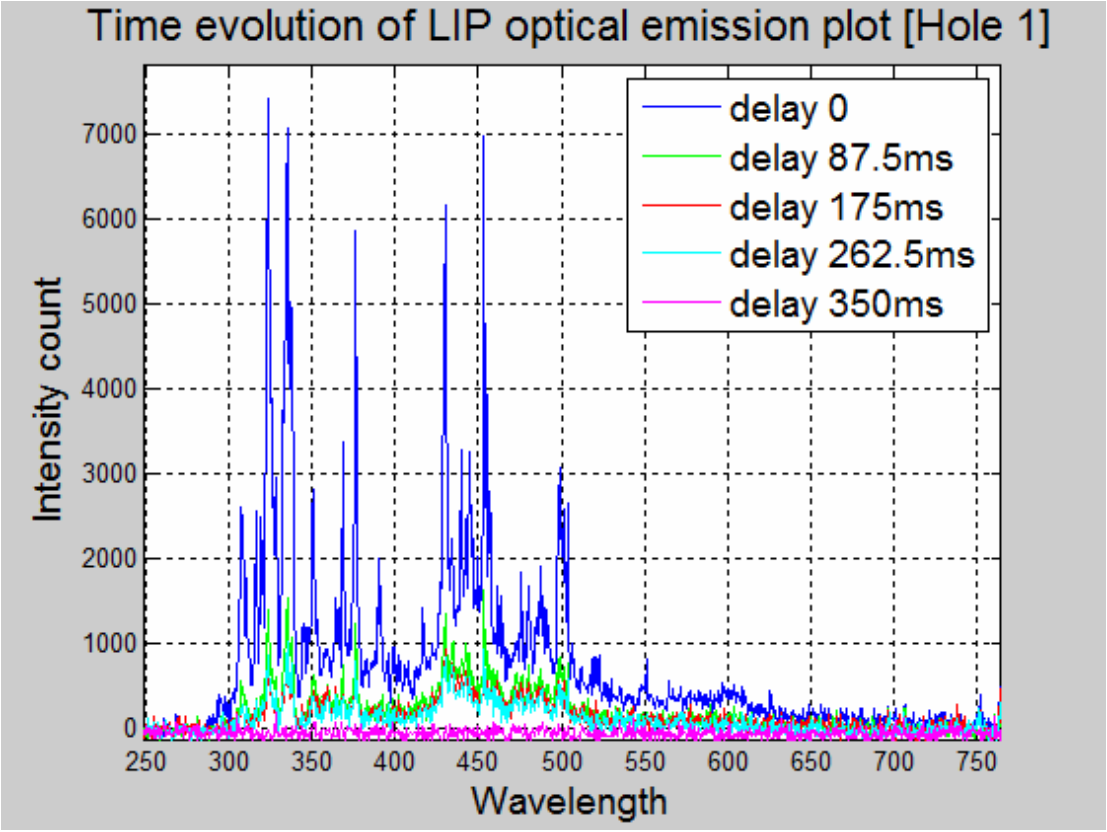

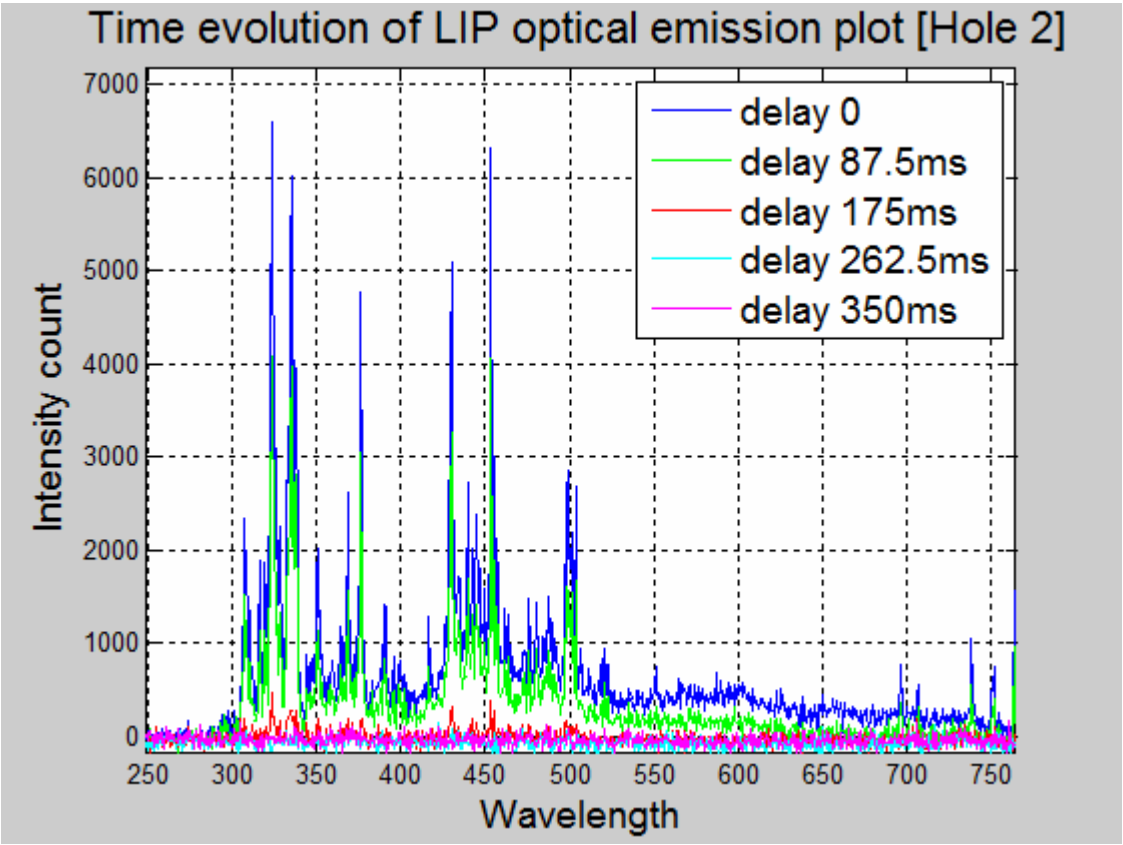

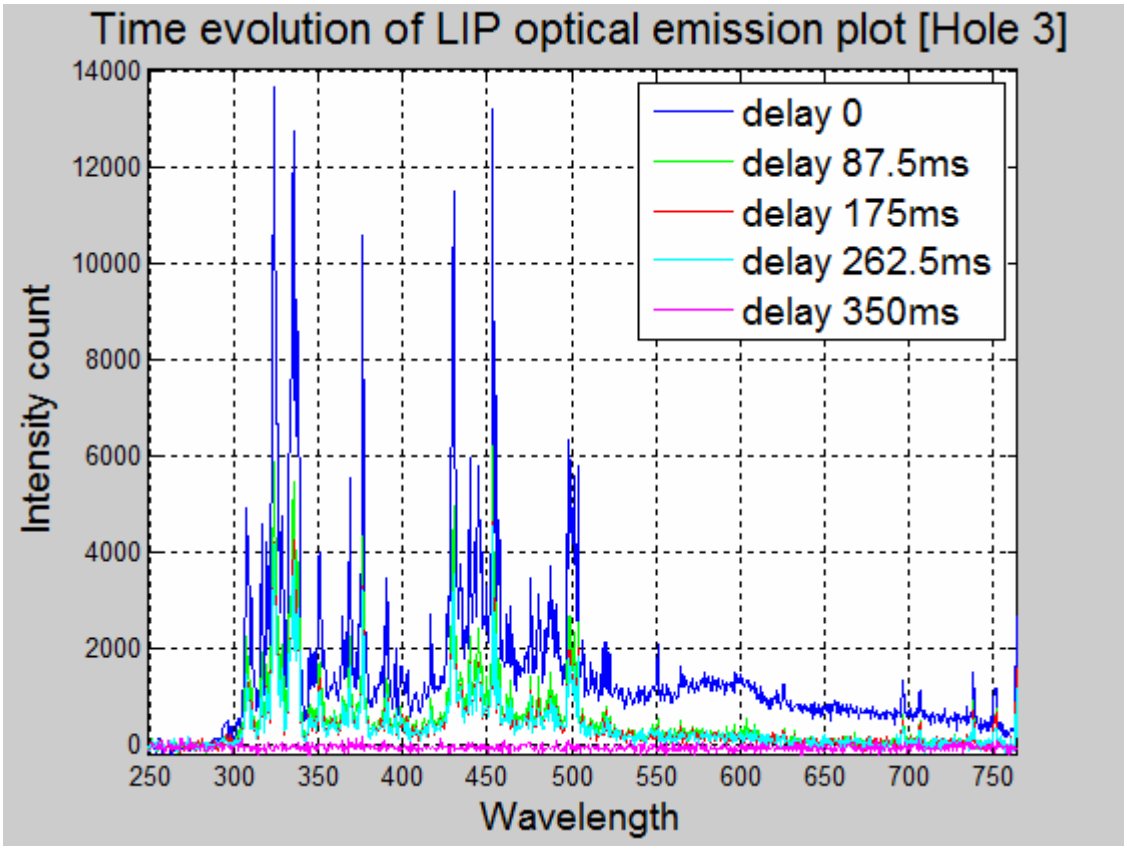
Time evolution of LIP optical emission plot [Hole 3]
Intensity count
Wavelength
delay 0
delay 87.5ms
delay 175ms
delay 262.5ms
delay 350ms
14000
12000
10000
8000
6000
4000
2000
0
250
300
350
400
450
500
550
600
650
700
750

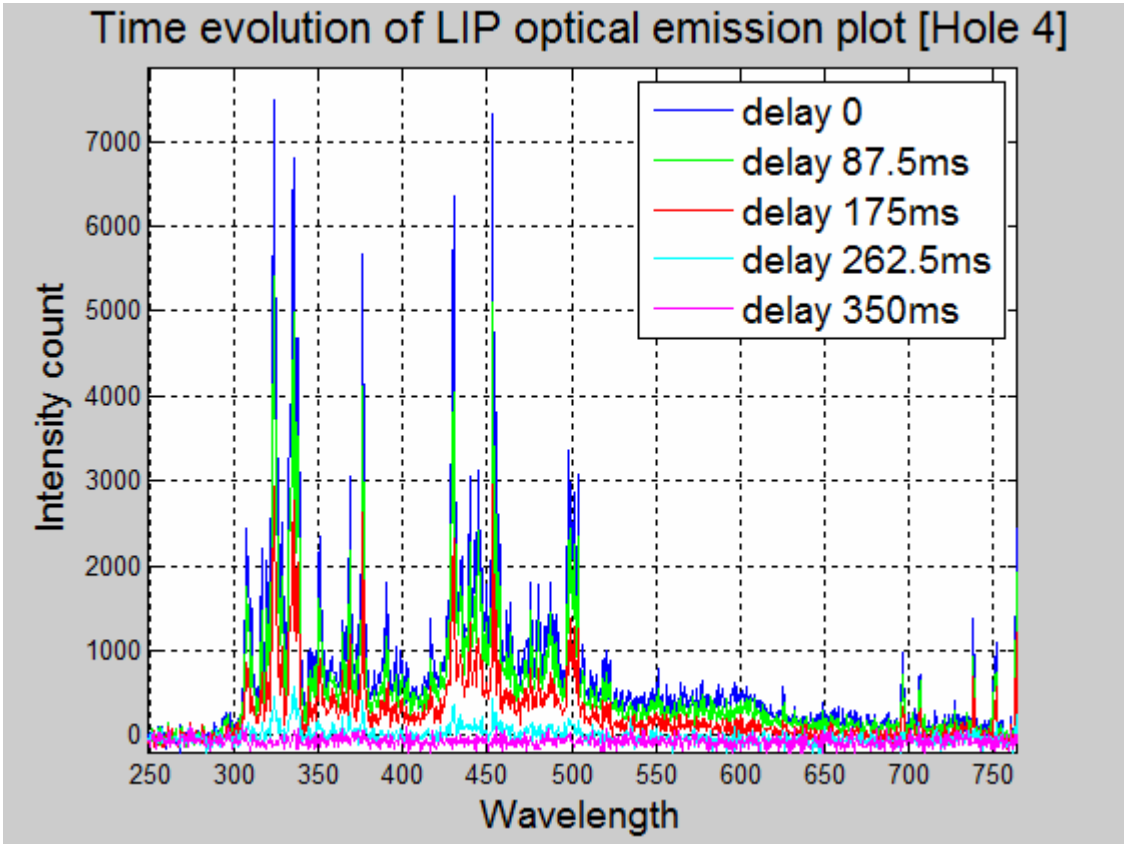
Time evolution of LIP optical emission plot [Hole 4]
Intensity count
Wavelength
delay 0
delay 87.5ms
delay 175ms
delay 262.5ms
delay 350ms
7000
6000
5000
4000
3000
2000
1000
0
250
300
350
400
450
500
550
600
650
700
750

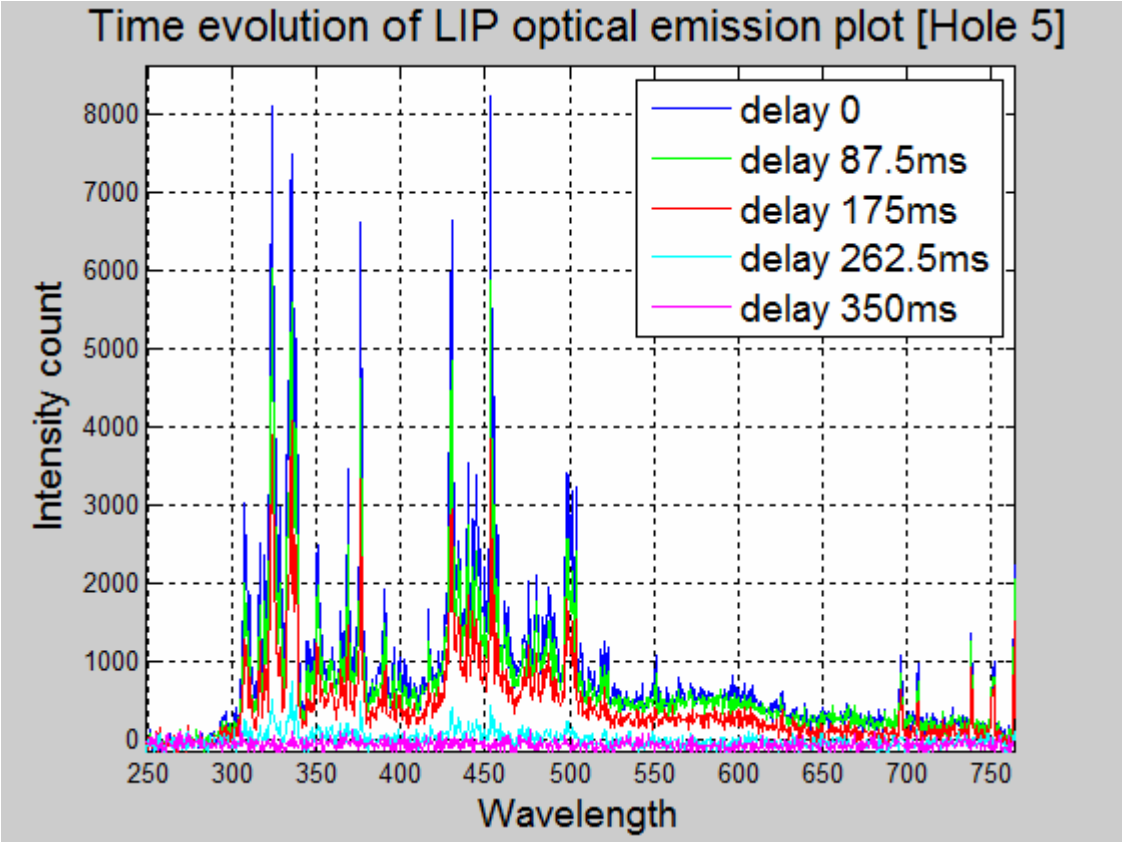
Time evolution of LIP optical emission plot [Hole 5]
delay 0
delay 87.5ms
delay 175ms
delay 262.5ms
delay 350ms
Intensity count
Wavelength
0
1000
2000
3000
4000
5000
6000
7000
8000
250
300
350
400
450
500
550
600
650
700
750